THE UNIVERSITY OF MICHIGAN

COLLEGE OF ENGINEERING
Department of Electrical Engineering

Technical Report

MEASUREMENT AND INTERPRETATION OF PLASMA PROPERTIES TO 100 KILOBARS OF PRESSURE

James W. Robinson

ORA Project 05742

supported by:

NATIONAL AERONAUTICS AND SPACE ADMINISTRATION
GRANT NO. NsG-415
WASHINGTON, D.C.

administered through:

OFFICE OF RESEARCH ADMINISTRATION ANN ARBOR

October 1965

TABLE OF CONTENTS

TABLE OF CONTENTS (Concluded)

MEASUREMENT AND INTERPRETATION OF PLASMA PROPERTIES TO 100 KILOBARS OF PRESSURE*

By James W. Robinson
The University of Michigan

SUMMARY

Plasmas were produced at near-liquid densities, and measurements of thermodynamic properties were made for these conditions. The range of pressures investigated was too high for static confinement, so the plasmas were generated under water which provided transient inertial confinement. Experimental data were obtained at pressures of 4, 7.7, and 115 kilobars. Pressure at the two lower levels was produced by the inertial restraint of the water which surrounded the expanding column of plasma. The pressure at the higher level was produced by detonating an explosive charge in the water in the vicinity of the plasma column.

At each level of pressure, the temperature, pressure, and internal energy of the plasma were determined experimentally. At the lower pressure levels, internal energy was predicted from temperature and pressure data by the use of the Debye-Hückel theory of shielding. The predicted values were lower than the measured values by a factor of five, so a different theoretical approach was sought. A calculation based upon the quantum mechanical virial theorem introduced the strong cohesive forces which were needed to explain the measurements. At the higher pressure where temperature was much lower, the plasma was treated as a partially dissociated gas of water molecules with a very low fraction of ionization. The equation of state was modified by the introduction of a covolume which was required because of the high density of the plasma.

INTRODUCTION

A plasma can be defined as an electrically conducting gas composed of charged particles of both polarities. Vast ranges of temperature and density are included in the scope of the definition. The greatest concentrations of plasma occur in stellar bodies where any semblance of atomic structure is completely destroyed because of the high density and temperature. At

*This paper was submitted in different format as a doctoral thesis at The University of Michigan.

the other extreme are the tenuous gases of space which are also considered to be plasmas.

No general theory can be applied to the description of all types of plasma. Although certain physical principles have general validity, the method of procedure for any particular range of density is established by the relative importance of the various physical processes which occur.

For a particular range of conditions, a model is constructed upon which computational procedures are based. The model is an idealized representation of the physical processes which predominate for those conditions. Any model sufficiently general to describe all cases would be hopelessly complex, so that the development of a general approach for all types of plasma is not feasible.

Often an experimental investigation depends upon so many variables that an accurate and simple model is not known. A realistic model may lead to mathematical complexities while an over-simplified model may predict grossly incorrect relationships. Error can also arise from the extension of a model beyond its range of applicability. Plasma research is concerned with the development of theoretical models from which experimental observations can be accurately predicted.

Not only is there a lack of theoretical knowledge of plasmas but also there is a lack of experimental data. Theory is not easily confirmed in terms of data because experimental variables are difficult to control and to measure. The method of confining the plasma often affects the properties of the plasma.

Most plasma research has occurred at densities below 10^{16} electrons/cm^3. Of great interest in this range are phenomena associated with communications, controlled nuclear fusion, radio astronomy, and gaseous electronic devices.

Considerable theoretical progress has been made in describing plasmas as the extreme densities of stellar interiors where atomic structure is completely destroyed. For this situation the Thomas-Fermi model describes the electrons of an atom as an ideal Fermi gas confined to a spherical volume. (1)

This paper deals with a range of densities lower than the densities where the Thomas-Fermi model is applicable, yet higher than densities where the great bulk of plasma research has been conducted. In this range from 10^{22} to 10^{23} electrons/cm^3, the interactions between particles are sufficiently strong that models based upon modifications of an ideal gas often do not apply. Although the Fermi gas of electrons in a metal is well understood at these densities, the behavior of a plasma with random ion locations is not. These densities are obtained in a plasma by confining it at pressures

of approximately 100 kilobars. In this study, such pressures were produced so that properties of the plasmas could be measured. Pressure, temperature, and internal energy were determined experimentally. These results were compared with theoretical predictions to determine the appropriateness of the physical models from which the theories were derived.

Historical Background

As experimentalists extended research to higher pressures and temperatures, the principal problem to be solved was that of plasma confinement. Not only would materials be too weak to maintain pressure, but they would be seriously eroded if they came in contact with the plasma being studied.

In the late 1930's, Suits measured properties of plasma under a static confinement of 1 kilobar. (2) The test chamber contained a window through which photographs and spectrographs of an arc discharge could be taken. However, his measurements represented a limit in static pressures which could not be easily surpassed. Although static pressure chambers have been constructed to produce pressures of hundreds of kilobars, they are not adaptable to plasma study.

E. A. Martin produced transient plasmas at several kilobars of pressure by using inertial confinement. (3) His techniques introduced an extension to the range of pressures which could be investigated with static confinement. However, the measurements then became dynamic instead of steady state measurements, so that the experimental problem was the development of accurate instrumentation with a fast time response.

Martin's plasma was produced by discharging a capacitor bank between electrodes submerged in water. A column of plasma was formed which grew by continuously ionizing water at its boundary. The electrical power delivered to the plasma was almost completely utilized in the formation of new plasma at the boundary. Pressure was maintained by the inertial restraint of the water which surrounded the column. As the column expanded and the surrounding water was displaced, a cylindrical shock wave was formed about the column. The confining medium of water was transparent so that photographic observations could be made.

Martin was able to measure pressure, temperature, and internal energy of the plasma. The measurements could be checked by computing internal energy from pressure and temperature. Although quantitative interpretation of the data was not conclusive, the methods were established by which more accurate measurements could be made.

Recently Sherk has made measurements of temperature for underwater exploding wires of different metals. (4) He used a relatively low-power dis-

charge with a relatively heavy wire so that the plasma consisted mainly of metal vapor and not of water as was the case for Martin's work. He found the temperature to be a function of ionization potential of the metal.

Several Russians have investigated the production of strong shock waves in water from underwater electric discharges. (5,6,7) However, they have made measurements of the shock waves and not of the plasmas.

Seay has produced a helium plasma at 10^{18} electrons/cm^3 and 20 000°K by passing a shock wave from a chemical explosive through the gas. (8)

E. A. Martin's Investigation

E. A. Martin developed several concepts and techniques in his work which have been retained in the present investigation. The more important of these are briefly presented here to supplement the historical account.

The plasma column was formed by electrically exploding a fine initiating wire which was stretched between the discharge electrodes. Without the wire the formation of the plasma was delayed many microseconds after the discharge circuit switch was closed, and when electrical breakdown did occur the path was very irregular. The wire contaminated the plasma but Martin showed that the effect was negligible. The plasma column rapidly inducted water so that after a few tenths of a microsecond the percentage of metal was very small.

When an initiating wire of 0.001 in. tungsten was used, the current flow began immediately without a dwell period after the switch was closed. The shape of the plasma column was a uniform cylinder which grew at a reproducible rate. The boundaries of the column were sharply defined. Thus, the volume of plasma could be computed as a function of time from photographs taken at various stages of growth.

By order-of-magnitude calculations and by various experimental modifications, Martin was able to establish two important properties of the plasma. To a good approximation, the plasma was in thermodynamic equilibrium and it was a black-body radiator. Both properties resulted from the high density. Thus, the temperature could be determined from an absolute measurement of the radiation in a narrow bandwidth by using the Planck distribution function.

As the plasma column grew by converting water at its boundary into new plasma, the energy for generating the plasma was transported to the boundary of the column through the mechanism of ion recombination at the boundary. Yet the temperature and current density were fairly constant throughout the column so that calculations could be based upon a uniform body of plasma.

The migration rate of atoms that were eroded from the electrodes was shown to be sufficiently small that electrode contamination of the plasma could be neglected.

Pressure was determined indirectly from the growth rate of the column. The rate at which the surrounding water was displaced was a function of the plasma pressure, which could be computed from the hydrodynamic properties of the water.

Scope of the Present Investigation

Measurements of plasma properties were made in two different ranges of pressure. Two series of tests were made in the range from 4 to 8 kilobars of pressure by using a procedure similar to that which Martin used. Then measurements were made at approximately 115 kilobars by using chemical explosives to generate additional confining pressure. The instrumentation was designed to have better resolution than Martin's equipment so that a more significant interpretation of data could be made.

The use of chemical explosives was introduced to extend the range of pressures under which plasma could be produced and investigated. An underwater detonation of an explosive produces a shock wave in the water which has a pressure in the range of 100 kilobars. When this shock wave is made to pass through an existing column of plasma, such as Martin studied, the plasma is compressed to the higher pressure.

The possibility exists, without the use of explosives, of producing much higher pressures than those obtained by Martin, because an increase in the rate of rise of discharge current results in a pressure increase. However, faster rates of current rise mean reduced confinement times. The use of explosives made possible a fairly steady pressure for an observation period of about 2 μsec, independently of the rate of rise of the current.

The formation of a uniform plasma in the high-pressure region of the explosive shock wave could not be accomplished directly. Therefore, the plasma was first formed in undisturbed water and then compressed by the passage of the shock wave. The direction of motion of the shock wave was normal to the axis of the plasma column so that it was distorted into a column with an elliptical cross section when the shock passed through it.

For each experimental condition that was investigated, the temperature, pressure, and internal energy per unit volume were determined experimentally. Thus, a basis existed for examining theories in terms of experimental data.

The plasma at 115 kilobars was adequately described as a gas of partially dissociated molecules with an excluded volume. Fractional ionization was very

low because of the relatively low temperature of 10 000°K.

However, in the 4 to 8 kilobar range the temperature was between 30 000 and 40 000°K and ionization was very significant. For this range, the apparently suitable model was a partially ionized gas which was subject to Saha's ionization equation and to the Debye-Hückel theory of shielding for ionized particles. However, the model was found to be very much unsuited to a description of the plasma. The theoretical prediction of internal energy from pressure and temperature was too low by a factor of five.

Therefore, a different approach to the theory was considered. The plasma was treated as a collection of ions and electrons subject to the quantum mechanical virial theorem. No distinction was made between neutral atoms and ionized atoms. The approach was found to be much more satisfactory than the Debye-Hückel theory although it was not sufficiently developed to yield quantitatively accurate results.

From the attempts to generate a plasma directly in the region of high pressure created by the chemical explosive, a type of discharge was produced which differed from that obtained by compressing an existing plasma column. The discharge path formed as a mixture of two types of plasma which had significantly different temperatures. The hotter type of plasma with temperatures in the range of 10 000°K was apparently the same as that which was obtained by compression of existing plasma. The cooler regions had temperatures in the range of 6000 to 7000°K.

Acknowledgments

Harold C. Early made numerous suggestions for the development of experimental techniques. William N. Lawrence designed and built the Kerr cell camera which was used in the investigation. Gunnar Hok participated in many discussions concerning the interpretations of the measurements.

I. USE OF EXPLOSIVES FOR CONFINING PLASMA

In this investigation, a chemical explosive was used as a means of confining plasma at a pressure of approximately 100 kilobars. There was no specific interest in extending the science of explosives, but rather in adapting explosive technology to the problem of confining plasma. The method of confinement had to be compatible with the techniques for measuring the plasma properties. In this section, the problems specifically related to the use of explosives and to the design of the explosive charge are discussed. The method of determining the pressure produced by the explosive is described and results are presented here.

Choice of Explosive

Chemical explosives are classified in two categories which are distinguished by the burning rates. (9, p. 215) If the velocity of the combustion front exceeds the velocity of sound in the unreacted explosive, the burning process is called a detonation. However, if the velocity is less than that of sound, the process is called a deflagration. This distinction, known as Jouguet's rule, separates explosives into two types which have very different physical characteristics.

The pressure generated in a medium which surrounds a detonating explosive is primarily a function of the density and compressibility of the medium. However, for a deflagration the pressure depends upon the mechanical strength of the container. Detonation pressures greatly exceed the yield strengths of most materials and thus they are much higher than deflagration pressures. In water, detonating explosives generate pressures exceeding 100 kilobars.

The idea of using explosives to confine plasma originated with the knowledge that pressures up to 100 kilobars were obtainable from detonating explosives. With such pressures as a goal, the choice of explosive was necessarily limited to those which detonate.

Many types of detonating explosives are known, the most familiar of which is TNT. The type chosen for this work, PETN is very similar to TNT in chemical properties. Pentolite, a mixture of these two types, could have been used as could other less known types. (10)

PETN was chosen because it was the most convenient to use. It is commercially available in small quantities and in various forms among which are flexible sheets of different thicknesses. The sheets are easily cut to any shape desired to provide versatility in the use of the explosive.

The abbreviation, PETN, stands for pentaerythritol tetranitrate which has the chemical formula, $C_5H_8(NO_3)_4$. The reaction of PETN liberates nitrogen and forms simple oxides. Energy released is from 1.3 to 1.5 kcal/g depending upon manufacture and conditions of use. The chemical is mixed with a binder to form the soft, plastic sheets which are sold commercially.

The sheets of explosive are very difficult to detonate except with a blasting cap. According to the manufacturer, some sheets burned when they were placed in a fire, but they did not detonate. Also the impact of rifle bullets upon a sheet with a steel backing plate failed to initiate a detonation. Yet the manufacturer warns that the sheets should be cut with a single-bladed knife and not with shears because of the possibility that small particles might be caught between moving metal parts of the shears and thus be detonated. Detonation was reliably initiated with common dynamite caps which were available locally.

Nominal detonation velocity for the sheet explosive was 6500 to 7500 m/sec according to the manufacturers specifications. The velocity was measured for this particular application to be 8000 m/sec. The higher value for measured velocity is attributed to the fact that the explosive was encased in steel for this application.

Explosive Charge Design

The peak pressure produced by an explosive in water depends upon the type of explosive and not upon the amount. However, the duration of the pressure pulse does depend upon the amount. Therefore, if an explosive is to be used to confine a plasma at high pressure, the amount of explosive depends upon the desired confinement time.

The pressure pulse from an explosive is in the form of a shock wave which propagates through the medium, water in this case, at high speed. The shock wave consists of a discontinuity or front between the undisturbed medium ahead of the front and the highly compressed medium behind the front. As the front moves through the undisturbed medium, it continuously inducts new material into the compressed region. The front has a finite thickness which, however, is too small for measurement. The thickness has been estimated at 10^{-5} or 10^{-6} cm. (11, p. 45)

The peak pressure of the shock wave occurs in the region immediately behind the front and the pressure decreases as a function of distance behind the front. Some pressure-distance profiles of a shock wave are shown in Fig. 1, which represents the progression of a wave in time. They show both the decay of peak pressure with time and the spacial pressure distribution.

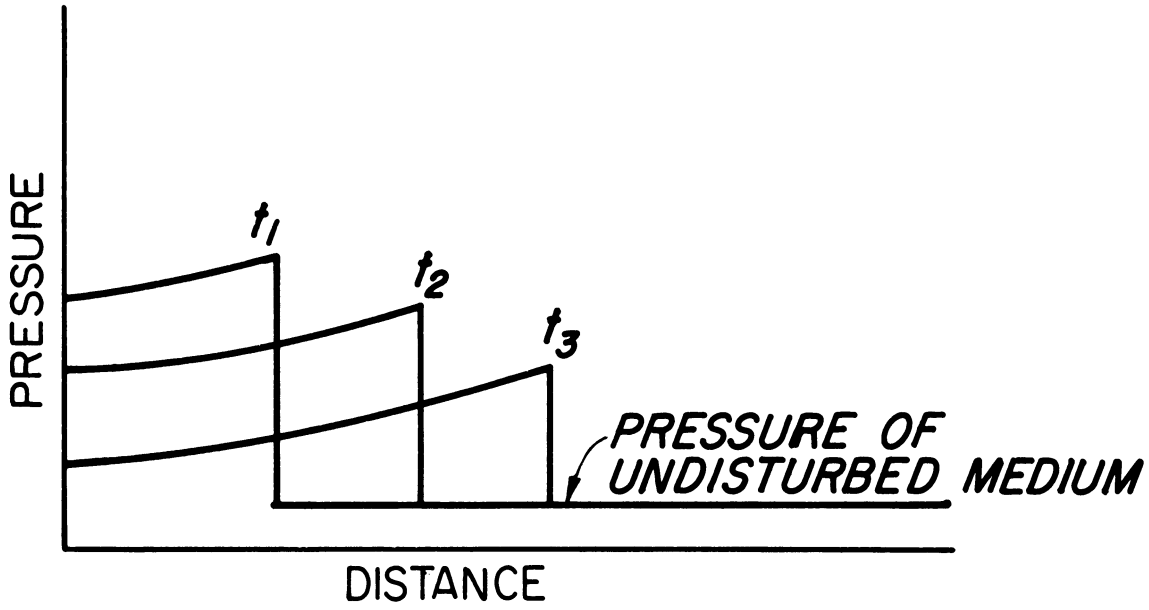

Fig. 1. Pressure distribution in a shock wave for different times with $t_3 > t_2 > t_1$.

The similarity principle is useful in calculating the size of an explosive charge needed for a particular application. (11) The principle is a scaling law which states that if dimensions and time of a particular experimental situation are multiplied by a constant factor, the pressure will remain unchanged. For example, suppose a spherical charge of radius a is detonated with a blasting cap at its center. At some radius $R > a$, a peak pressure of P occurs after T seconds and the pressure decays to P' after T' seconds. Then, if a sphere of radius ka is detonated, peak pressure P occurs at kR after kT seconds and the pressure decays to P' after kT' seconds. Viscous effects cause small deviations from the scaling law, and the effect of gravity invalidates the law after the pressure has dropped to a low level.

An estimate of the required charge size was made by using the scaling law with the results of some theoretical calculations by Bethe and Kirkwood. Various theories have been developed which predict pressure by analyzing the detonation process with an equation of state of the explosive gases, and by accounting for the nature of shock propagation in the water which surrounds the explosive charge. The theories require many approximating assumptions and lengthy calculations. Yet the results are reasonably accurate for order-of-magnitude estimates. The theory of Bethe and Kirkwood has been applied to a sphere of pentolite (50% TNT—50% PETN) which has a density of 1.60 g/cm^3, with the results shown in Table 1. (11, p. 123) The table is expressed in terms of ratios which are invariant under the scaling law.

TABLE 1

THEORY OF BETHE AND KIRKWOOD APPLIED TO A SPHERE OF PENTOLITE WITH RADIUS a IN WATER

Normalized radius, R/a	Peak pressure, psi	Normalized decay time constant θ/a, sec/cm
1	606 000	0.310×10^{-5}
10	21 200	1.37
25	6 310	2.22

Assume that a confinement time of 2 μsec is desired for a plasma which will be located near the surface of a sphere of explosive. If pressure decay can be approximated by an exponential function of time, then a decay time constant of 20 μsec is a reasonable requirement. According to the table, the charge radius would then be 6.46 cm and the weight would be 1800 g for the condition that R/a = 1.

A sphere is not a reasonable shape for the explosive charge because a strong pressure wave propagates in all directions from a sphere while a pressure wave concentrated at the plasma location is required. Still, the results from the spherical case can be interpreted is a useful manner. If a conical sector of the sphere in question is removed from the sphere and placed in a matching hole in some dense backing material, then the sector alone will produce a pressure wave along its axis equivalent to the pressure wave from the entire sphere of explosive along that same axis. The substitution of backing material for explosive is illustrated in Fig. 2. Of course no backing material

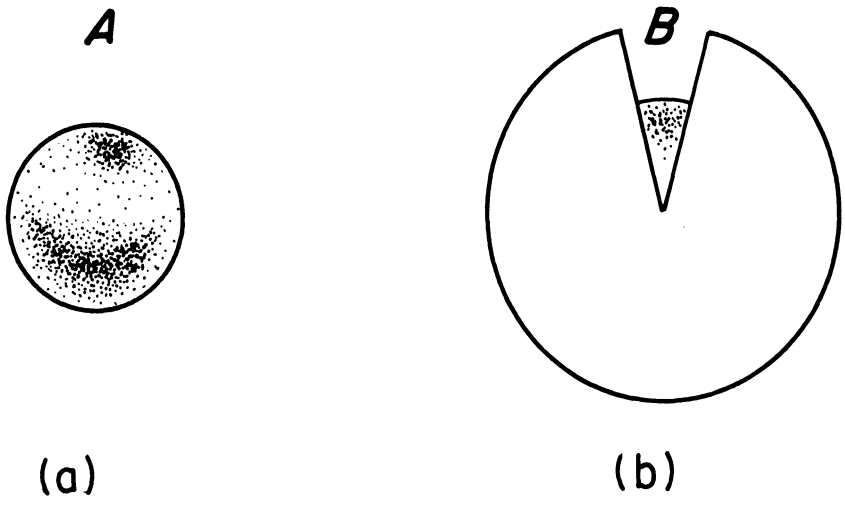

Fig. 2. Two equivalent configurations of explosive for generating pressure at points A and B: (a) a sphere; (b) a conical sector backed with a dense medium.

can be perfectly rigid so that the substitution of backing material is not exactly equivalent to using the entire sphere of explosive. However, experience has shown that the use of backing material is practical. For an area of 2 cm^2 on the face of the sector, the required mass of explosive would be only 6.9 instead of 1800 g.

The actual configuration used for this research was a cylindrical column of explosive which weighed 9.6 g. The column consisted of discs cut from the sheet explosive which were stacked in a hole bored along the axis of a 3 in. diameter steel cylinder. The hole was 2 in. long and 31/64 in. in diameter, and the explosive column was flush with the end of the steel cylinder. A smaller diameter hole was bored as an extension of the 31/64 in. hole to receive the cap which detonated the explosive. The assembly is shown in Fig. 3.

The assembly was modified by bolting an extension to the end of the steel cylinder. The extension, conveniently fabricated from brass bar stock, contained a 1/2 in. hole which was aligned with the hole in the cylinder and which contained water. The extension prevented the shock wave produced in the water from diverging as rapidly as it would have done without the extension. Thus pressure was maintained for a longer period of time.

The steel cylinder was destroyed by the explosive charge. Figure 4 shows one cylinder ready to receive the explosive and another cylinder after the detonation.

Test Facility

Because of the small size of the explosive charge, the experiments could be conducted at an indoor test facility. Indoor testing was desirable because of the convenience of nearby shop facilities and because of weather problems associated with outdoor testing. A few preliminary tests were conducted out-of-doors to determine that it would be safe to move inside.

The problems to be considered for indoor work were ventilation, personnel protection, noise suppression, and prevention of blast wave damage. These were successfully solved. The work was conducted in areas which were isolated from other personnel and were well ventilated. The detonations were always under water so that the noise was muffled. Furthermore, the water prevented the occurrence of high-velocity projectiles.

The water tank in which the experiments were conducted was a section of steel tubing 1 ft in diameter and 1 ft long with walls 1 in. thick. It was lined with a replacable polyethylene bag. The tank was set on a concrete floor with a shock-absorbing spacer between the steel base and the concrete to lessen the impact on the concrete. No damage was done either to the tank

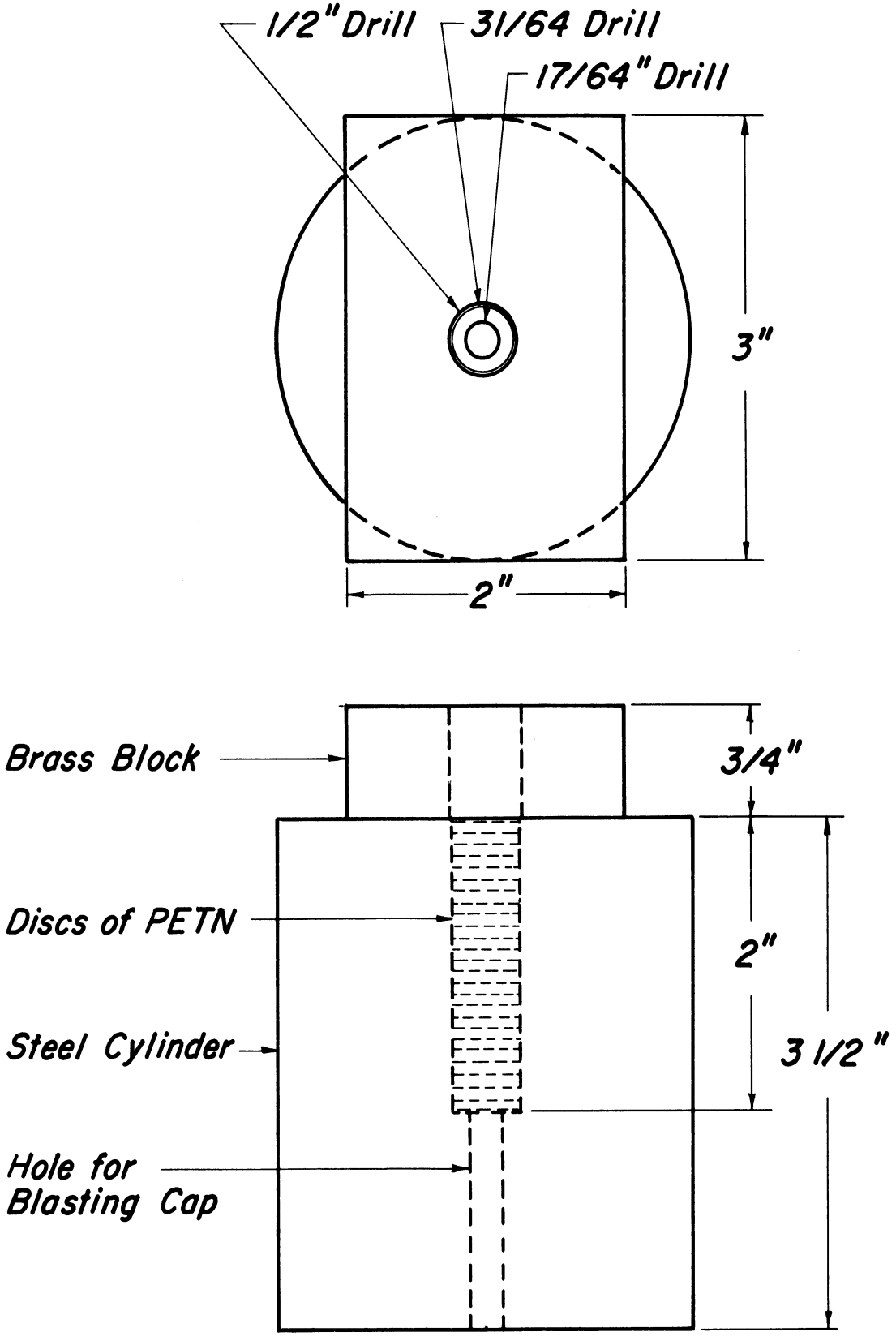

Fig. 3. Explosive charge assembly.

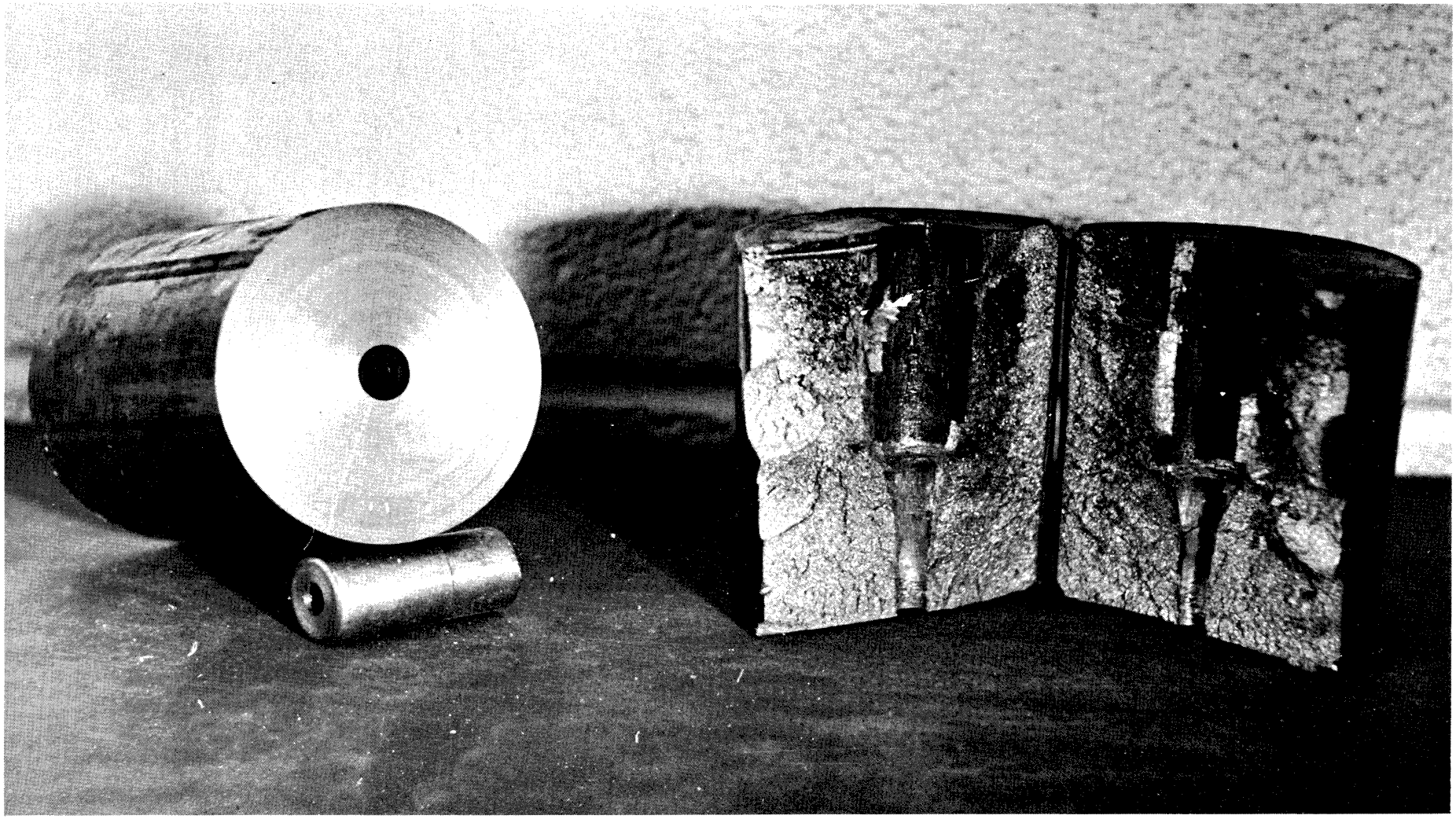

Fig. 4. One steel cylinder ready to receive the explosive charge and another after detonation of the charge.

or to the floor. Typically, the tank moved a few inches during a test. Baffles were erected to contain the water spray and to stop any projectiles which might occur. The tank and a baffle to catch the water are shown in Fig. 5.

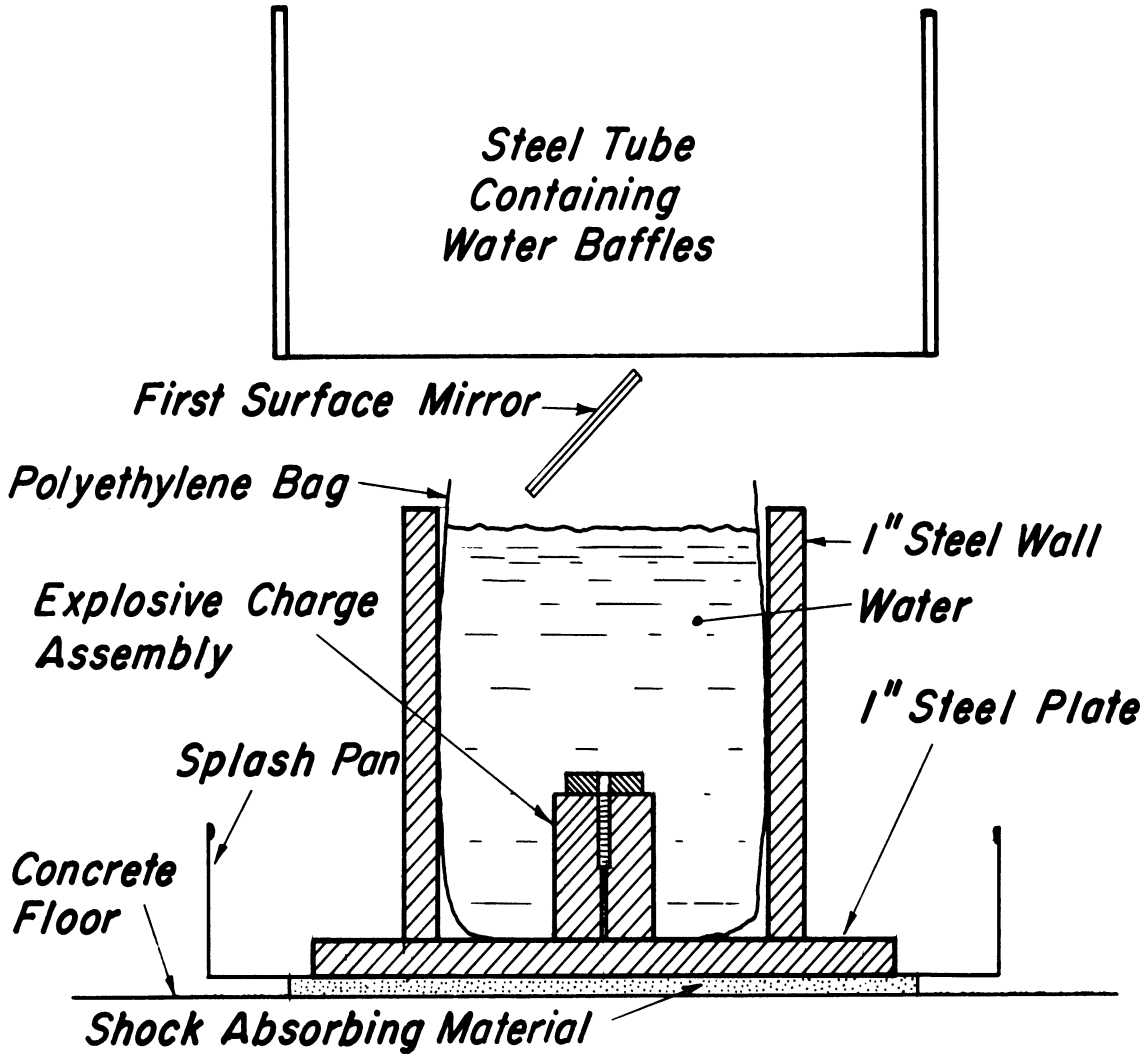

Fig. 5. Explosive charge in test chamber.

Handling Methods

Certain precautions were observed in the testing procedure. Although PETN is not easily detonated, blasting caps are sensitive to mechanical shock and to electrical transients. Thus, precautions were established regarding use of the caps. The placement of the blasting cap was the last operation to be performed in the assembly of the test equipment. Also the electrical leads from the blasting cap were not connected to the firing circuit until all preliminary circuit testing had been completed. The actual experiments were conducted by remote control from behind barricades.

Timing of Detonation and Plasma Formation

The occurrences of the explosive detonation and the capacitor discharge had to be related through some timing system so that the plasma confinement could be achieved consistantly. Two methods were considered for solving this problem.

The method which was adopted used the detonation front of the explosive to close a switch. The switching action initiated an electrical signal which triggered the capacitor discharge after a delay of 2 μsec.

Various switching mechanisms were tried which depended upon the rupture of a dielectric material separating the two switch electrodes. The final choice of switch used the PETN itself as the dielectric material. Other investigators have used this technique. (12)

The switch was constructed by grounding the steel cylinder and inserting an electrode into the PETN. The electrode carried a potential of 5 kilovolts. As the detonation wave propagated through the explosive, it converted the explosive from an insulator to a highly conductive medium and shorted the electrode to ground. A very precise and rapid switching action occurred because of the steepness of the detonation front.

The electrode, which was simply the end of a No. 20 vinyl insulated wire, was inserted into the PETN through a small hole drilled in the steel cylinder. The tip of the wire, to be designated as a sensor wire, was offset slightly from the hole so that the tip would be in the conductive region of the PETN before the wire was sheared off at the hole. The wire tip was precisely located relative to the end of the steel cylinder by setting its position with a depth gage. Because of the finite velocity of the detonation wave in the explosive, the placement of the wire tip determined the relative timing of the initiation of the capacitor discharge and the arrival of the shock wave at the plasma location.

Another method which was considered was the use of a master control unit which would emit a sequence of timed pulses to initiate the detonation, to trigger the capacitor discharge, and to operate the instrumentation. However, the firing time for a common blasting cap is measured in milliseconds and time jitter was to be less than 0.1 μsec. The method was not feasible without the use of a special cap with a firing time of less than 1 μsec. Such a commercially available cap is fired by a spark gap instead of a conventional bridgewire. Even with such a cap, the prospect of obtaining low jitter was poor because of the time of about 10 μsec required for the detonation to propagate through the column of explosive.

Pressure Measurement

The pressure produced in water by the exploding PETN was calculated from a measurement of the velocity of the shock wave. There is no pressure transducer which has the strength and response time to measure the 100 kilobar pressure of the shock wave. Thus, the method based upon shock velocity has become standard for work with explosives.

For water in a given initial state, the velocity of a shock wave has been uniquely determined as a function of the peak pressure. (13) Thus, a measurement of velocity can be converted directly into pressure. The method is valid only for high-pressure nonlinear shocks, because for low pressures the shock velocity is equal to the sound velocity. At high pressures, the shock velocity greatly exceeds the sound velocity.

Not only can peak pressure be determined from shock velocity, but the pressure gradient behind the shock front can be computed from the acceleration of the shock front and the curvature of the front. (14) Details of the calculation are described in Section 4.

Two methods were tried for measuring the velocity of the shock wave in the water. One method was based upon the change of conductivity of water which occurs when a shock front passes through it. (12) Wire pairs were placed in the water in the path of the shock front to record the change. Some useful data was obtained but the method was quite susceptible to electrical interference because of the low potential circuits which were used to measure the conductivity.

A more convenient method was found which depended upon the emission of light by a bubble of argon gas when it was struck by a shock wave. This method has been widely used in research with explosives as a time-of-arrival indicator. (15)

The argon flash units were constructed by drilling a 0.375 in. hole through a 0.040 in. metal plate and applying a piece of transparent tape to either side. The space between the tapes was filled with argon.

A flash unit was placed in the water above the PETN at a known distance from the end of the steel cylinder. When the detonation front reached the end of the column of explosive, a flash of light was emitted from the explosive, and later, when the shock front in the water reached the argon, a second flash of light was emitted from the argon. The two light flashes were recorded with a phototube and an oscilloscope so that the time between them could be determined. In addition to the light flashes, an electrical pulse was obtained from the sensor wire in the PETN. From the time intervals and the positions of the sensor wire and argon flash unit, the shock and detonation wave positions could be plotted as functions of time. Several tests with different argon flash unit spacings provided a curve of the shock position as a function of time.

The phototube was a type 921 vacuum photodiode. The load resistor for the tube was chosen to be 10 000 ohms which is smaller than usual practice requires. The choice of resistor was made to provide a sufficiently short rise time for observing the light flashes. The oscilloscope input capacitance of 20 pF was in parallel with the load resistor to produce a time constant of 0.2 μsec. Although the response was not fast enough to reproduce the light flashes accurately, the important data, which was the time the flash first began to be visible, was obtained satisfactorily. The load resistor was large enough that no amplification of the signal was needed to place it within the range of the oscilloscope sensitivity.

Shock position measurements were made for conditions with and without the brass-block extension which was described previously. The results of the measurements are shown in Fig. 6. The graph shows the detonation wave as well as the shock waves in the water.

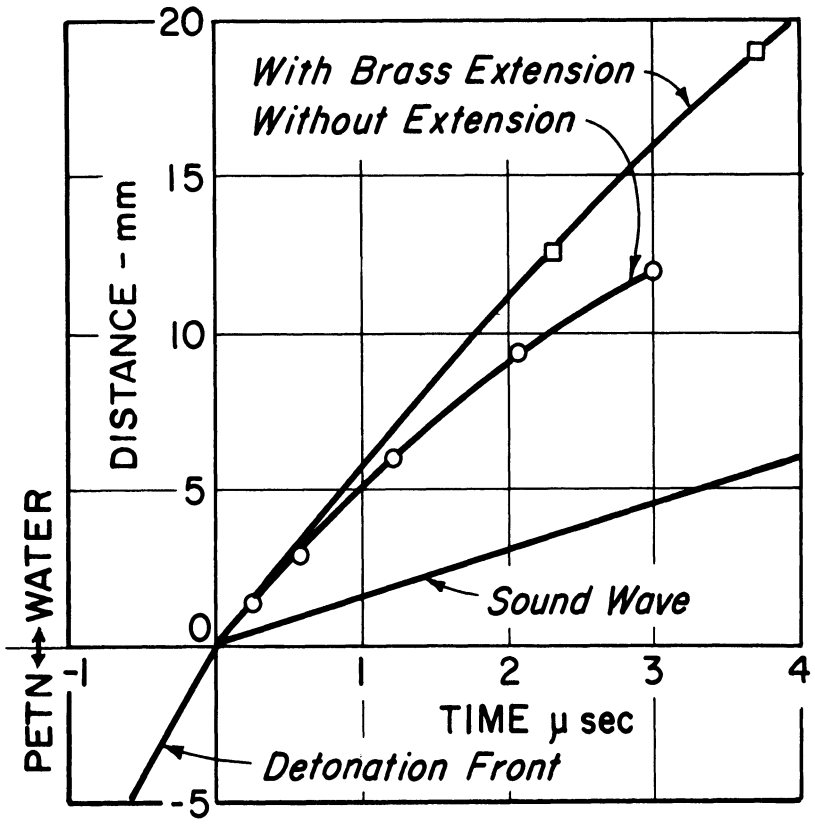

Fig. 6. Shock front propagation with and without the brass extension to confine the shock wave.

Velocity was determined from Fig. 6 as a function of time and from it the pressure was determined. Also the pressure gradient was estimated. Figure 7 shows the variation of peak pressure as a function of the distance of travel of the shock front. The figure shows that the effect of the brass

extension was to prevent divergence of the shock wave and to maintain pressure for a longer period of time than without the extension. With the brass extension, the pressure gradient was estimated to be 6 kilobars/mm, whereas without the extension the gradient was 10 kilobars/mm.

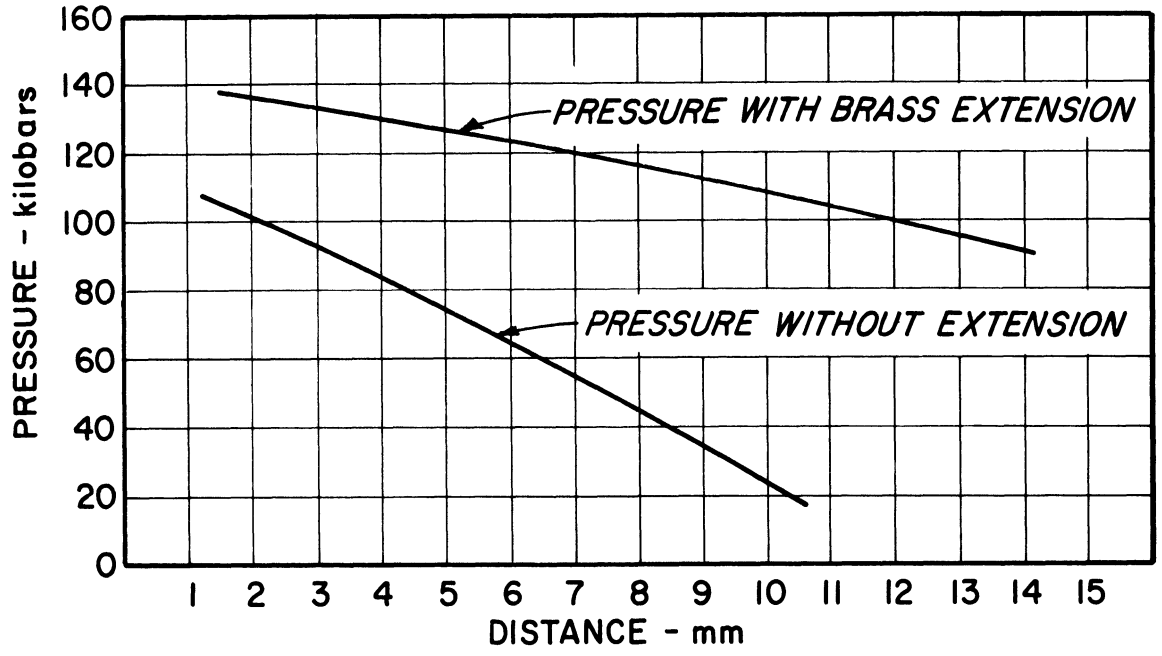

Fig. 7. Shock front pressure as a function of distance traveled.

Shock Curvature and Distortion

The argon flash units were useful in another way than for velocity measurement. When used with an open shutter on a camera, they provided flash illumination which stopped the motion of the shock wave. Thus, the shape of the shock front and the distortion of images by the shock front could be determined.

The amount of distortion was important for interpreting photographs of plasma which was behind the shock front. There was practically no distortion when the direction of viewing was along the axis of the cylindrical explosive charge, but distortion was severe at right angles to the axis.

Figure 8 shows a photograph taken with an argon flash. The grid lines were ruled on a paper which was located in the high pressure region behind the front, and the photograph was taken from a viewpoint slightly off the axis of the hole in the brass block. The partial shield hides the argon flash unit from direct view. Clearly the distortion from this view is negligible, even in the regions near the edge of the hole.

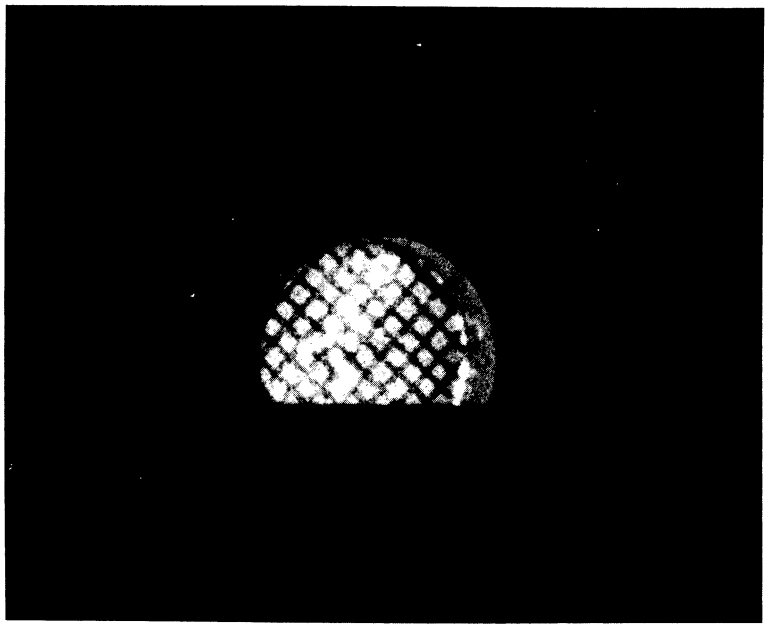

Fig. 8. Photograph through shock front with argon flash illumination.

II. EQUIPMENT FUNCTION AND DESIGN

The experimental apparatus consisted of several subsystems which were designed for specific purposes, and yet which were also designed to function together as a unified system. The explosive-charge assembly, which was previously described, served the purpose of generating a high-pressure shock wave. However, the assembly was designed so that it would be an integral part of the more complex assembly which included the electrodes for plasma generation. The total system included a triggered capacitor discharge circuit, a Kerr-cell camera, oscilloscopes, current and voltage probes, and a timing circuit which controlled the various functions of the system.

The experimental system was designed for producing a plasma at high pressure and for measuring the properties of the plasma. The latter function imposed many restrictions upon the design that would not have been necessary otherwise. Furthermore, the system operation had to be reproducible over a series of tests so that results could be accumulated to provide much more complete and accurate data than could be obtained from a single test.

Electrode Design

The plasma was located in the region of high pressure behind the front of the explosively produced shock wave. Thus, the electrodes had to be similarly located. The electrodes were as close as possible to the explosive charge so that time jitter and pressure decay could be minimized. However, the electrodes would have been short-circuited by the explosive by-products if they had been too close to the charge. The electrodes were designed so that photographs could be taken of the plasma, and so that the shock-wave contour would not be distorted. Also, the electrodes were electrically insulated to prevent the discharge from forming in an unwanted position. Finally, the electrode assembly was designed so that many such assemblies could be built in identical fashion because each assembly was destroyed when it was used.

Of many designs considered, the one shown in Fig. 9 was chosen for the taking of data. Other designs were used for some tests but the results of those tests are not included because they were not as accurate or complete as the later tests with the design which is shown.

Previous electrode designs were based upon the concept that electrodes made of lightweight copper sheet would move with the water behind the shock front and thus not be overtaken by the cloud of explosive by-products. Significant data were taken with such designs, but their use was discontinued for several reasons. The brass extension, which prevented a rapid pressure decay, could not be used with the electrodes. Also the electrodes were difficult

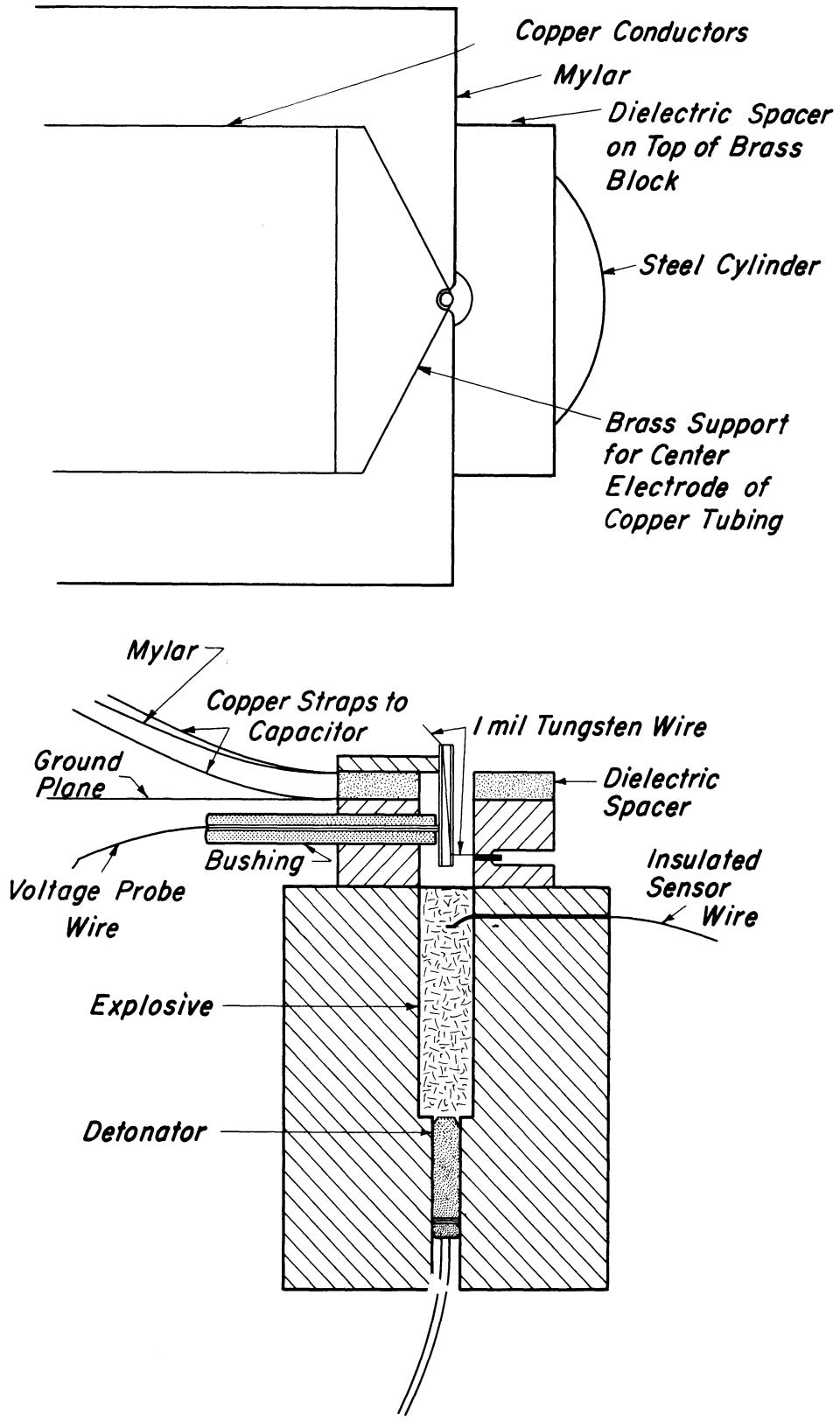

Fig. 9. Electrode assembly and explosive charge.

to construct and assemble with precision. Finally, the system which used the lightweight electrodes had a poor grounding arrangement.

Some consideration was given to the use of a high-density dielectric material for confining the shock wave in place of the brass block extension. However, common dielectric materials have densities not greatly different from the density of water. High-density dielectric materials are almost exclusively glass or ceramic compositions which would be very difficult to machine into a usable form. A mixture of tungsten powder in epoxy resin was considered but it would have been expensive to use, especially as an expendable material.

Thus, the system shown in Fig. 9 was developed. Although nothing can be considered stationary when subjected to the explosive shock wave, the electrodes in the system are relatively stationary compared with the adjacent water and plasma.

One electrode is the wall of the 1/2 in. diameter hole and the other electrode is the copper tube which is centered in the hole. The center electrode, which was the cathode, had a high potential relative to the grounded anode. The unsymmetrical placement of the plasma relative to the explosive charge was no problem in that the shock front had no significant distortion over the entire cross section of the 1/2 in. diameter hole. The parallel electrode surfaces did not restrict the motion of the plasma as it was carried along by the water.

The outer electrode was grounded along with the explosive casing. However, the inner electrode was kept about 6 mm away from the surface of the explosive. With a mass velocity of 2 mm/μsec, the explosive gases required 3 μsec to reach the electrode. However, the shock front, with a velocity of 5 mm/μsec, reached the electrode and the plasma in a little more than 1 μsec. Thus, a period of 2 μsec was available for measurements of the plasma properties before the electrodes were short-circuited by the explosive gases.

A fine tungsten wire was stretched between the electrodes to initiate the plasma formation. Without the wire, the plasma formation would have been unpredictably delayed, perhaps many microseconds, and the plasma would have been very irregular. However, with the wire a uniform cylindrical column of plasma was formed with no significant delay. A 0.0005 in. diameter wire introduced time jitter into the discharge but a 0.001 in. diameter wire was adequate. The tungsten did contaminate the plasma but to a first-order approximation the effects of the tungsten could be neglected. (3, p. 265) After 0.3 μsec the number of tungsten atoms was a small fraction of the number of hydrogen and oxygen atoms.

The tungsten wire was mounted by threading one end through a No. 80 hole (0.0013 in. diameter) in the side of the center electrode and by threading the other end through a much larger hole in the side of the outer electrode. A snuggly fitting wire was pressed into the hole in the outer electrode to hold one end of the tungsten wire in place. The other end was drawn up through the center of the inner electrode and pulled tight.

A probe wire was attached to the center electrode for measuring voltage. The wire ran along the ground plane to a voltage probe which was a few feet away. The probe had an attenuation of 1000 to 1 and a rise time of 14 μsec for the system in which it was used. The peak voltage rating was 40 000 volts.

The capacitor discharge circuit was grounded at the brass block by being attached to the ground plane at that point and that point only. All other elements of the discharge circuit were floating, including the capacitor case and the triggered spark gap. Thus, the voltage measured by the probe was the same as the voltage from the center electrode to the outer electrode. When the probe wire was attached to the outer instead of the center electrode the measured voltage was negligible.

Equipment Protection

Reliable operation of the instrumentation depended upon the adequate protection of electrical and optical systems from the effects of the explosion. Water spray caused trouble by dirtying optical surfaces and shorting high-voltage circuits. The spray and blast wave from a test had no effect on the instrumentation for that particular test because the measurements were taken long before the shock wave had time to break the surface of the water. The protection was necessary to avoid frequent repairs of equipment between tests.

The protection was achieved by separating the instrumentation from the water tank with plywood walls which had portholes for taking photographs and passing electrical connections. Photographs were taken through a glass window which was frequently splashed but never broken. The baffle above the tank caught most of the water spray and the plywood walls served only to stop indirect splashing. As further protection against occasional droplets of water, polyethylene sheets were placed over the electrical equipment before each test.

Photographs were taken of the plasma from a view above the water tank through the surface of the water. A front-surface mirror was placed directly above the tank at a 45° angle so that the camera could be placed at the side of the tank behind the plywood wall. The mirror was expendable.

Capacitor Discharge System

The energy for generating the plasma was stored in a 14.8 (nominal value of 15) μF capacitor which was rated at 20 000 volts. The capacitor was designed with low-inductance terminations for applications requiring a fast discharge. The capacitance was measured with a General Radio bridge, type 1650 A.

A three-electrode spark-gap switch was designed to be mounted on the capacitor itself. The switching occurred between a hemispherical electrode on the high-potential terminal of the capacitor and a flat plate electrode, which contained the trigger electrode. The trigger wire mounting was similar to that for a Lovotron where the wire protrudes into the gap from a hole in the electrode. A dielectric sleeve separated the trigger from the main electrode. (16) The flat plate electrode was mounted on a collector plate in such a way that the spacing of the gap could be set as desired. The collector plate and another plate, which was bolted to the capacitor case, served as terminations for closely spaced copper straps which led to the electrodes in the water tank. The termination plates were insulated from each other with Mylar and dielectric paper.

A positive trigger pulse was obtained through a pulse transformer which isolated the pulse generator from the capacitor discharge circuit. The capacitor was negatively charged so that the electrode containing the trigger wire was the anode. A positive trigger pulse on the anode is considered as the best arrangement of polaraties for dependable firing of the gap. (16)

The inductance of the assembly of capacitor, switch, and connecting straps was measured. The connecting straps were joined together to short-circuit the system, so that a ringing discharge occurred when the spark-gap switch was closed. The ring frequency of the discharge was 172 kc/sec corresponding to an inductance of 58 nH.

The copper connecting straps were a permanent installation up to the plywood barricade. At the barricade they were clamped to flexible copper straps which entered the water tank and which were attached to the discharge electrodes. The latter straps were destroyed with each test and had to be replaced. The straps were closely spaced with Mylar insulation so that their inductance could be minimized. The total length of the copper connecting straps was approximately 3 ft. A schematic of the discharge circuit is shown in Fig. 10.

Grounding System

Because of the high current discharge, the electrical systems had to be carefully grounded to avoid spurious effects on the measurements. All

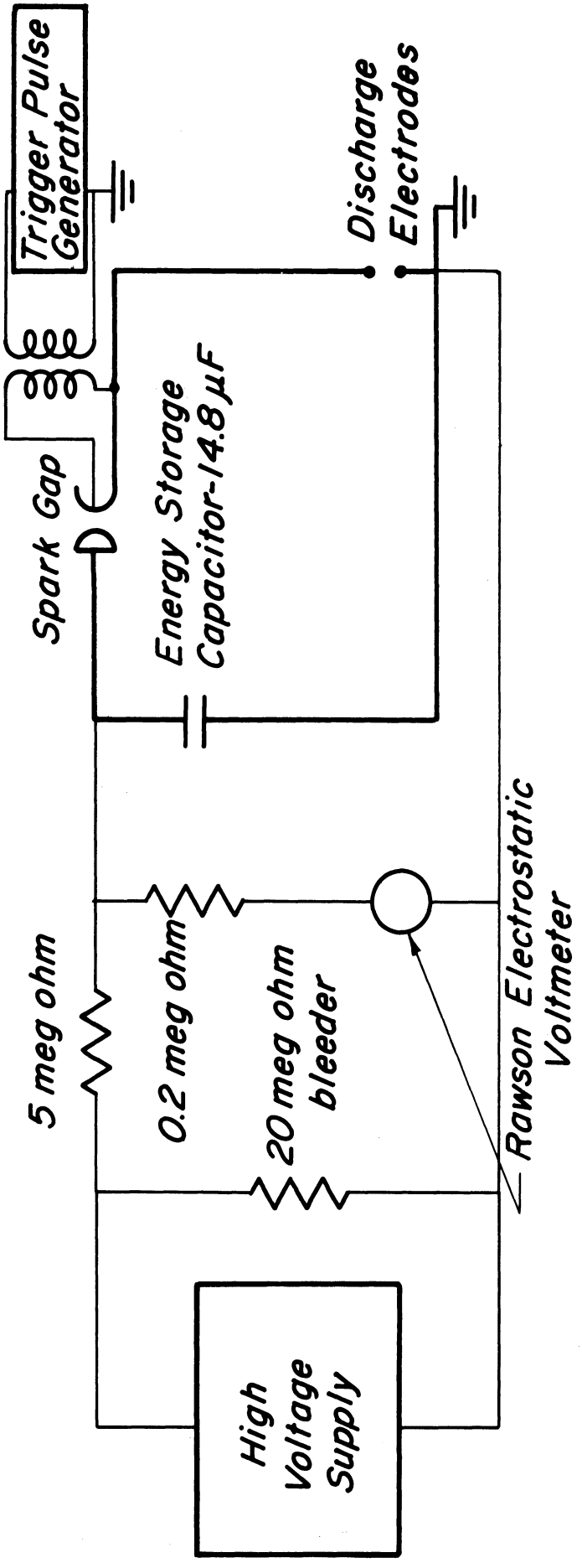

Fig. 10. Energy storage capacitor circuit.

instrumentation chassis were connected to a copper ground sheet. The ground sheet was connected to the oscilloscope room, to a galvanized steel enclosure around the capacitor and spark gap switch, to the water tank, and to the discharge circuit at the low potential electrode in the water tank.

The grounding of the discharge circuit in the water tank was necessary because of the way in which voltage was measured. The portion of the ground plane in the water tank was destroyed with each test and needed replacement.

Signal cables to the oscilloscopes were grounded at the point where they entered the oscilloscope room, and they were run through copper braid which was in contact with the ground sheet.

Timing System

The timing of the various electronic functions was determined by the sensor wire which was buried in the PETN and which acted as a switch. This wire, a No. 20 vinyl-covered copper wire about 3 ft long, ran from a hole in the steel cylinder out of the water tank and through the splash protecting shields to a terminal on the pulse generator.

The pulse generator, which is shown in Fig. 11, produced three simultaneous output pulses of approximately 100 volts amplitude. The generator itself was a modification of a capacitive divider. A charge was established on the high potential capacitor of the divider circuit. Then the sensor wire in the PETN discharged the capacitor into the low potential circuit of the divider to produce a step voltage output. The low potential circuit was actually a combination of capacitors which provided multiple outputs. The 48 ohm resistor, which was a few inches of resistance wire, provided damping to reduce the tendency of the circuit to ring. The 6800 ohm resistor was necessary to establish the correct DC potentials in the circuit.

Even with the damping resistor, some ringing occurred at the output terminals. However each terminal was connected to a 1000 ohm delay line which filtered out the ring and also served the primary purpose of delaying the pulses. The pulses which were available from the delay lines were free from ring and had rise times of 0.2 μsec.

The block diagram of Fig. 12 shows the arrangement of the different circuits which were operated from the pulse generator. The three delay elements were designed so that the order of events was: (1) the triggering of oscilloscopes; (2) the triggering of the capacitor discharge; and (3) the triggering of the Kerr cell shutters.

The pulse generator could be triggered manually instead of by the PETN switch. This feature allowed checking of the operation of the circuits just

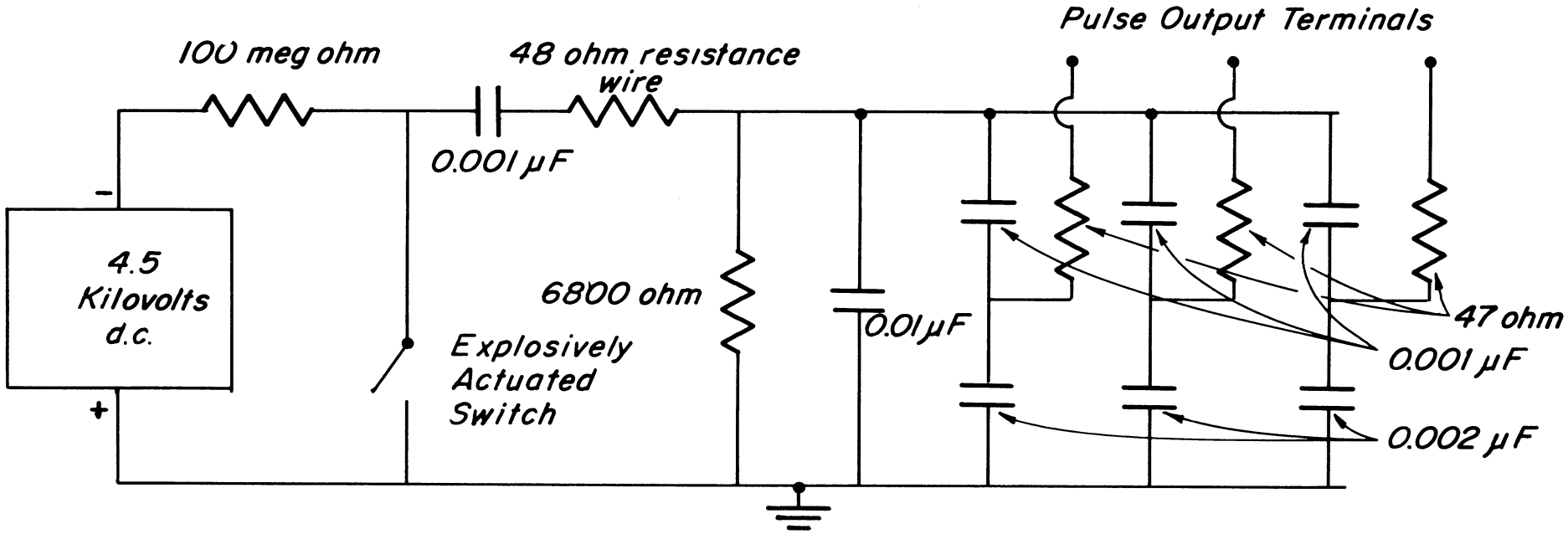

Fig. 11. Pulse generator to produce three simultaneous pulses.

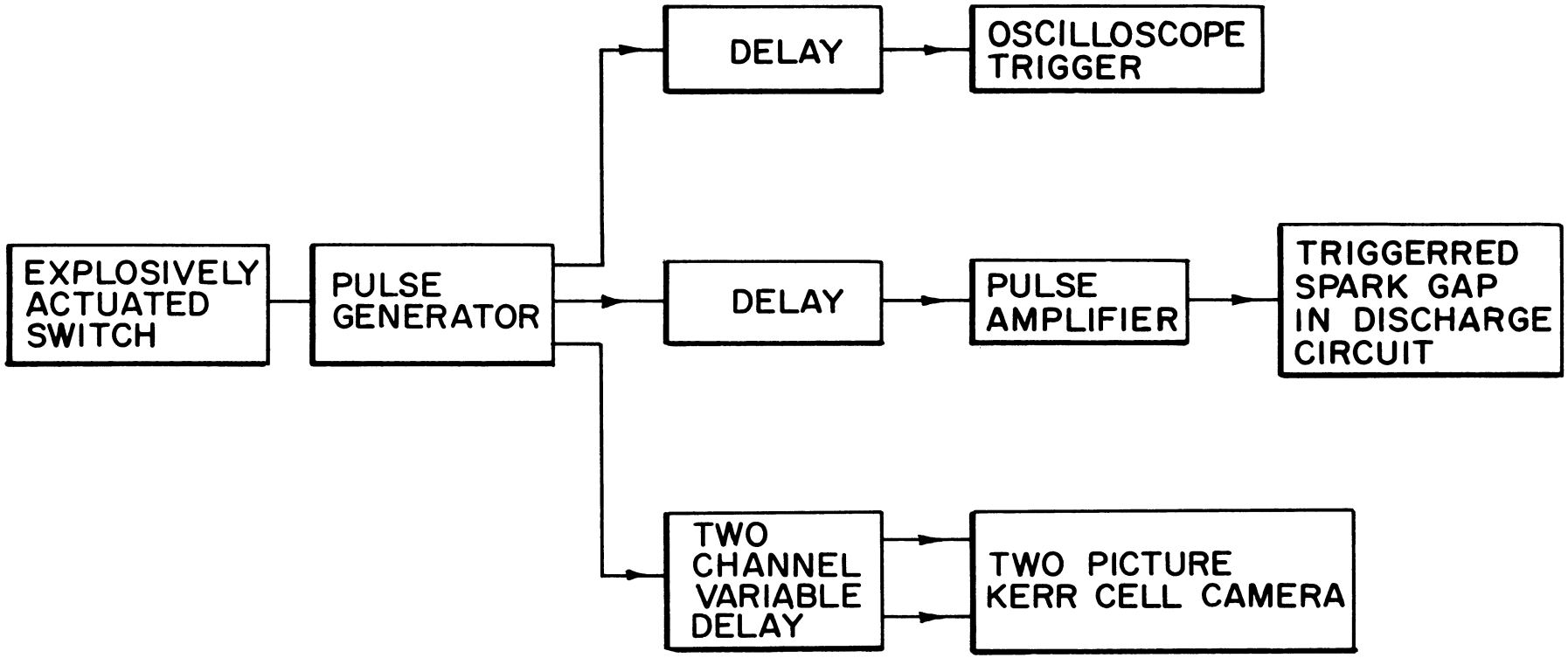

Fig. 12. Block diagram of control system.

before a test. Also, experiments without explosive could be performed without modifying the system.

Camera System

The camera was designed and built specifically for the requirements of this project by William N. Lawrence. The system requirements and the past experience of staff personnel with Kerr cells determined that the camera should be designed with Kerr cell shutters.

Although Kerr cell cameras require much higher levels of light intensity than image converter cameras, the Kerr cell shutter provides a much better resolution. For the small object size and high intensity of the plasma under investigation, the Kerr cell was therefore more appropriate.

To obtain a sufficiently large image, the camera was required to have a magnification of approximately unity. Yet, because of the destructiveness of the explosive charge, the camera had to be placed some distance away from the object. These two requirements were met by using a lens of long focal length.

The camera was required to take two photographs of an event through a single lens in order to show growth patterns of the plasma under investigation. Thus, the camera was designed with a beam splitting mirror behind the lens to form two separate images. Each image was then controlled with a Kerr cell shutter. The necessary mirrors and shutters could be installed between the lens and film holder because the design for a magnification of unity required a fairly long optical path between the lens and the film.

The geometric f number of an optical system is determined by a single diaphram, even if several are included in the system. All others act as field stops instead of f stops. For this system the lens settings determined the f stop over the range of f/11 to f/32 and the Kerr cell aperature was a field stop. However, for lens settings less than f/11, the lens diaphram became a field stop and the shutter aperature was the f stop. The camera was operated in the range from f/11 to f/32.

The actual f number of the system was different from the lens settings for two reasons. First, it was different by the factor M+1, where M represents the magnification factor. This factor is negligible for most photographic applications where M is much smaller than 1. However, for this camera, M was approximately equal to 1. Also, the f number did not account for the absorption of light by the polaroids and the nitrobenzene in the shutters. The effect of absorption was not determined, although it may have been equivalent to several f stops.

Two identical pulse generators were built to provide pulses of 30 000 volts to the Kerr cell electrodes. The pulse widths were 0.1 μsec. Zarem's circuit was used in the design of the pulsers. (17) A thyrite resistor in series with the triggered spark gap switch prevented undesirable ringing and provided a monitor signal.

Voltage and Current Measurements

The technique of measuring voltage was described in the section on electrode design. When the discharge circuit was grounded at some point other than the outer electrode, a significant correction to the voltage measurement was necessary. Even without the need for that correction, another correction was necessary to account for the inductance of the electrodes and for the inductance of the plasma itself. The correction was determined by measuring the voltage of the center electrode relative to ground with a No. 18 copper wire substituted for the plasma column. The inductance measured by this method, 5 nH, was approximately the same as the inductance which was estimated from the geometry of the electrodes. The difference between the inductance of the plasma and the inductance of the copper wire was shown to be negligible. The inductive correction was typically 10 to 20 percent of the total measured voltage.

The current of the capacitor discharge was measured by sampling the magnetic flux of the discharge with a wire loop. The voltage generated in the loop was proportional to the rate of change of flux through the loop. Also the flux was proportional to the current in the discharge. Thus, the loop voltage was proportional to the time derivative of the current. The loop was connected to a 70 ohm cable which transmitted the signal to an integrating circuit which was mounted next to the input terminals of an oscilloscope. The integrated signal which was proportional to current was recorded by the oscilloscope camera.

Two precautions were necessary in the design of the current-measuring system. The inductance of the loop had to be sufficiently small that the loop would act as an ideal voltage source in driving the 70 ohm line. Also, the integrating circuit had to have a time constant which was long compared to the time of duration of the experiment. The integrating circuit, with a time constant of 44 μsec, is shown in Fig. 13. The circuit was designed to terminate the 70 ohm cable in a matched load as well as to integrate the signal.

The loop design underwent several changes until one particular design was found which met the needs of the project. The final design actually was much simpler than many of its predecessors. Early versions of the loop were inserted into a cavity between the current carrying copper straps through a slot in one of the straps. These versions required that the discharge circuit be grounded at the location of the loop. However, the need for ground-

ing the circuit at the discharge electrode led to the loop design which was finally adopted.

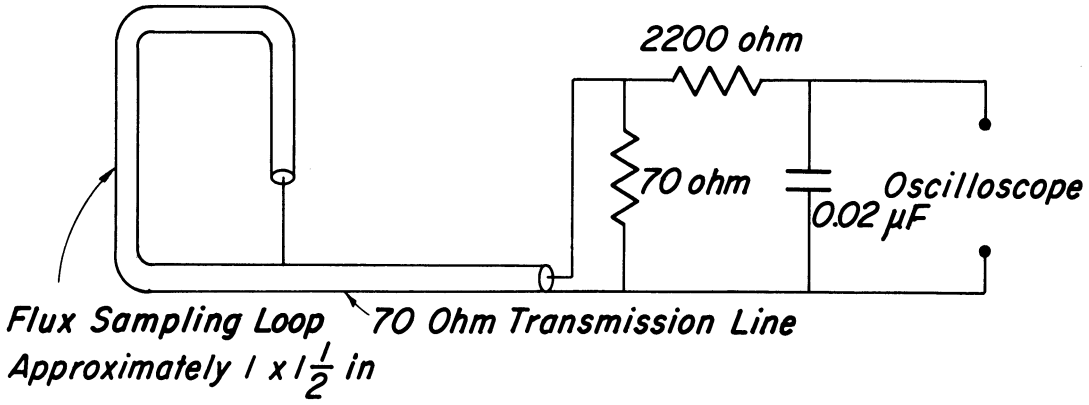

Fig. 13. Integrating circuit for current measurement.

The loop was made by soldering the center conductor of the coaxial line to a point on the braid a few inches from the end of the cable to form a loop. The braid provided electrostatic shielding for the loop without forming a closed metallic loop which would distort the flux. The braid was attached to the ground sheet but not to the discharge circuit. The loop was placed near the discharge circuit to link the flux which issued from the space between the current carrying conductors. The space between the current carrying conductors was widened in the vicinity of the loop to increase the number of flux lines which would link the loop. The loop and the conductors were firmly clamped in place with dielectric materials.

The current-measuring system was calibrated by making an oscillographic record of the output of the integrating circuit for a ringing discharge. A short circuit was clamped across the current-carrying straps and the capacitor was discharged after being charged to a known potential. From the data, the radian frequency and the decrement of the discharge could be computed. These results, when combined with values for capacitance and charging voltage, were sufficient to compute the peak current of the discharge. From the oscilloscope trace, the peak voltage output of the integrating circuit was known. Thus, a calibration factor in amperes per volt could be calculated. The calibration factor for the system was 930 000 amperes per volt. Occasional checks of the factor showed that it was reproducible within the limits of error of the current measurement.

Oscilloscopes

Two oscilloscopes were used to record data. One was a dual-trace oscilloscope which recorded both voltage and current of the capacitor discharge.

The other monitored the Kerr-cell shutter operation.

The former had a 25 megacycle band width and the latter had an 18 megacycle band width. Both oscilloscopes were equipped with P-11 phosphors. Traces at 0.2 μsec/cm were recorded at f/1.9 on film with an ASA rating of 3000.

The dual-trace oscilloscope was triggered externally in its single-sweep mode by a pulse from the generator which has been described previously. The other oscilloscope was triggered by the plus gate from the dual-trace oscilloscope.

A mixer circuit was developed to monitor the two signals from the Kerr cell pulsers and the plus gate from the dual trace oscilloscope. The signals were capacitively coupled together in this circuit to form a composite signal which showed the increments of time between the individual signals.

III. TEMPERATURE MEASUREMENT

The plasmas under investigation radiated with black-body spectral distributions. Thus, temperatures could be determined by measurements of radiation intensity in a selected spectral band. The Kerr cell camera with Kodak Royal Pan film was used as the radiation measuring device.

The photographic measurement of temperature required that the film density scale be calibrated as a function of temperature. With an exposure time of 0.1 μsec, the reciprocity law for photographic exposures was not valid, so that a method of calibration had to be found which did not depend upon that law. Explicitly the law states that if changes are made in both radiation intensity and exposure time so that their product is not changed, then the density of the film image is not changed.

All photographs were taken with the same exposure time of 0.1 μsec so that the problem of reciprocity failure was circumvented. However, it was necessary to photograph a source of known temperature with exactly the same procedures as were used with the unknowns in order to determine the film density corresponding to that temperature. From that one point, the temperature-density scale was developed.

The first step in calibrating the film was to obtain a source of known temperature. The source had to be a black-body radiator at a sufficiently high temperature to be photographed with the Kerr cell camera. The light duration had to be sufficiently short that the film would not be fogged by light leakage through the crossed polaroids of the Kerr cells. The source had to be reproducible.

An underwater spark was chosen to fill the requirements for a reference source. A simple electrode system was developed which could be substituted in place of the electrodes used for the principal investigation. With the substituted electrodes, a plasma with a reproducible and easily measured temperature was generated to meet the need for a reference source.

The temperature of the reference source was determined by the method that E. A. Martin used in his research on underwater sparks. (3) The sensitivity of a vacuum photodiode for a narrow spectral band was determined by measuring its response to a hot tungsten ribbon which had known temperature, emissivity, and area. Tests showed that the photodiode response accurately followed the inverse square law for distance from source to sensor. Then the photodiode response was measured for radiation from the plasma. Tests showed that the diode response was linear and not saturated. The radiating area of the plasma was measured as a function of time by photographing the plasma with the Kerr cell camera. From these measurements, the temperature of the shouce was determined.

A correction which was neglected by Martin was introduced into the measurement of temperature. The correction arose from the refraction of light from the plasma when it passed through the interface between water and air as it traveled to the photodiode. The refraction caused the light rays to diverge so that the phototube measurement was less than if no refraction had occurred. The correction factor can be shown to be the square of the ratio of indexes of refraction of the two media. For water and air the factor is 1.77.

With no interface effect, suppose that light rays in solid angle φ would reach the photosensitive surface of the tube. Then with the effect taken into account, the solid angle would be φ/n^2. Thus, the measured radiation had to be corrected by the factor of n^2. If d is the distance from the source to the interface and D is the distance from the source to the sensor then the exact expression for the correction is:

$$n^2[1-d/D(1-1/n)]^2 \qquad (3.1)$$

This becomes n^2 if d is small compared with D.

Many sources of error arise in the measurement of plasma temperature with a phototube. Reasonable estimates of the errors were combined by the root mean square method to estimate the uncertainty in the temperature measurement. The measured value is believed to be within 10 percent of the plasma temperature.

The spectral band of the Kerr-cell camera included all of the optical region with a cutoff in the ultraviolet because of the absorption of the glass elements of the camera and of the nitrobenzene in the Kerr cells. The blue radiation had the most significant effect upon the film because the spectral distribution of the plasma was peaked in the ultraviolet region making the intensity of blue greater than the intensity of red. No attempt was made to limit the bandwidth of the camera because over the optical band the relative intensity of radiation as a function of temperature was practically the same regardless of the band chosen. Figure 14 shows relative black-body radiation for various optical bands. A multiplicative scaling factor was determined for each of the three curves so that they could be superimposed for comparison.

The developing procedure was standardized so that variations in film density from development would be minimized. The Royal Pan film with an ASA number of 400 was developed in D-76 at 70°F for 7 min with tray agitation. The film was transferred to an acetic acid stop bath for 15 sec and then to F-5 fixer for 6 min. After one-half hour of washing the film was treated with a solution which reduced surface tension as an aid to drying.

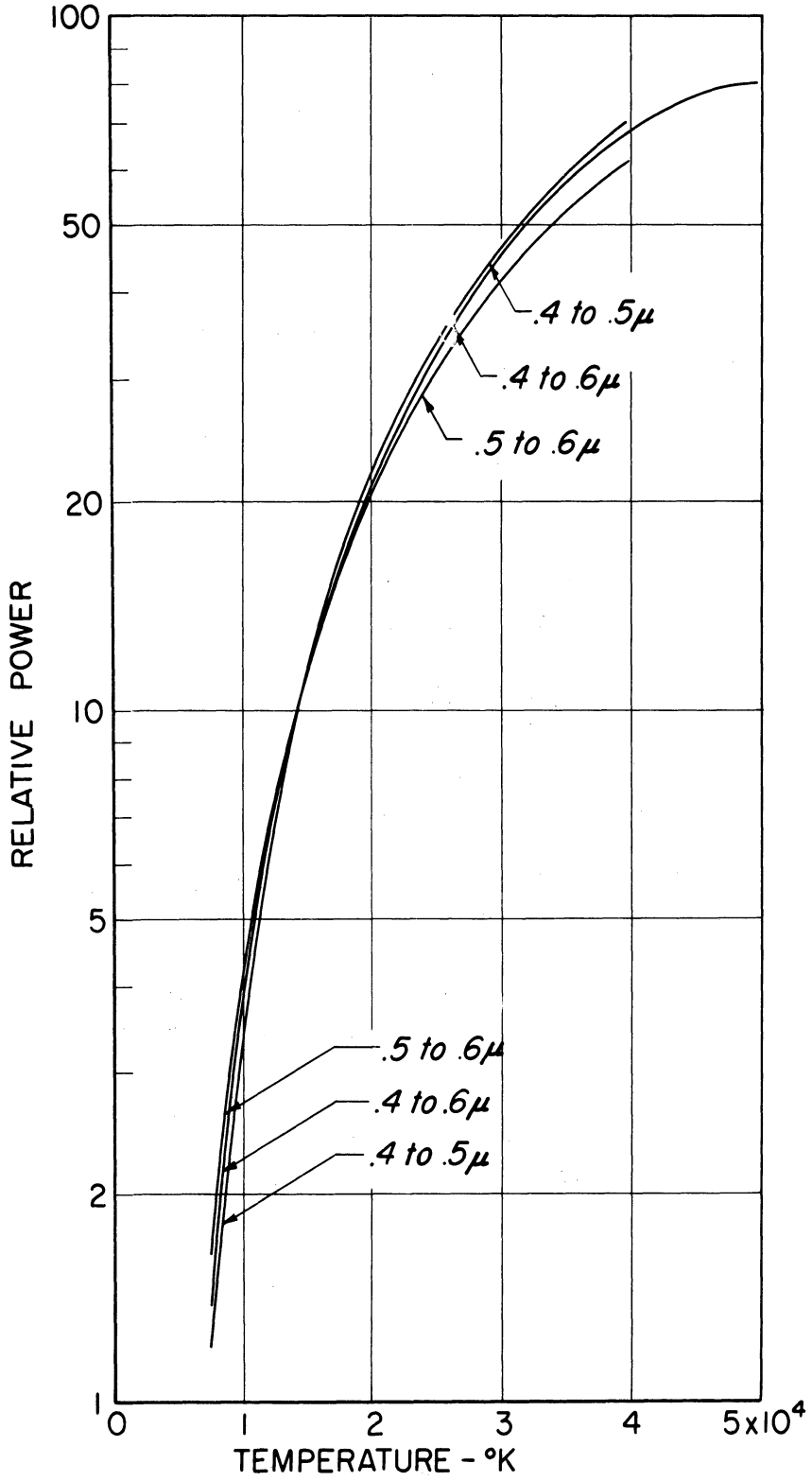

Fig. 14. Variation of black-body radiant power with temperature for various spectral bands.

In order to account for minor variations in development and film characteristics a certain area of each negative was given a known exposure. This exposure was made through a print projection scale which is a set of neutral density filters arranged like pieces of pie. The scale was placed in contact with the film so that the image formed on the film was composed of sectors of different densities. The film was exposed through the scale for 0.1 sec with a conventional camera shutter. The lens of the camera was pointed toward a white background illuminated with tungsten light and it was deliberately misfocused to produce diffuse illumination.

The density scale which was established on each negative served two purposes. It determined variations in image density because of variations in development. It also established a relationship between intensity of exposure and image density. This relationship was used to extend the calibration of the film density for one particular temperature to a calibration for other temperatures within the density range.

The method of extending the calibration is subject to two criticisms. First, the calibration extension was done with tungsten light which differed from the light of the underwater plasmas. Second, the calibration was done with exposures of 0.1 sec instead of 0.1 μsec. However, these criticisms were shown to be unimportant by photographing the known temperature source at 0.1 μsec with different f numbers and observing that the shift in film density corresponded to the shift in f number.

The use of an exposure of 0.1 sec to establish the density scale was based on an assumption about the reciprocity law. For the law to be valid the film density D is given by some function of the product of intensity and exposure time, It. Yet, if instead of $D = f(It)$, the equation can be written $D = f[I\, g(t)]$, then the procedure which was used is valid. This modified equation does describe the situation within the accuracy of the experiment previously described.

The range of temperature from 10 000 to 30 000°K corresponded to a range of 3 f stops or an image density range of 1.0 where density is the log base 10 of relative light transmission of the film. Density was measured with a recording microphotometer.

In actual practice the plasma temperature was anticipated and the f stop on the lens was set so that the film density would be in the middle of the density range where microphotometer measurements were most accurate. The range of measurement was thus determined by the range of f stops of the lens. The discussion on camera design indicated the range to be from f/11 to f/32 which covers 3 f stops. Plasmas were photographed with temperatures estimated to be as low as 6000°K and as high as 50 000°K with the most accurate range being from 10 000 to 30 000°K.

IV. PRESSURE MEASUREMENT

The means of determining plasma pressure depended upon whether or not explosive was used to confine the plasma. Without explosive, the pressure was computed from the rate of plasma column expansion. Also the pressure produced by the magnetic pinch effect was included. However, with explosive the pressure was primarily that produced by the explosive shock wave with minor corrections for the effects of magnetic pinch and column expansion.

The properties of shock waves in water are involved in calculations of pressure both with and without explosives. When explosives are used, the explosive by-products act as a piston which pushes water ahead of it in the 1/2 in. diameter chamber. In either case, the plasma column is a radially expanding cylinder which displaces water to create a cylindrical shock wave about the column. The expanding column may be considered as a generalized form of piston.

A shock wave is a region of high pressure ahead of the piston which is producing the shock wave. The region is bounded by the piston and by the shock front which propagates ahead of the piston. Regions ahead of the shock front remain undisturbed until the front sweeps through them.

Shock Front Equations

Regardless of the shape or decay rate of a shock wave, the conditions at the shock front can all be calculated from one measured quantity such as the shock front velocity. The shock front equations and an equation of state determine the pressure, density, and mass velocity of the medium directly behind the front in terms of the shock front velocity and the properties of the undisturbed medium ahead of the front.

A shock front model is shown in Fig. 15 where subscript (0) refers to conditions ahead of the front and subscript (1) refers to conditions immediately behind the front. The front velocity is u_S and mass velocity behind the front is u_1. Let P represent pressure; V, specific volume; and m, mass flow rate per unit area of shock front.

The three conservation laws for mass, momentum, and energy can be applied to the transition which occurs across the shock front. However, the energy equation is not needed because of the property of water known as separable energy. (9, p. 7) If S is entropy, then energy E can be written approximately as

$$E = E'(V) + E''(S) \qquad (4.1)$$

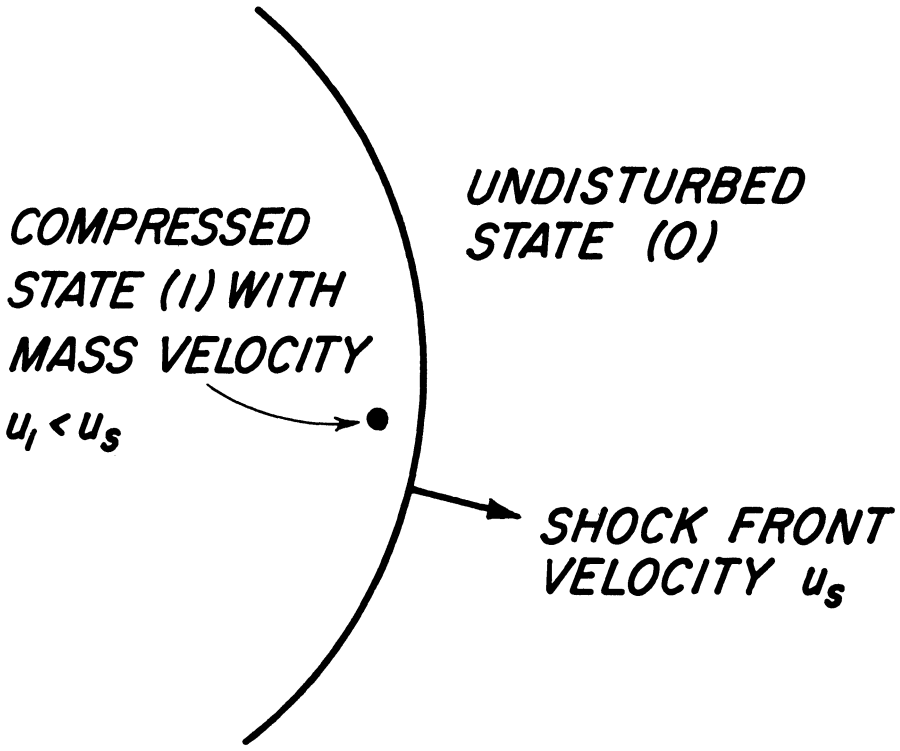

Fig. 15. Shock front model.

The pressure is given by

$$P = -\left.\frac{\partial E}{\partial V}\right|_s = -\frac{dE'}{dV} \tag{4.2}$$

Therefore, pressure is a function of specific volume alone and the irreversible effects which occur during the passage of the shock front can be neglected. Thus, the energy conservation equation is not needed.

The conservation laws of mass and momentum are the following:

$$\text{Mass:} \qquad \frac{u_s}{V_o} = \frac{u_s - u_1}{V_1} = m \tag{4.3}$$

$$\text{Momentum:} \qquad mu_1 = P_1 - P_o \tag{4.4}$$

These two conservation laws can be written in the following form:

$$u_S = V_O\sqrt{\frac{P_1-P_O}{V_O-V_1}} \tag{4.5}$$

$$u_1 = u_S\left(1 - \frac{V_1}{V_O}\right) \tag{4.6}$$

With these equations, the shock front problem is completely solved when an equation of state is known which gives P as a function of V.

The equation of state which is used is the integrated form of the modified Tait equation of state. (11, p. 39)

$$P_1 = (P_O+B)\left(\frac{V_O}{V_1}\right)^n - B \tag{4.7}$$

The quantities, B and n, are slowly varying functions of entropy which are treated as constants according to the assumption of separable energy. The constant n is taken as 7 and the constant B is taken to be consistent with the velocity of sound in the limit that V_1 approaches V_O. For a sound velocity of 1483 m/sec, B is 3140 x 10^5 N/m^2 or 3140 bars.

If both u_S and u_1 are measured, then P and V can be determined directly from the conservation equations without an equation of state. Such measurements have been made by Walsh and Rice to verify that the modified Tait equation of state is a valid representation of the properties of water. (13)

For the simple case of a plane shock front with constant velocity, the pressure and mass velocity are uniform and constant throughout the entire region between the shock front and the piston which is producing the shock wave. The piston moves with a velocity equal to the mass velocity of the compressed medium. Thus, the shock front conditions alone are sufficient to determine the pressure distribution over the entire shock wave.

Nonuniform Pressure Distributions in Shock Waves

In the ideal case just described, the pressure is uniform over the entire compressed region. However, if the shock front is curved or if the piston velocity is not constant, the pressure varies with both time and space coordinates. The pressure immediately behind the front is still determined from the front velocity, but the pressure varies over the region between the front and the piston. The shock front equations are then used as boundary conditions for the more general problem of the nonuniform shock wave.

If the time rate of change of the shock velocity and the shock front curvature are known in addition to the shock velocity, then it is possible to compute the pressure gradient and mass velocity gradient in the region imme-

diately behind the front. (14) The equation for the pressure gradient is:

$$\left.\frac{\partial P}{\partial r}\right|_1 = \frac{\frac{c_1^2}{V_1}\frac{du_1}{dt} + 2\frac{c_1^2}{r_1 V_1}u_1(u_s-u_1) + (u_s-u_1)\frac{dP_1}{dt}}{(u_s-u_1)^2 - c_1^2} \qquad (4.8)$$

The sound velocity c_1 is computed as a function of P_1 from the equation of state, and r_1 is the radius of curvature of the shock front. This equation was used for estimating the pressure gradients given in Section I.

The general approach to finding pressure and velocity distributions for the shock wave consists of solving differential equations for mass and momentum conservation subject to the equation of state for water. Once again the energy equation is dropped because of separable energy. For a cylindrical shock wave, the differential equations become: (9, p. 29)

$$\text{Mass:} \qquad \frac{\partial}{\partial r}(r\rho u) = -r\frac{\partial \rho}{\partial t} \qquad (4.9)$$

$$\text{Momentum:} \qquad \rho\left(\frac{\partial u}{\partial t} + u\frac{\partial u}{\partial r}\right) = -\frac{\partial P}{\partial t} \qquad (4.10)$$

where ρ is density, r is radius, u is mass velocity, and t is time. These equations must be solved subject to the shock front conditions and subject to the condition that at the piston face, the piston velocity equals the mass velocity.

The Cylindrical Shock Wave

The cylindrical shock wave is of interest because the expanding column of plasma generates such a shock wave. The pressure of the column of plasma relative to its surroundings determines the rate of expansion of the column. Thus, a measurement of column expansion rate can be used to compute the pressure. However, the apparent expansion rate of the column exceeds the effective rate for computing pressure because the column itself is continually converting water into plasma at its boundary. The problem can be interperted in terms of expansion of a fixed amount of plasma if the expansion rate is corrected.

For a given piston velocity, corresponding to a given column expansion rate, the piston pressure is certainly less for a cylindrical geometry than for a plane geometry because of the divergence of flow in the cylindrical case. The effect of divergence can be seen in an elementary way by making the assumption that pressure is constant over the shock wave. If pressure and therefore

density are constant, the mass velocity must be inversely proportional to the radius if mass is to be conserved. With the added assemption that the variable quantities are functions only of the ratio of radius to time, $r/t = y$, then uy is a constant. If the shock front is denoted by subscript (1) and the piston by subscript (2), then the condition that piston velocity be equal to mass velocity at the piston face determines that $uy = y_2^2$. At the shock front the equation becomes $u_s u_1 = u_2^2 = y_2^2$ where $u_s = y_1$. Thus, $u_1 < u_2$ because $u_s > y_2$. Therefore, the pressure, which is a function of the mass velocity at the shock front, is less than that which would have been computed for a plane wave with the same piston velocity.

The preceeding analysis is not adequate because the momentum equation is not satisfied. The mass velocity is not constant so that the pressure gradient must be different from zero, which is contradictory to the assumption. Actually the pressure is higher near the piston than it is at the shock front, although the piston pressure is not as high as it would be for a plane geometry.

The problem has been treated in detail by G. I. Taylor for a spherical geometry. (9, p. 424-429) The treatment assumes that the dependent variables are functions only of r/t which is y. The assumption restricts the applicability of the solution to cases where the piston velocity is constant. The method of solution can be used for a cylindrical geometry with only a slight change in the form of the equations. Fortunately, the expansion rate of the cylindrical plasma column is nearly constant so that it is possible to use the solution of Taylor.

Taylor's method reduces the problem to solving a first-order nonlinear differential equation and to performing two quadratures. All three operations require numerical methods which are best handled by a computer. Some computations were done with this method by hand for comparison with results obtained by a more simple, yet less accurate, method to be described shortly. The uncertainties in the growth rate data were sufficiently large that a precise computer solution would have been of little more value than the solution to be described presently.

The assumption that dependent variables are functions only of y was included in the approximate calculation which was used to determine plasma pressure as a function of growth rate. The calculation was based upon the following expression:

$$\rho u = C y^q \qquad (4.11)$$

C is a constant and q is an undetermined exponent. For $q = -1$, the method reduces to that described earlier where pressure was held constant. The pressure was allowed to vary by letting q be different from -1 so that a more realistic calculation could be made.

The functional relation for ρu was combined with the mass conservation equation to obtain expressions for ρ and u in terms of y and an integration constant K.

$$\rho = \frac{q+1}{q-1} C y^{q-1} + K \tag{4.12}$$

$$u = \frac{C y^{q}}{\frac{q+1}{q-1} C y^{q-1} + K} \tag{4.13}$$

The previously used subscript notations are continued in this calculation. In terms of the notations, the boundary conditions at the shock front and at the piston are written:

$$u_1 = y_1\left(1 - \frac{\rho_0}{\rho_1}\right) \tag{4.14}$$

$$u_2 = y_2 \tag{4.15}$$

From the boundary conditions, the quantities at the piston can be described in terms of the quantities at the shock front, the quantities ahead of the shock front in the undisturbed medium, and the parameter q.

$$C = \frac{\rho_1 - \rho_0}{y_1^{q-1}} \tag{4.16}$$

$$K = \frac{q+1}{q-1}\rho_0 - \frac{2}{q-1}\rho_1 \tag{4.17}$$

$$\rho_2 = \rho_1 - \frac{q+1}{2}\rho_0 \tag{4.18}$$

$$y_2 = u_2 = u_s\left(\frac{\rho_2}{\rho_1 - \rho_0}\right)^{1/q-1} \tag{4.19}$$

The problem is solved if q is determined from the momentum equation, but the problem is too complex for such a simple approach to yield an exact solution. There is no value of q which satisfies the momentum equation. However, q can be chosen so that the integral of the momentum equation is satisfied. That is, the average negative pressure gradient is equated to

the average time rate of change of momentum over the region occupied by the compressed water. The equation can be integrated by separating the variables, ρ and y, if one makes the assumption that

$$\frac{q-1}{q+1}\frac{K}{C} \gg y^{q-1} \tag{4.20}$$

The assumption was valid for the cases of interest. The integrated equation is as follows:

$$\begin{aligned}\frac{7B}{6\rho_0{}^7}(\rho_2{}^6-\rho_1{}^6) &= \frac{y_1{}^{q+1}-y_2{}^{q+1}}{(q+1)b}(-qa) \\ &+ \frac{y_1{}^{2q}-y_2{}^{2q}}{2qb^2}[qa+(2q+1)a^2] \\ &+ \frac{y_1{}^{3q-1}-y_2{}^{3q-1}}{(3q-1)b^3}[-qa+(4q+2)a^2-(q+1)a^3]\end{aligned} \tag{4.21}$$

with $a = q-1/q+1$, $b = aK/C$, and with B equal to the constant from the equation of state.

In practice a value of q was assumed and with it the piston conditions were computed in terms of specified shock front conditions. The results were substituted into the integrated momentum equation to check the validity of the choice of q. From the check, a new value of q was estimated and the procedure was repeated. The calculation usually converged with 3 or 4 cycles.

Plasma pressure was computed as a function of expansion rate for several points so that the curve of Fig. 16 could be drawn. A second curve in the figure shows the pressure which would be obtained if the shock wave were plane rather than cylindrical.

Plasma Column Growth

The growth rate of the plasma column was measured by time resolved photography using Kerr cells. Two photographs with exposure times of 0.1 μsec were taken during each test. The timing of the exposures could be varied from one test to the next so that the growth rate could be determined over the entire time of interest. The exposure pulses were monitored with an oscilloscope so that a record of the timing could be obtained for each test.

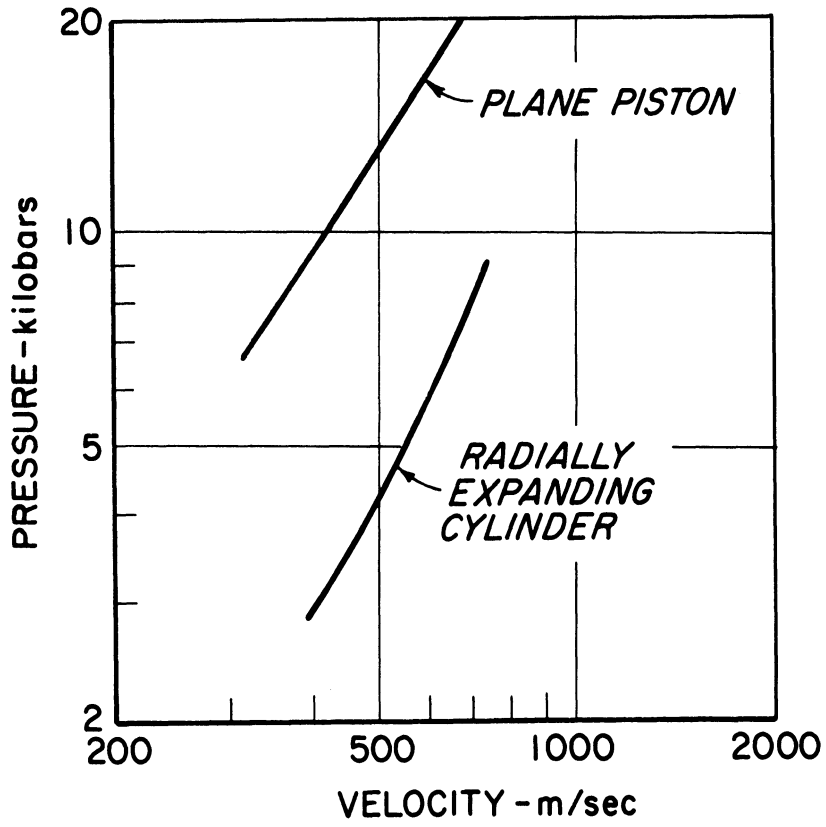

Fig. 16. Pressure as a function of velocity for a plane piston and for a radially expanding cylinder.

Each discharge electrode assembly carried two parallel scratch marks on the brass block which were a known distance apart. Those marks served as a reference from which the dimensions of the plasma column could be determined. The Kerr cell camera was focused by rotating one of the polaroid windows so that the cell would pass light. Then, before the cell was closed in preparation for the test, a time exposure was made to record the scratch mark spacing on a separate sheet of film. The sheet of film with the scratch marks was compared to the sheet of film with the plasma image to determine the plasma dimensions.

The actual measurement of dimensions was done with a projector which produced a 10X enlargement on a ground glass screen. A ruler was used to measure the plasma images on the screen and to compare them with the image of the scratch marks.

The boundaries of the plasma column appeared to be quite definite. However, the existance of a diffuse boundary would have meant that the apparent plasma dimensions depended upon the amount of exposure of the film, with the more dense image appearing to be larger. Yet highly overexposed photographs did not appear to be any larger than normally exposed photographs. Thus, the possibility of a diffuse boundary was dismissed.

The cylindrical shock front which propagates outward from the plasma column causes distortion of the image of the column because of light refraction. Thus, the measurement of column dimensions must be corrected for the distortion. No data could be found for index of refraction of water as a function of pressure at high pressures, so that a calculation of distortion was not feasible. However, the effects of distortion were determined experimentally.

A steel pin was placed in a position normal to the tungsten initiating wire with the pin point being nearest the wire. A time exposure was taken of the arrangement before the plasma was formed to record the relative positions of the wire and the pin. Then a Kerr cell exposure was made after the plasma was formed and the cylindrical shock wave had swept over the pin point. A reflector behind the pin produced a silhouette of the pin point. The pin did not move appreciably in the time interval of interest because of its high density and its shape. Thus, by comparison of the two photographs, the apparent displacement of the pin point could be used to determine the amount of distortion.

The amount of distortion would be more severe at the pin point than at the surface of the plasma column which was nearer the center of the cylindrical shock front. Even so, the distortion could barely be observed. As an estimate it was on the order of 5 percent. For the calculations of pressure the distortion was then completely neglected.

The creation of new plasma at the plasma column boundary makes the growth rate greater than what it would be for a constant amount of expanding plasma. In fact, the plasma does not undergo any significant expansion once it is formed because the temperature and pressure of the plasma column are practically constant. Yet the water surrounding the column is pushed outward as new plasma is formed from water adjacent to the column. As the water is converted into plasma it expands to occupy a volume much larger than its original volume so that the remaining water is forced outward. As the ratio of plasma volume to the volume of water which produced the plasma becomes large, the distinction between the actual growth rate and the rate caused by pressure alone becomes negligible. For a typical volume ratio of 10 to 1, a cylinder of water of unit radius expands into a cylinder of plasma of radius $\sqrt{10}$ or 3.16. Thus, the pressure-related growth rate is $100(3.16-1)/3.16$ or 68.4 percent of the apparent rate.

With the various considerations of this section, the growth rate of a plasma column can be determined with an uncertainty of about 10 percent. Then, from cylindrical shock wave theory the uncertainty is magnified to approximately 20 percent of the pressure.

Pinch Pressure

The force on the plasma current from its self magnetic field is significant when the plasma has no explosive confinement. The force, known as a pinch force, contributes to the pressure of the plasma. The total confining pressure then becomes the sum of the shock wave pressure and the pinch pressure.

The pinch pressure is not uniform through the plasma but it is greatest at the center. When current is uniformly distributed over the plasma cross section the expression for pressure is (18)

$$P = \frac{\mu I^2}{4\pi^2 R^4} (R^2 - r^2) \qquad (4.22)$$

where R is the radius of the plasma column and r is the independent radius variable. I is current and μ is the permeability of the plasma which is taken to be that of free space for this analysis. The average pressure over the plasma volume was used for calculations of the plasma properties. The average pinch pressure is given by

$$P = \frac{\mu I^2}{8\pi^2 R^2} \qquad (4.23)$$

Explosive Confinement of Plasma

When no explosive is used, the plasma pressure is determined from the growth rate and the pinch effect. The ambient pressure is negligible. Yet when explosive is used the ambient pressure is approximately 115 kilobars and the other effects become secondary. The plasma pressure is then equal to the ambient pressure plus some small corrections.

The ambient pressure which is established by the shock wave from the explosive has been determined in Section I to be 115 kilobars. The corrections are determined in the same way as the contributions to pressure were determined for the case without explosive except that the plasma column does not have a circular cross-section but rather an elliptical one. The column is distorted when the shock front passes through it. As an approximation the column may be considered to have a circular section.

The calculation of pinch pressure is identical to the calculation for the other case.

The calculation of the pressure differential between the plasma and the surroundings proceeds in the same manner as previously except that the undisturbed medium into which the cylindrical shock propagates is considered to be water at 115 kilobars. Plasma pressure was calculated as a function of column growth rate for an ambient pressure of 115 kilobars. The results are shown in Fig. 17. Once again the growth rate which is measured exceeds the rate to be used in the pressure calculation because of the formation of plasma at the column boundaries.

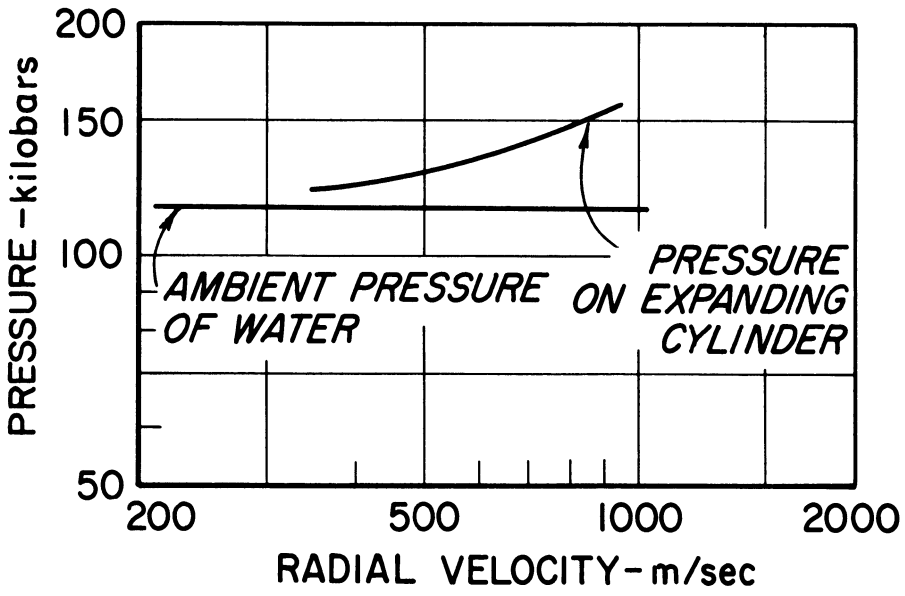

Fig. 17. Pressure of a radially expanding cylinder in water with an ambient pressure of 115 kilobars.

The plasma column is somewhat more complicated than the preceeding analysis implies. After the shock wave has swept through the plasma column and compressed it, the plasma is still being traversed by reflected shock waves. The dimensions of the plasma are sufficiently small that the transit time of the reflected shocks is about 0.1 μsec, so that pressure equilibrium should be established fairly quickly. The effects of the reflected shocks upon pressure are completely neglected.

The other correction to the plasma pressure arises from the existance of a pressure gradient behind the shock front. If the gradient is 6 kilobars/mm and the plasma is 2 mm behind the shock front, then the pressure correction is -12 kilobars.

The negative correction from the pressure gradient is offset by the positive corrections from the pinch effect and column expansion. The net correction is such a small percentage of the ambient pressure that it has been ignored in the calculations which are to follow. The plasma pressure is con-

sidered to be 115 kilobars with an uncertainty of about 10 percent which arises from the uncertainty in the shock velocity measurements.

V. EXPERIMENTAL RESULTS

The experimental results are presented in three sections which represent three different series of experiments at different pressures. The first two are measurements of plasma properties at 4 and 7.7 kilobars which were made without the use of explosives to confine the plasma. The third series was made with explosives which established a plasma pressure of 115 kilobars.

The only difference in procedure between the 4 kilobar tests and the 7.7 kilobar tests was in the amount of inductance included in the discharge circuit. Inductance was deliberately increased for the 4 kilobar tests so that the rate of current rise would be less than for the 7.7 kilobar tests.

The only difference between tests at 7.7 kilobars and 115 kilobars was in the use of explosives at the higher pressure level.

For all tests, the storage capacitor was charged to 14 kilovolts as measured with an electrostatic volt-meter. Stored electrical energy was 1450 joules.

For all tests, the length of the plasma column was approximately 3/16 in. The electrode separation was measured with a ball gage before each test to account for minor variations in spacing caused by variations in electrode manufacture and assembly.

Some auxiliary tests (without explosive) were run with plasma columns of different lengths to show that length was not a significant variable in determining the properties of the plasma per unit length. Plasma voltage was found to be proportional to the length of the plasma column. As a result, electrode phenomena were unimportant in the analysis of the plasma.

The plasma was replaced with a No. 18 copper wire for certain tests to determine the inductance of the plasma and electrodes. For various rates of current rise the voltage was found to be proportional to the rate of rise. From the data the inductive correction for a particular test with plasma could be determined as a function of the rate of current rise for that particular test.

The assumption was made for computing the inductive correction that the current for any particular test could be represented by a normalized current-time function multiplied by appropriate constants. This was not strictly true in that during the first 0.2 μsec the rate of current rise through a plasma column was lower than it would have been through No. 18 copper wire given the same average rate of rise over the entire time interval of interest. The high initial inductance and resistance of the tungsten initiating wire were the

cause of the slower rate of rise until the plasma column had grown somewhat. This minor effect was neglected in determining the inductive correction to the voltage of the plasma.

The accuracy of the current measurement was very low during the first 0.2 μsec when the current was nearly zero. Thus, the early data should not be given much significance. At later times the integrated electrical energy is subject to the error in the early data, yet the percentage error in the total energy is small. Thus, the significant results are found in the range of time beyond about 0.5 μsec.

Tests were performed both with and without explosive to show that there was no significant fraction of the discharge current passing through the water surrounding the discharge electrodes instead of through the plasma column. The tests were conducted in the usual manner except that no tungsten initiating wire was used. No plasma column or other visible conducting path was formed during the first 2 μsec so that any current flow had to be leakage current through the water. No discharge current could be detected even though the potential across the electrodes rose to the level of the charging voltage of the energy storage capacitor.

Plasma at 4 kilobars

The plasma was produced with a discharge current which had a rate of rise of approximately 50 000 A/μsec. Several tests were performed which were as nearly alike as possible with tests being discarded when some obvious malfunction of equipment occurred.

Data points were taken from photographs of oscilloscope traces of current and voltage. Kerr cell photographs were obtained for the purposes of determining the plasma dimensions and temperatures. The oscilloscope traces for monitoring the Kerr cell exposures were photographed.

The graph of Fig. 18 shows the growth of the plasma column diameter as a function of time. The symbols occur in pairs to identify the photographs taken during each test. The times are taken as the midpoints of the 0.1 μsec exposure intervals. Two photographs of the plasma column are shown in Fig. 19.

There was no apparent variation of temperature of the plasma with time over the interval represented by the photographs. Thus, the plasma temperature was considered to be the average of all the temperatures from all the photographs. The result was 38 000°K with a root mean square deviation of 8000°K. In this particular series, the temperature was somewhat above the range where temperature measurements were most accurate, and thus the deviation was quite high.

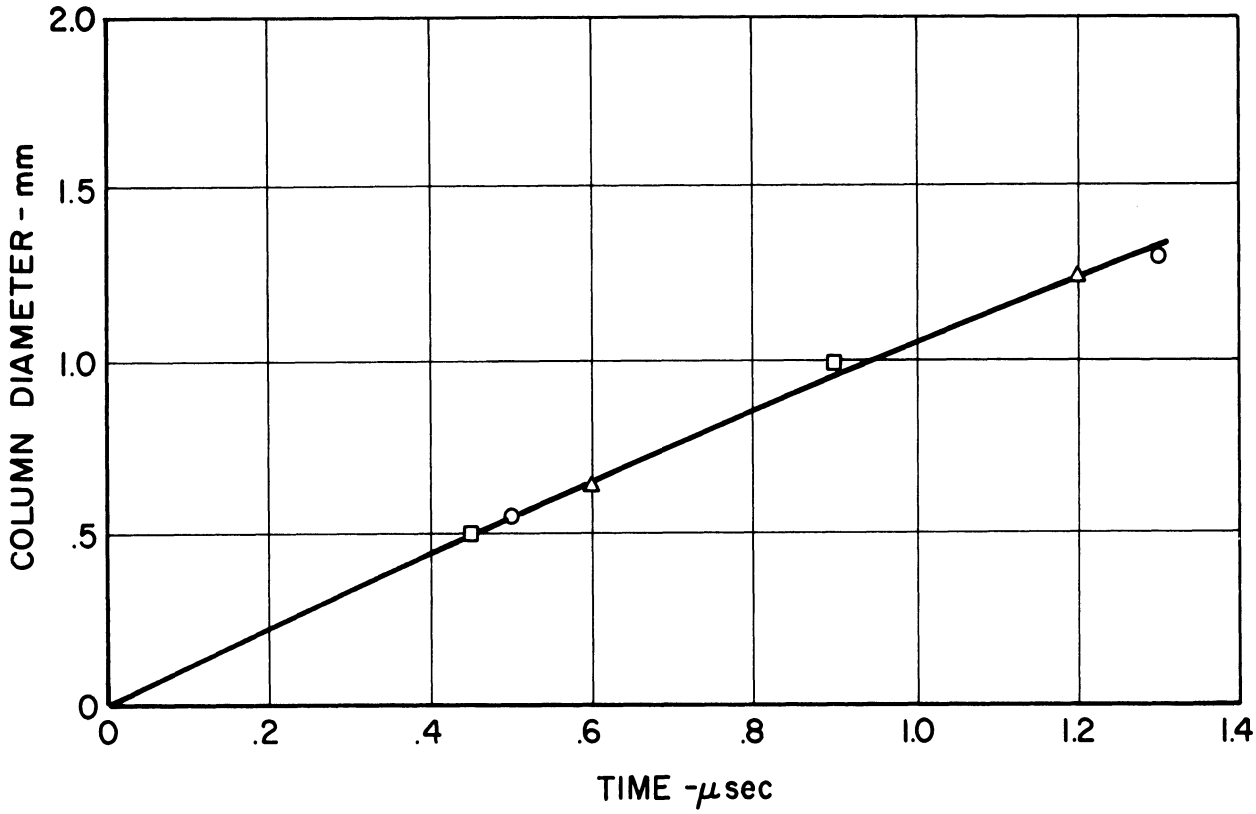

Fig. 18. Growth of the 4 kilobar plasma column.

Fig. 19. Two photographs in sequence of the 4 kilobar plasma column.

From the current and voltage data, the electrical power and electrical energy per unit length of plasma were computed as functions of time. The computations are summarized in Table 2. The average voltage was corrected for the inductive effects and multiplied by the average current to obtain power which was divided by the length of the plasma column to obtain power per unit length. The power function was graphically integrated to determine the electrical energy which had been absorbed by the plasma as a function of time. Electrical power is plotted as a function of time along with results from the other series of tests in Fig. 20.

TABLE 2

CALCULATION OF ELECTRICAL ENERGY FOR 4 KILOBAR PLASMA COLUMN

(4.23 mm average length)

Time, μsec	Average current, kA	Average voltage, kV	Inductive voltage correction, kV	Corrected voltage, kV	Electrical power per mm of column length, MW/mm	Electrical energy per mm of column length, J/mm
0.0	0.0	--	---	--	0.0	0.0
0.1	--	--	---	--	--	--
0.2	4.65	3.57	0.2	3.37	3.7	0.37
0.3	9.30	2.77	0.2	2.57	5.6	0.83
0.4	13.9	2.16	0.2	1.96	6.5	1.43
0.5	20.1	1.93	0.2	1.73	8.2	2.21
0.6	27.9	1.73	0.2	1.53	10.1	3.09
0.7	32.5	1.53	0.2	1.33	10.2	4.12
0.8	41.7	1.43	0.2	1.23	12.1	5.17
0.9	43.4	1.33	0.2	1.13	11.6	6.35
1.0	48.1	1.23	0.2	1.03	12.8	7.56
1.1	54.3	1.20	0.2	1.00	12.8	8.8
1.2	59.0	1.17	0.2	0.97	13.5	10.2
1.3	63.5	1.10	0.2	0.90	13.5	11.6
1.4	69.7	1.07	0.2	0.87	14.3	12.9

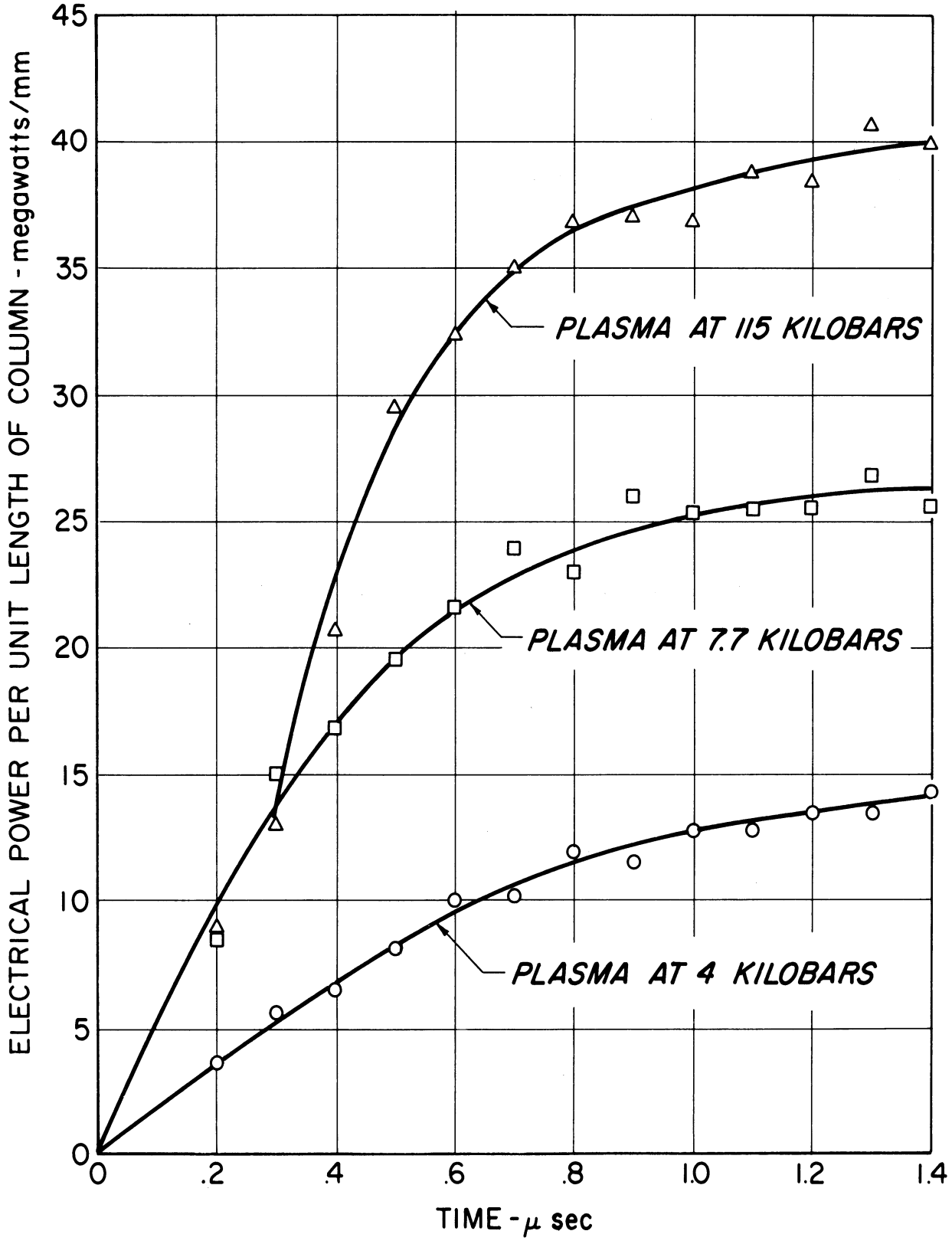

Fig. 20. Electrical power as a function of time for the three series of tests.

Further calculations for the plasma are summarized in Table 3.

The pressure determined as a function of channel expansion must be based upon a corrected expansion rate. Water has a density of atoms of 10^{29} m^{-3}. If a cylinder of water of unit radius expands to form plasma with a density of n atoms per cubic meter, then the plasma column will have a radius of $(10^{29}/n)^{1/2}$. The actual expansion velocity is determined from the difference between the plasma column diameter and the diameter of the original column of water so that the effective diameter D' is given by a function of the actual diameter D and the density n.

$$D' = D \frac{\left(\frac{10^{29}}{n}\right)^{1/2} - 1}{\left(\frac{10^{29}}{n}\right)^{1/2}} \tag{5.1}$$

The diameter D was determined from the growth curve and then D' was computed on the basis of $n = 5 \times 10^{27}$. The choice of n was determined from theoretical discussions to follow in later sections. One half the time rate of change of D' was used as the velocity of radial expansion in determining the pressure from cylindrical shock wave theory which was discussed in the preceeding section.

The plasma column diameter growth rate was not exactly constant so the shock wave theory was not strictly applicable. Yet, the deviations in growth rate were small. Thus, the theory was used and the pressure at any particular time was determined from the slope of the corrected growth rate curve at that time.

Pinch pressure was determined as a function of time from the current and the actual diameter D.

Then the sum of the two pressure contributions was found. The sum was assumed to be the confining pressure which is equal to the combined effects of kinetic motion of the plasma particles and interaction among the particles.

Radiation and mechanical work done upon the water surrounding the plasma are energy losses which must be subtracted from the electrical energy to determine the net energy of the plasma relative to the energy of the water from which the plasma was formed.

Radiation losses were computed for the plasma on a basis of black-body radiation at 38 000°K from the surface area of the plasma column. The power loss was integrated as a function of time to determine energy loss.

TABLE 3

CALCULATION OF PRESSURE AND INTERNAL ENERGY PER UNIT VOLUME FOR 4 KILOBAR PLASMA

Time, μsec	Column diameter, mm	Volume per mm of column length, mm^2	Pressure calculated from corrected column expansion rate, kilobar	Magnetic pinch pressure, kilobar	Total pressure, P, kilobar	Energy lost by radiation per mm of column length, J/mm	Mechanical work of expansion per mm of column length, J/mm	Internal energy, u, J/mm^3
0.0	--	---	---	--	---	--	--	--
0.1	--	---	---	--	---	--	--	--
0.2	0.23	0.042	3.2	0.26	3.5	0.0083	0.0108	8.43
0.3	0.34	0.091	3.1	0.48	3.6	0.0189	0.0259	8.63
0.4	0.44	0.152	3.0	0.64	3.6	0.0234	0.0433	8.94
0.5	0.55	0.237	3.0	0.85	3.9	0.0418	0.0677	8.87
0.6	0.66	0.342	2.9	1.14	4.0	0.0642	0.0975	8.63
0.7	0.76	0.453	2.9	1.16	4.1	0.0905	0.129	8.62
0.8	0.86	0.581	2.9	1.49	4.4	0.1205	0.166	8.40
0.9	0.97	0.738	2.9	1.28	4.2	0.1545	0.210	8.12
1.0	1.07	0.893	2.8	1.43	4.2	0.1923	0.254	7.96
1.1	1.17	1.08	2.8	1.37	4.2	0.2338	0.308	7.70
1.2	1.24	1.21	---	1.44	---	--	--	--
1.3	1.33	1.39	---	--	---	--	--	--

Mechanical work was the integral of $P\ dV$ with a special interpretation of the quantities P and V. P included only the expansion pressure contribution and V was a corrected volume which was less than the actual volume by the factor $(1-n/10^{29})$. The plasma, once formed, was nearly motionless so that expansion against the magnetic field was not a contributing factor.

The losses were subtracted from the electrical energy to determine plasma internal energy which was normalized per unit volume. The losses were minor corrections to the energy.

From the calculations the three quantities which are of significance for the theoretical analyses to follow are:

Internal Energy u — 8.4×10^9 J/m^3

Pressure P — 4 kilobars

Temperature T — 38 000°K

The numbers are chosen to represent the measured properties within a small percentage over the time interval from 0.5 to 1.1 μsec.

Plasma at 7.7 Kilobars

For the series at 7.7 kilobars, the rate of current rise was approximately 100 000 A/μsec. The results were computed from data averaged over several tests. Calculations were performed in the same way as for the series of measurements at 4 kilobars.

The average plasma temperature was 32 000°K with a root mean square deviation of 4000°K. Once again no trend of temperature variation with time was observed. The growth rate as determined from Kerr cell photographs is plotted in Fig. 21.

The corrections of growth rate and volume expansion were based upon a value of $n = 10^{28}$ for this series.

The calculations are tabulated in the same form that was used for the first series in Table 4 and Table 5. Power as a function of time is shown in Fig. 20.

The results for this series of measurements are as follows:

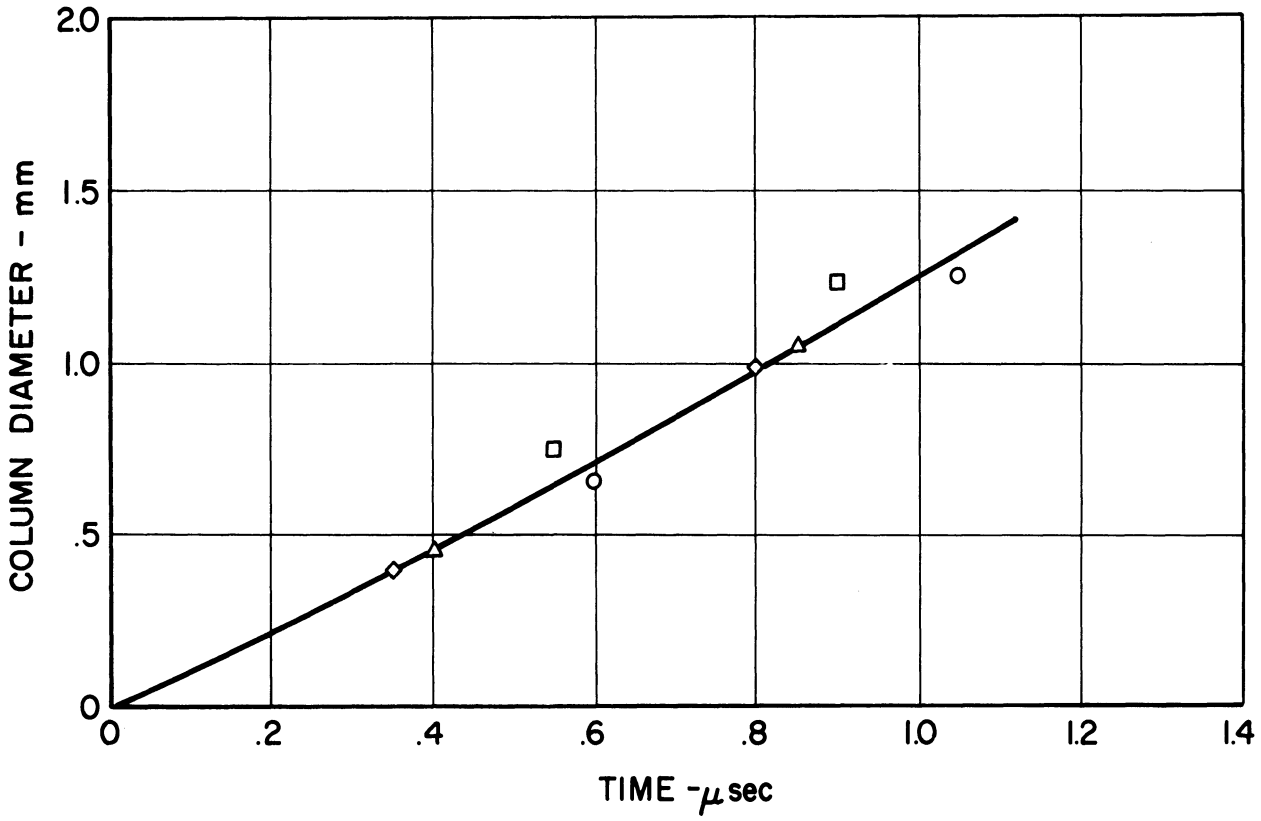

Fig. 21. Growth of the 7.7 kilobar plasma column.

Internal energy u — 16 x 10^9 J/m^3

Pressure P — 7.7 kilobars

Temperature T — 32 000°K

Plasma at 115 Kilobars

In addition to the quantitative measurements, several qualitative observations were made of the behavior of the high pressure plasma. However, a discussion of these observations will be reserved for a later section. For the quantitative measurements, a plasma column was formed in exactly the same way as in the case of the 7.7 kilobar measurements. Then in the time interval from 0.3 to 0.4 μsec, the shock front from the explosive swept laterally through the plasma column to compress it to the high level of pressure. The measurements of the high-pressure plasma were made over the interval from 0.5 to 0.9 μsec.

When the shock wave swept through the plasma column, the circular cross-section of the column was flattened to an elliptical section. The major axis of the section was easily measured by photographing the plasma through the

TABLE 4

CALCULATION OF ELECTRICAL ENERGY FOR 7.7 KILOBAR PLASMA COLUMN

(4.37 mm average length)

Time, μsec	Average current, kA	Average voltage, kV	Inductive voltage correction, kV	Corrected voltage, kV	Electrical power per mm of column length, MW/mm	Electrical energy per mm of column length, J/mm
0.0	0.0	--	---	--	0.0	0.0
0.1	--	--	---	--	--	0.27
0.2	9.3	4.5	0.5	4.0	8.5	1.12
0.3	21.7	3.53	0.5	3.03	15.1	2.16
0.4	31.0	2.87	0.5	2.37	16.8	3.68
0.5	43.4	2.47	0.5	1.97	19.6	5.51
0.6	55.8	2.20	0.5	1.70	21.7	7.57
0.7	68.2	2.03	0.5	1.53	23.9	9.81
0.8	77.6	1.80	0.5	1.30	23.1	12.3
0.9	89.9	1.67	0.4	1.27	26.1	14.8
1.0	97.7	1.53	0.4	1.13	25.3	17.3
1.1	108.0	1.43	0.4	1.03	25.5	19.9
1.2	116.0	1.37	0.4	0.97	25.6	22.5
1.3	122.0	1.26	0.3	0.96	26.8	25.1
1.4	129.0	1.17	0.3	0.87	25.7	27.7

TABLE 5

CALCULATION OF PRESSURE AND INTERNAL ENERGY PER UNIT VOLUME FOR 7.7 KILOBAR PLASMA

Time, μsec	Column diameter, mm	Volume per mm of column length, mm^2	Pressure calculated from corrected column expansion rate, kilobar	Magnetic pinch pressure, kilobar	Total pressure, P, kilobar	Energy lost by radiation per mm of column length, J/mm	Mechanical work of expansion per mm of column length, J/mm	Internal energy, u, J/mm^3
0.0	--	--	---	--	--	---	---	--
0.1	--	--	---	--	--	---	---	--
0.2	0.22	0.0381	2.9	1.14	4.04	0.004	0.014	28.9
0.3	0.34	0.0907	3.0	2.60	5.59	0.009	0.023	23.5
0.4	0.46	0.166	3.1	2.89	5.99	0.017	0.045	21.8
0.5	0.58	0.264	3.3	3.57	6.87	0.027	0.072	20.4
0.6	0.71	0.396	3.6	3.95	7.55	0.038	0.117	18.7
0.7	0.85	0.568	3.7	4.09	7.79	0.053	0.171	16.9
0.8	0.98	0.754	3.8	3.98	7.78	0.070	0.234	15.9
0.9	1.12	0.985	3.8	4.09	7.89	0.090	0.315	14.6
1.0	1.26	1.25	3.9	3.82	7.72	0.112	0.405	13.5
1.1	1.40	1.54	---	3.79	--	0.137	---	--
1.2	1.54	1.86	---	3.61	--	---	---	--

shock front in a direction parallel to the shock propagation. The distortion was negligible in that direction. However, the minor axis was difficult to measure because a side view photograph had to be taken obliquely through the shock front. Distortion was severe.

A hole was bored in the brass extension from the side so that a photograph could be taken of the plasma from that direction. Distortion of the dimensions in the photograph was estimated from photographs with argon flash illumination as described in Section I. A correction factor of 0.6 was applied to the measurements of the minor axis to obtain the true dimension.

Useful side view photographs of the plasma column were obtained for times of 0.5 to 0.6 μsec. At later times distortion was so severe that useful photographs could not be obtained. The ratio of major axis to minor axis was determined for that time interval and the ratio was assumed to be valid for all times from 0.4 to 0.9 μsec. The ratio was 3.4.

Figure 22 is a graph of the major axis as a function of time. The diameter of the 7.7 kilobar plasma column is also shown for comparison.

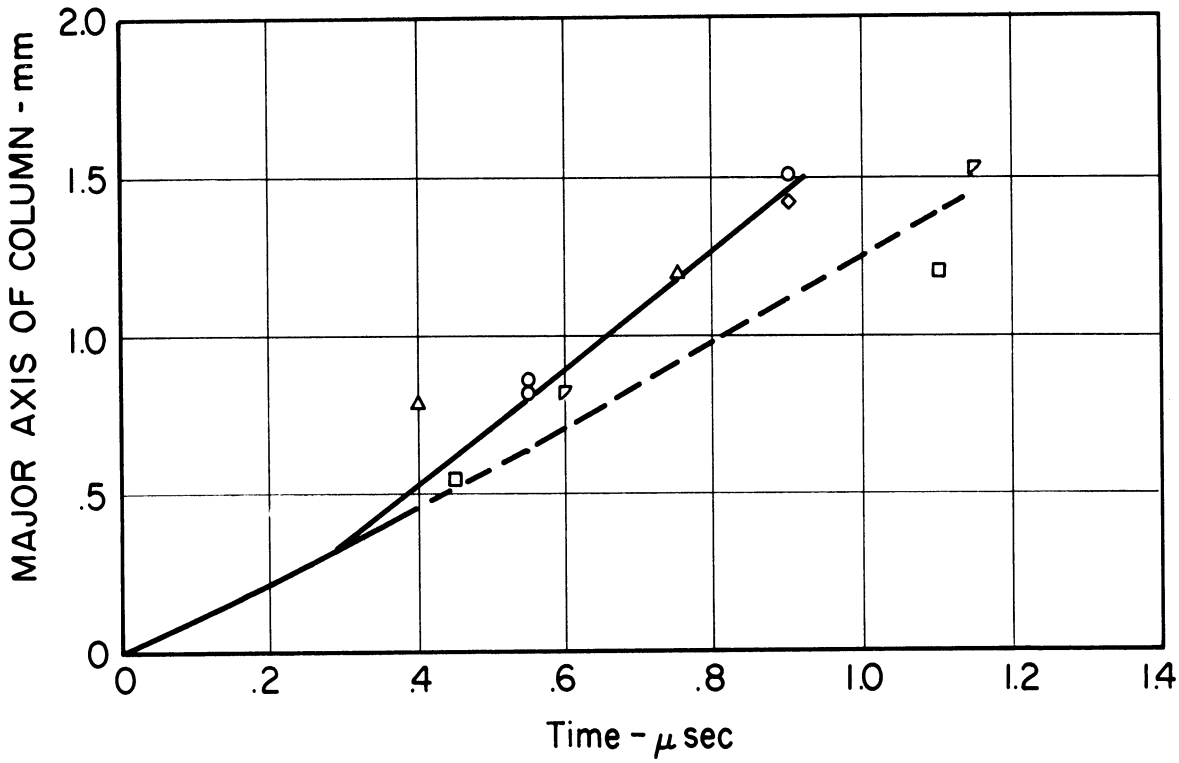

Fig. 22. Growth of the 115 kilobar plasma column along the major axis of its elliptical cross-section.

A photograph of the current and voltage traces for a typical test is shown in Fig. 23. The upper trace shows current. The voltage trace is of

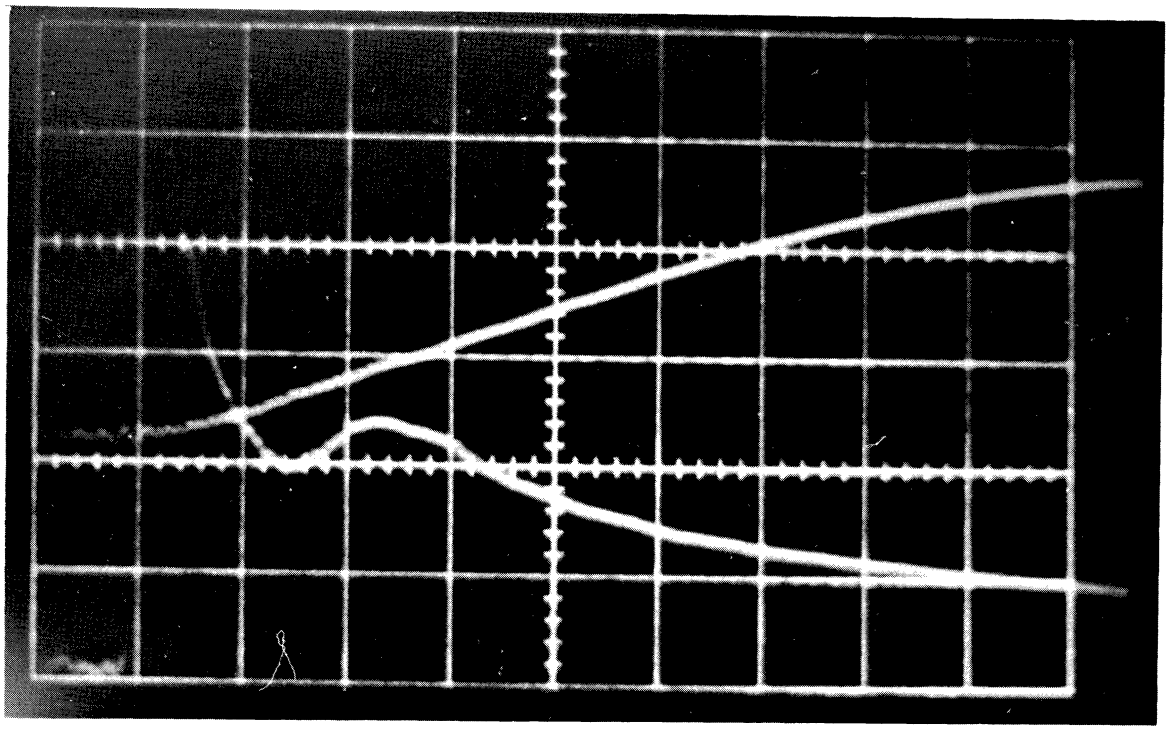

Fig. 23. Photograph of the oscilloscope trace for current and voltage when explosive was used.

particular interest because of the way it varies when the shock wave passes through the plasma. Without any explosive the voltage trace is a monotonically decreasing function. However, the resistance of the plasma column increases when the shock wave compression occurs so that the voltage across the plasma is raised. When the voltage is raised, the rate of current rise is decreased so that the current does not reach as high a peak value as it would if no explosive were used. The irregularity on the voltage trace indicates that the compression of the plasma occurred at the time which was determined from the measurements of shock velocity which were described in Section I.

Before the compression, the temperature was characteristic of the plasma without explosive confinement. When the plasma was compressed the temperature fell from above 30 000°K to approximately 10 000°K. After compression the temperature showed a tendency to decrease slowly with time until about 1.0 μsec after the plasma was formed. A later section will describe the variations in plasma temperature in more detail.

Electrical power and energy were computed from current and voltage in the same way as they were computed for the other series of tests. The power is plotted as a function of time in Fig. 20 and the computations are shown in Table 6.

TABLE 6

CALCULATION OF ELECTRICAL ENERGY FOR 115 KILOBAR PLASMA COLUMN

(4.39 mm average length)

Time, μsec	Average current, kA	Average voltage, kV	Inductive voltage correction, kV	Corrected, voltage, kV	Electrical power per mm of column length, MW/mm	Electrical energy per mm of column length, J/mm
0.0	0.0	--	---	--	0.0	0.0
0.1	--	7.73	0.5	7.23	--	---
0.2	9.3	4.80	0.5	4.30	9.1	1.12
0.3	17.0	3.86	0.5	3.36	13.0	2.16
0.4	24.8	4.07	0.4	3.67	20.7	4.08
0.5	34.1	4.20	0.4	3.80	29.5	6.73
0.6	41.8	3.80	0.4	3.40	32.3	9.73
0.7	51.2	3.40	0.4	3.00	35.0	13.1
0.8	60.5	3.07	0.4	2.67	36.8	16.7
0.9	69.7	2.73	0.4	2.33	37.0	20.3
1.0	75.9	2.53	0.4	2.13	36.8	24.3
1.1	83.7	2.33	0.3	2.03	38.7	28.2
1.2	90.0	2.17	0.3	1.87	38.3	32.0
1.3	97.7	2.13	0.3	1.83	40.7	36.0
1.4	103.5	2.00	0.3	1.70	39.9	39.9

Further calculations for the plasma are given in Table 7. Up to 0.3 μsec the calculations are identical to those for the 7.7 kilobar plasma. Then the compression occurs and the calculations become different.

For these calculations the pressure has been assumed to be 115 kilobars. Corrections from plasma expansion, pinch forces, and shock wave pressure gradient have been neglected. The corrections are a small percentage of the total pressure and furthermore they are of opposite signs so that they tend to cancel.

Radiation power loss was completely neglected because of the much lower temperatures which occurred at high pressure.

When the plasma was compressed, work was done on the plasma which was equivalent to a negative contribution to the integral of $P\ dV$. The contribution was estimated by multiplying the difference in plasma volume at 0.4 μsec for the 7.7 and 115 kilobar series by the average of 8 and 115 kilobars. The result was -0.6 J.

Work done by the plasma in expanding against the water at 115 kilobars was added to -0.6 to determine the total contribution to the work integral. Work done prior to 0.3 μsec was negligible.

The change in volume was found by subtracting the volume at 0.4 μsec from the volume at the time of interest and multiplying by the factor $(1-n/1.6 \times 10^{29})$ with n being 10^{29}. The change was then multiplied by 115 kilobars to obtain the work done.

The numerical results for the high-pressure plasma are the following:

Internal energy u — 50×10^9 J/m^3

Pressure P — 115 kilobars

Temperature T — 10 000°K

Comparison

From the results of the three series of tests, some observations can be made. The behavior of temperature as a function of pressure is of particular interest. The highest temperature occurred in the plasma with the lowest pressure and the temperature at 115 kilobars was much less than the temperatures at the lower pressures.

For an ideal gas the internal energy per unit volume is proportional to the pressure, regardless of what the temperature might be. Yet for the plasmas,

TABLE 7

CALCULATION OF INTERNAL ENERGY PER UNIT VOLUME FOR 115 KILOBAR PLASMA

Time, μsec	Major axis of elliptical cross section, mm	Minor axis, mm	Volume per mm of column length, mm^2	Pressure, P, kilobar	Mechanical work per mm of column length, J/mm	Internal energy, u, J/mm^3
0.0	--	--	--	--	--	--
0.1	--	--	--	--	--	--
0.2	0.22	0.22	--	3.04	--	--
0.3	0.34	0.34	0.0909	4.70	+0.026	23.4
			Compression of plasma by shock wave			
0.4	0.53	0.16	0.0666	115	-0.6	70.3
0.5	0.71	0.22	0.123	115	-0.354	57.6
0.6	0.89	0.27	0.188	115	-0.048	52.0
0.7	1.08	0.33	0.280	115	+0.041	48.2
0.8	1.26	0.39	0.396	115	+0.83	44.2
0.9	1.45	0.45	0.513	115	+1.33	42.1

the relationship between energy and pressure is greatly different. For a 30 to 1 increase in pressure from 4 to 115 kilobars, the increase in the internal energy is only a factor of 6.

VI. DEBYE-HÜCKEL THEORY

The plasmas which were formed without the explosive confinement were analyzed with the Debye-Hückel shielding theory. The plasma temperature was in the range where a large fraction of the atoms were ionized. Thus, the theory, which deals with interactions of charged particles, could be applied. However, the application was not extended to the plasma with explosive confinement because the temperature and charged particle density were much lower than for the plasmas at lower pressures.

The Debye-Hückel theory for partially ionized plasma has found considerable application in the computation of thermodynamic properties of plasmas under high pressures such as those which occur in stellar bodies. Rouse published numerical results for several elements from machine calculations based on the Debye-Hückel theory. (19, 20) Yet at the same time he acknowledged that the theory was inadequate. In his calculations the correction term to the ionization potential in Saha's equation became so large that it exceeded the original potential.

The Debye-Hückel theory has a rigorous theoretical basis and it is certainly valid for computing correction terms to be inserted in ideal gas equations if the correction terms do not become too large. Any attempt to extend the theory so that the corrections are of major significance is open to question because of the classical formulation of the theory. At high particle densities where the corrections are large, quantum effects are significant.

The theory was originally proposed by Debye and Hückel in 1923 to explain phenomena in electrolytic solutions. (21) Their somewhat intuitive derivation was rigorously proved in 1950 by Mayer who also showed an equivalence between the problems for an electrolytic solution and for an ion gas. (22)

Numerous authors have presented theoretical derivations using a variety of methods and their results reduce to the Debye-Hückel theory in the limit of low density. Yet the extension of these methods to higher orders of correction becomes unfeasible because of computational difficulties. Villars has shown that for a computational method devised by Green, machine computations become very lengthy or even divergent for temperatures less than 10^5°K. (23)

Before further discussion of the various derivations which have been made, the general theoretical approach will be described. All methods are oriented toward the calculation of the partition function of the plasma from which all thermodynamic properties can be determined.

General Theory

In general, the partition function for a system of particles is defined as the sum over all possible configurations of the system of the quantity, $e^{-E/kT}$. The partition function Z is then

$$Z = \sum e^{-E_i/kT} \tag{6.1}$$

where E_i is the energy of a particular configuration of particles. (24) Several assumptions are made under which Z can be written in a more specific form:

1. The system contains three types of indistinguishable particles which are atoms, positive ions, and electrons.

2. The particles, particularly the electrons, behave classically.

3. The energy of the system is the sum of the thermal energies of the particles, the internal energies of the particles, and the energy of interaction between particles.

The first assumption implies that all molecules are dissociated into atoms of oxygen and hydrogen. Martin has shown that the number of undissociated molecules is a small fraction of the number of atoms for a temperature of 30 000°K. (3, p. 264) The assumption is not valid however for the 115 kilobar plasma at 10 000°K.

With these assumptions, Z can be written as the following function: (24)

$$Z = \prod_{\gamma} \left[\frac{1}{N_\gamma !} \left(\sum_j e^{-E_j^\gamma/kT} \right)^{N_\gamma} \right] \sum_q e^{-E_c/kT} \tag{6.2}$$

The index γ ranges over the particle types; E_j^γ is the sum of kinetic and internal energies for a single particle of type γ in the state j; N_γ is the number of particles of type γ; E_c is the coulomb interaction energy for all particles in the system; q is the summation index over all spacial configurations of the system of particles.

The various factors of Z are considered separately. First the energy E_j is written as the sum of kinetic energy E_t and internal energy E_s. Σ_j is replaced by Σ_s Σ_t and Σ_t is converted into an integral over the continuum of kinetic energies.

The degeneracy of kinetic energy levels, dg, is given by

$$dg = 2\pi \left(\frac{2m_\gamma}{h^2}\right)^{3/2} \sqrt{E}\, dE \tag{6.3}$$

per unit volume where m_γ is the particle mass and E is the kinetic energy. (25) The kinetic energy factor of Z then becomes

$$\int_0^\infty e^{-E/kT}\, dg = \left(\frac{2\pi mkT}{h^2}\right)^{3/2} \tag{6.4}$$

The internal energy sums are taken over the excited states of the particles. The contribution from the electron is simply

$$2\, e^{-E_o^e/kT} = B_e\, e^{-E_o^e/kT} \tag{6.5}$$

where $B_e = 2$ is the electron spin degeneracy and E_o^e is the zero energy. The neutral atom can exist in different states with different energy levels which have corresponding degeneracies. Thus, the contribution from the atom is

$$\sum_s g_s\, e^{-E_s^n/kT} \tag{6.6}$$

where E_s^n is the energy of the s excited state of the neutral particle represented with the index n. This sum is commonly expressed as

$$B_n\, e^{-E_o^n/kT} \tag{6.7}$$

which contains the same information in terms of the ground state energy E_o^n and the partition function over excited states B_n.

In like manner, the contribution from the ion is

$$B_i\, e^{-E_o^i/kT} \tag{6.8}$$

where the index i represents the ion. If the ion is a bare nucleus without orbital electrons, then B_i reduces to unity.

The ground-state energies have significance only in their relative magnitudes which are related to the ionization energy χ through the equation

$$E_o^i + E_o^e = \chi + E_o^n \tag{6.9}$$

The sum over spacial configurations is converted to an integral over the volume of the plasma. The integral is a multiple integral over the coordinates of each of the particles and is given by

$$Q = \int \ldots \int e^{-E_c/kT} \, dr_1 \ldots dr_{3n} \tag{6.10}$$

where E_c is a function of the coordinates.

The partition function is then the product of the various factors which have been described and it is given by

$$Z = \prod_\gamma \left\{ \frac{1}{N_\gamma!} \left[B_\gamma \, e^{-E_o^\gamma/kT} \left(\frac{2\pi mkT}{h^2} \right)^{3/2} \right]^{N_\gamma} \right\} Q \tag{6.11}$$

The evaluation of Q in terms of temperature T, volume V, and numbers of particles N_γ is the principal problem which must be treated to obtain a theory for properties of the plasma. Once Z is known the desired equations can be found by differentiation. Internal energy is given by

$$U = kT^2 \frac{\partial(\ell n Z)}{\partial T} = \frac{\partial\left(\frac{A}{T}\right)}{\partial\left(\frac{1}{T}\right)} \tag{6.12}$$

where free energy A is $-kT \, \ell n \, Z$. Pressure is given by

$$P = kT \frac{\partial(\ell n Z)}{\partial V} \tag{6.13}$$

Chemical potential μ_γ is given by

$$\mu_\gamma = - kT \frac{\partial(\ell n Z)}{\partial N_\gamma} \tag{6.14}$$

Finally, the ionization equation or Saha's equation is obtained from the condition for equilibrium which is given by

$$\mu_e + \mu_i = \mu_n \tag{6.15}$$

Evaluation of Q

The configuration integral, Q, can be found quite simply by using a nonrigorous method which does give physical insight into the limitations of the theory. The method deals with finding the potential energy of an ion which is shielded with a charge cloud.

Poisson's equation is written for the potential around an ion with the assumption that the potential is altered by the presence of a negative charge cloud.

$$\nabla^2 \psi = - \frac{\rho}{\epsilon_o} \tag{6.16}$$

The charge ρ is the net charge of a collection of positive and negative particles which is given by

$$\rho = e(n_i' - n_e') \tag{6.17}$$

where n_i' and n_e' are densities of the ions and electrons.

The n' quantities are determined from a Boltzmann distribution factor for charge distribution in a region of nonuniform potential. If n_e represents the average density of ions which equals the average density of electrons then n_i' and n_e' are given by

$$\begin{aligned} n_i' &= n_e \, e^{-e\psi/kT} \\ n_e' &= n_e \, e^{+e\psi/kT} \end{aligned} \tag{6.18}$$

The preceding equations can be combined to obtain a differential equation for ψ which is

$$\nabla^2 \psi = \frac{en_e}{\epsilon_o} \left(e^{e\psi/kT} - e^{-e\psi/kT} \right) \tag{6.19}$$

To solve the equation let $\psi = a_o \varphi / r$ so that

$$\nabla^2 \psi = \frac{a_o}{r} \frac{\partial^2 \varphi}{\partial r^2} \tag{6.20}$$

where a_o is the Bohr radius. Let x and a be defined by

$$x = \frac{rkT}{a_o e}, \quad a = \frac{e^4 n_e a_o^2}{\epsilon_o (kT)^3} \tag{6.21}$$

Then the differential equation becomes

$$\frac{\partial^2 \varphi}{\partial x^2} = ax(e^{\varphi/x} - e^{-\varphi/x}) \tag{6.22}$$

Assume that φ/x is much less than unity for $r > a_o$. An equivalent assumption is that

$$\frac{e\varphi}{kT} \ll 1 \quad \text{or} \quad \frac{e\psi}{kT} \ll 1 \tag{6.23}$$

The exponential terms may then be expanded in a series to linearize the equation with the result that

$$\frac{\partial^2 \varphi}{\partial x^2} = 2a\,\varphi \tag{6.24}$$

The solution is

$$\varphi = \frac{e}{4\pi\epsilon_o a_o} e^{-\sqrt{2a}\,x} \tag{6.25}$$

or in terms of the original variables, the solution is

$$\psi = \frac{e}{4\pi\epsilon_o r} e^{-r/h} \tag{6.26}$$

The quantity, h, called the Debye length, is given by

$$h = \sqrt{\frac{\epsilon_o kT}{2e^2 n_e}} \tag{6.27}$$

The coefficient of the exponential factor in the solution is determined by the condition that as a becomes small in the limit where the density n_e goes to zero, the potential around the ion in question must approach the free-space value.

By differentiation of the potential, the charge density about the ion can be determined. The density ρ is given by

$$\rho = - \epsilon_o \nabla^2 \psi = - \frac{e}{4\pi r h^2} e^{-r/h} \tag{6.28}$$

The calculation of the charge cloud density is restricted to a range of temperature and density which meets certain conditions. First of all, the assumption that $e\psi/kT \ll 1$ for $r > a_o$ introduces a restriction. The assumption is equivalent to the statement that the temperature must be sufficiently high that the probability of the existence of an electron in a bound state is very small. The limitation of r to values greater than a_o arises from the quantum theory where an electron cannot exist in an arbitrarily low energy state about an ion.

The validity of the concept of a charge cloud is restricted by the discrete nature of the charged particles. For the analysis to be valid, a great many particles of both charge polarities must exist in the cloud. Thus, the shielding distance must be sufficiently large that many particles are included. The number of particles within the Debye radius is given by

$$N = \frac{4\pi}{3} h^3 n_e \tag{6.29}$$

By expressing h in terms of n_e, N is given by

$$N = \frac{4\pi}{3} \left(\frac{\epsilon_o kT}{2e^2} \right)^{3/2} n_e^{-1/2} \tag{6.30}$$

Thus, as the density becomes large the approximation of a distributed cloud of charge becomes poor. The ion is shielded by strong interactions with a very few particles rather than by weak interactions with many particles.

To continue the derivation, the potential energy of the central ion in the field of the charge cloud is given by

$$\alpha = \int \frac{e}{4\pi\epsilon_o r} \rho \, dV \tag{6.31}$$

The volume integral over dV is replaced with the integral from o to ∞ of $4\pi r \, dr$ and the result of the integration is

$$\alpha = - \frac{e^2}{4\pi\epsilon_o h} \tag{6.32}$$

The energy of an electron in the field of the other particles is given by the same expression as for the ion. Thus, the total energy of the system is the sum over all charged particles of the system with a factor of 1/2 because the interactions between particle pairs are counted twice in the sum. The total energy per unit volume is

$$\frac{1}{2}(n_e\alpha+n_i\alpha) = -\frac{n_e e^2}{4\pi\epsilon_o h} \tag{6.33}$$

With this result for the interaction energy of the coulomb forces, the configuration integral Q can be determined. If the internal energy states of the various particles are temporarily neglected, the internal energy of the plasma is given by

$$U = \frac{2}{3}(N_e+N_i+N_n)kT - \frac{N_e e^2}{4\pi\epsilon_o h} \tag{6.34}$$

where N_γ is the product of volume and n_γ. Q can be deduced by working backward from this equation for U.

A similarity method described by Landau and Lifshitz (26) can be used to show that the general form of the partition function is

$$Z = T^{3N/2} V^N f(VT^{-3/n}) \tag{6.35}$$

where f is an arbitrary function, n is the degree of homogeniety of the potential function, and N is the sum of all the numbers of particles of different types. For Coulomb forces n is -1. The result stated by Landau and Lifshitz is somewhat less general than the one given here because they did not include the factor V^N.

If the function f is a constant then the equation is that for an ideal gas. The internal energy is

$$U = kT^2 \frac{\partial(\ell nZ)}{\partial T} = \frac{3}{2} NkT \tag{6.36}$$

and the pressure is

$$P = kT \frac{\partial(\ell nZ)}{\partial V} = \frac{NkT}{V} \tag{6.37}$$

For a nonideal gas, f is not a constant and the contribution to u from f is

$$kT^2 \frac{\partial(\ell nf)}{\partial T} = \frac{3kT^4V}{f} \frac{df}{d(T^3V)} \tag{6.38}$$

This quantity is equal to the energy of coulomb interaction, $\alpha/2\ (N_e+N_i)$, which may be expressed in terms of T, V, and N_e rather than h. Thus, a differential equation is obtained for the function f.

$$\frac{3kT^4V}{f} \frac{df}{d(T^3V)} = -\frac{b(N_i^{3/2}+N_e^{3/2})}{(VT)^{1/2}} \tag{6.39}$$

The constant b is given by

$$b = \frac{\sqrt{2}\ e^3}{8\pi\epsilon_o^{3/2}\sqrt{k}} \tag{6.40}$$

The equation for f has separable variables of f and T^3V and can be integrated to obtain

$$\ell n\ f = \frac{2b(N_i^{3/2}+N_e^{3/2})}{3k(T^3V)^{1/2}} \tag{6.41}$$

Thus the configuration integral Q can finally be written as

$$Q = V^{N_i+N_e+N_n} \exp \frac{2b(N_i^{3/2}+N_e^{3/2})}{3k(T^3V)^{1/2}} \tag{6.42}$$

Numerous authors have evaluated Q with a variety of methods. Their results are equivalent to the value just given when they are simplified from what is usually a more complex analytical description. Their more general calculations include higher order corrections than the Debye-Hückel theory yet the computations of higher-order effects are extremely complex.

Theimer and Gentry evaluated Q by expressing the potential energy of the system in terms of Fourier components of the particle density. (27, p. 93) They were able to obtain an integral of a product of functions of single variables whereas the potential energy is normally a complicated function of many variables.

Green developed an iterative procedure for evaluating the configuration integral and he obtained the Debye-Hückel result with some simplifying approximations. (28)

Mayer used the method of cluster expansions which has been described in detail by various authors. (22)

Equation of State

When the partition function is evaluated, the equation of state of the plasma can be determined. Here the phrase, equation of state, is considered to be a group of three equations which are commonly called the thermal or kinetic equation of state, the caloric equation of state, and Saha's equation. The equations are:

$$P = \frac{kT}{V} \sum_{\gamma} N_{\gamma} - \frac{b(N_e^{3/2}+N_i^{3/2})}{3V\sqrt{TV}} \tag{6.43}$$

$$U = \frac{3}{2} kT \sum_{\gamma} N_{\gamma} - \sum_{\gamma} N_{\gamma} E_o^{\gamma} - \frac{b(N_e^{3/2}+N_i^{3/2})}{\sqrt{TV}} \tag{6.44}$$

$$\frac{n_e n_i}{n_n} = \frac{B_e B_i}{B_n} \left(\frac{2\pi mkT}{h^2}\right)^{3/2} \exp \frac{\left(-\chi+2a\sqrt{\frac{n_e}{T}}\right)}{kT} \tag{6.45}$$

The equations are subject to the condition for charge conservation that $n_e = n_i$. Then for two variables such as T and P, the equations can be solved for the other variables.

Molecular formations were neglected in the partition function formulation so that the expression for U does not include the energy of dissociation of the water molecule. If U is to represent internal energy relative to the normal state of water then a correction term must be added to account for dissociation and other minor effects such as the energy of vaporization. If d is the energy per atom, which is $5.2\ 10^{-19}$ J, then U is increased by the term

$$(N_n+N_i)d \tag{6.46}$$

Modification of the Debye-Hückel Theory

Because of the limitations of the Debye-Hückel theory, numerous authors have suggested corrections to the theory.

Theimer and Gentry showed that any classical theory which attempts to calculate a finite energy for a system of point charges without a repulsive core must produce the Debye-Hückel result. (27, p. 95) Thus, they suggest that the Debye-Hückel energy be multiplied by the factor $1/(1+\sigma/n)$ to introduce the effect of a repulsive core of radius σ.

Ecker and Kroll determined a correction to the ionization potential in Saha's equation which was based upon the Debye-Hückel theory for low densities but which was modified for densities above a certain critical density. (29)

Rouse has suggested that the correction to the ionization potential should be the Debye-Hückel correction times the factor

$$\left(\frac{1}{1+\sqrt{\frac{2a_o}{h}}}\right)^2 \tag{6.47}$$

where a_o is the Bohr radius. (20, p. 663) The modified correction asymptotically approaches the ionization potential in the high density limit.

Comparison of Theory and Experiment

The plasma consisted of both hydrogen and oxygen ions. An analysis of the plasma would normally require a Saha equation for each type of ion. However, because the two types of ions have nearly identical ionization potentials, the calculations could be simplified.

Average ionization potentials and average ratios of excited state partition functions were used in a single Saha equation as if there were a single type of ion. Sample computations with two Saha equations showed that the approximation of using one equation was very good. With one equation the computations were much simplified.

Ionization of oxygen beyond the first level was neglected because the temperature was too low for significant ionization to occur in the second level. The condition was thus imposed that the number of free electrons was equal to the number of ions.

Excited state partition functions, B_i and B_n, were computed from tables of energy levels and degeneracies for the various particles. Figures were taken from a tabulation by Moore. (30) For hydrogen the first two terms of the summation were included. For oxygen, terms were taken through the level of 9.13 eV, and for the oxygen ion, terms were taken through 5.01 eV. The selection of terms was based upon the relative magnitudes of the terms

and upon the amount of volume available to each particle.

Harris has suggested that the perturbations of internal energy levels should be included in a calculation of plasma properties. (31) Such perturbations are not a part of the Debye-Huckel theory and they would be difficult to compute. Therefore, they are not included.

The correction factor which was proposed by Rouse was introduced into the equations for P and U as well as into the Saha equation. The results with the correction factor were not significantly different from the Debye-Huckel results when the ionization potential correction term was less than the ionization potential. The Rouse modification was significant for conditions where the Debye-Hückel correction term exceeded the ionization potential.

Calculations were performed by determining P, u, n_i and n_n as functions of n_e for some temperature which was treated as a parameter. Results of the theoretical calculations for two different temperatures are plotted in Fig. 24 as a function of the density of ions and atoms taken together.

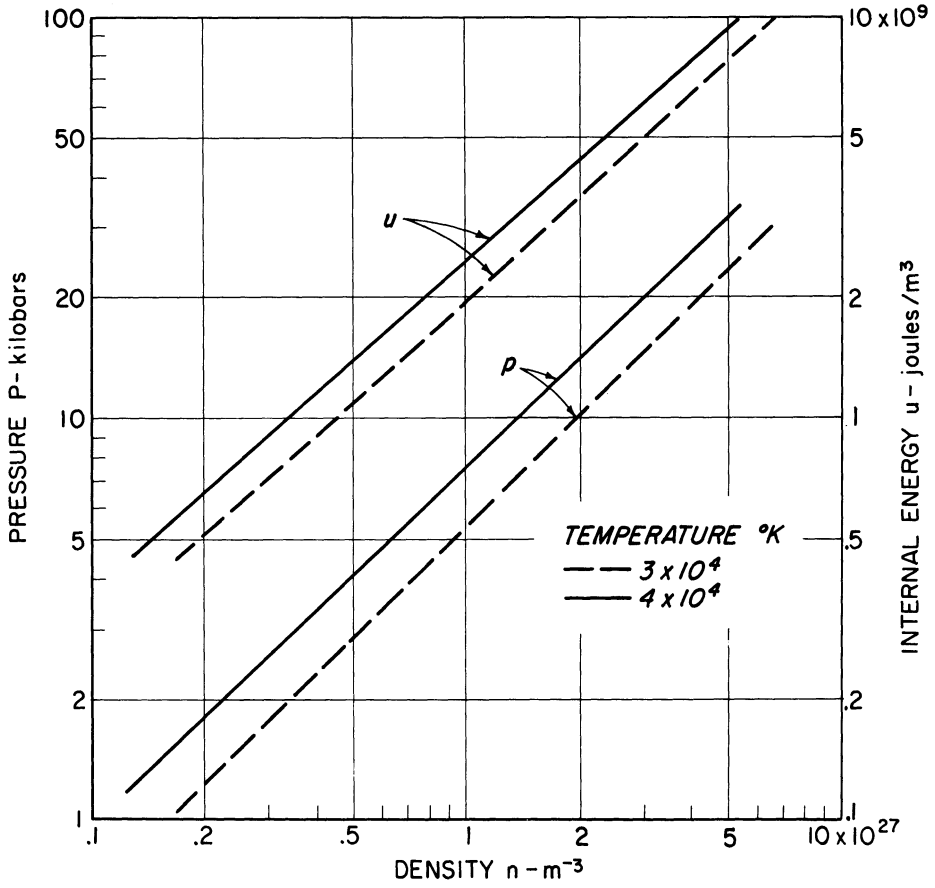

Fig. 24. Calculations of pressure and internal energy as functions of density from the Debye-Hückel theory.

A comparison of theory and experiment is shown in Table 8. For a given pressure, the predicted value of internal energy is much lower than the measured value. The theory is so inadequate that modifications or extensions can hardly be expected to be of much help. Thus an entirely new approach is necessary.

TABLE 8

COMPARISON OF DEBYE-HÜCKEL THEORY WITH MEASURED DATA

Pressure, kilobars	Temperature, °K	Measured internal energy, J/mm^3	Internal energy from theory, J/mm^3
4	38 000	8.4	1.4
7.7	32 000	16	2.8

The failure of the Debye-Huckel theory is not surprising because of the number of particles included in the Debye sphere. If the number is evaluated for a temperature of 30 000°K and an electron density of 5×10^{26}, the result is that $N = 0.113$ when it should be much larger than unity if the theory is to be valid.

VII. VIRIAL THEOREM

The virial theorem is used here as the basis for the derivation of an equation of state to replace the result of the Debye-Hückel theory. The use of the virial theorem is fundamentally equivalent to the use of the partition function. (32, p. 136) However, the form of the virial theorem is adaptable to a different interpretation of particle interactions which leads to significantly different results.

Once again the discussion is limited to the case of the plasma without explosive confinement. Although the method is sufficiently general to include the results at high pressure the interpretation would be exceedingly difficult.

In the preceding chapter the inherent classical limitations of the Debye-Hückel theory were noted. To avoid those limitations, the computations of this chapter are based upon the quantum-mechanical form of the virial theorem which, for particles with coulomb interactions, is (32, p. 69)

$$\int \psi^* \left(\sum_j \frac{-h^2}{2m_j} \frac{\partial^2}{\partial x_j^2} \right) \psi \, dr = -\frac{1}{2} \int \psi^* \varphi \, \psi \, dr + \frac{3}{2} P \qquad (7.1)$$

The differential dr is the product of the factors, dx_j, for each of the coordinates and the potential φ is the sum over all particle interactions. ψ is the wave function. $3/2\ P$ describes the effects of external pressure upon the system of particles for unit volume.

Virial Theorem for a Single Atom

As an illustration of the interpretation of the quantum mechanical formulation, the virial theorem is applied here to a hydrogen atom. The wave function for the atom is a product of wave functions for translational motion of the atom and for orbital motion of the electron. When normalized to a unit volume, the wave function for the ground state is

$$\psi = \prod_{j=x,y,z} \exp\left(\frac{i \sqrt{2ME_j}\, x_j}{\hbar} \right) \frac{1}{(\pi a_o)^{3/2}} e^{-r/a_o} \qquad (7.2)$$

E_j is translational energy for the j coordinate; M is atomic mass; a_o is the Bohr radius given by $4\pi\epsilon_o \hbar^2/me^2$. The potential energy is

$$\varphi = \frac{-e^2}{4\pi\epsilon_o r} \qquad (7.3)$$

The sum over j of the second partial derivatives with respect to the coordinates is expressed as the sum of the Laplacian of the center of mass in rectangular coordinates plus the Laplacian of the electron coordinates relative to the ion in spherical coordinates. The terms in the virial equation can then be evaluated.

The integration is performed over the volume for both sets of coordinates. Unit volume is selected for the translational coordinates. For the electron motion, the integral includes all of space with the differential volume in spherical coordinates being

$$r^2 \sin\theta \, dr \, d\theta \, d\varphi \tag{7.4}$$

The result of the calculations is

$$\sum_j E_j + E_o = -\frac{1}{2}(-2E_o) + \frac{3}{2}P \tag{7.5}$$

The sum over E_j is identified in terms of temperature as $3/2\ kT$; E_o is the energy of motion of the electron given by $e^2/8\pi\epsilon_o a_o$; $-2E_o$ is the expectation value for the potential energy; P is the pressure. The kinetic energy of the electron is one half the absolute value of the potential energy.

For n noninteracting atoms per unit volume the result is

$$n\left(\frac{3}{2}\ kT\right) + n\,E_o = n\,E_o + \frac{3}{2}P \tag{7.6}$$

which is the ideal gas equation. The contributions from the electron states cancel.

Virial Theorem for Interacting Particles

The virial theorem can be written for a collection of charged particles without distinguishing whether or not the particles exist in atomic states, molecular states, or ionized states. All different forms are manifestations of coulomb interactions so that the equation is perfectly general. However, for this analysis the molecular states will not be considered. The description of such states would be very difficult.

The term in the virial theorem which arises from the expectation value of the potential energy is denoted by A and the term from the expectation value of the Laplacian operator is denoted by B. The terms correspond to

potential energy and kinetic energy of classical physics. Thus, the virial theorem is

$$\frac{3}{2} P = B + \frac{1}{2} A \tag{7.7}$$

where B includes the kinetic energy of bound electron states as well as the kinetic energy of translation. With n electrons and n ions per unit volume the equation can be written in terms of average kinetic and potential energies per pair of particles as

$$\frac{3}{2} \frac{P}{n} = b + \frac{a}{2} \tag{7.8}$$

or

$$\frac{P}{n} = \frac{2b}{3} + \frac{a}{3} \tag{7.9}$$

Energy Equation

The internal energy per unit volume of the plasma is determined relative to the internal energy of water under normal conditions. The energy is determined which would be used in an imaginary process to convert water from its normal state to a state of complete dissociation and ionization at zero temperature. Then the kinetic and potential energies, B and A, are added to that energy to obtain the complete expression for internal energy.

The energy for the imaginary process of separating the electrons and ions at zero temperature is principally the sum of dissociation energy and ionization energy times the number of particles. Also, included in the sum are minor terms such as the energy of vaporization. For water the dissociation energy of a molecule is 15.03×10^{-19} joules or 5.01×10^{-19} joules per atom. The ionization energy for either type of atom is 13.55 ev or 21.7×10^{-19} joules. From other effects there is a contribution of 0.2×10^{-19} joules so that the sum of all effects is 26.9×10^{-19} joules which will be denoted by f. Thus, internal energy is given by

$$u = n(f+a+b) \tag{7.10}$$

Limiting Cases

The virial equation and the energy equation reduce to ideal gas equations for appropriate conditions. The case is considered here of a partially ionized gas of noninteracting particles.

If the fraction of atoms which are ionized is X, then the kinetic energy per particle pair is

$$b = (1+X)\frac{3}{2}kT + (1-X)E_o \tag{7.11}$$

which is the sum of translational energies of the free particles and orbital kinetic energies of the bound electrons. The potential energy is

$$a = (1-X)(-2E_o) \tag{7.12}$$

Therefore, P and u can be expressed in terms of X as follows:

$$\frac{P}{n} = (1+X)kT \tag{7.13}$$

$$\frac{u}{n} = f + (1+X)\frac{3}{2}kT - (1-X)E_o \tag{7.14}$$

When X is zero, the equations represent a neutral ideal gas and when X is unity, the equations represent a fully ionized ideal gas

Plasma Model

A plasma model must be constructed for the evaluation of the quantities, a and b, so that the virial equation and the energy equation can be used for calculating the plasma properties. A very simple model is presented here, not with the intention of obtaining an accurate theory, but with the intention of illustrating the type of particle interaction which causes the plasma to be so very different from the Debye-Hückel description. Improvements upon the model might eventually lead to a quantitatively accurate theory.

The model consists of a collection of hydrogen ions and electrons. Although the plasma also contains oxygen ions, they are treated as if they were hydrogen. The approximation is supported by the fact that hydrogen and oxygen have the same ionization potential.

According to the criterion mentioned by Harris, an electron is considered to be free if its energy is greater than zero. (33, p. 1834) More explicitly, the kinetic energy of the electron must exceed the depth of the potential well in which it is located. For an electron near an ion the criterion becomes

$$\frac{3}{2}kT \geq \frac{e^2}{4\pi\epsilon_o r} \tag{7.15}$$

At 30 000°K, r must be greater than 3.71 Å if the electron is to be free.

Each ion can be assigned a radius determined by the average volume per ion by the equation

$$\frac{4\pi}{3} r_o^3 = \frac{1}{n} \tag{7.16}$$

and for a typical density of 10^{28} m^{-3}, r_o is 2.88 Å.

Therefore, the electron cannot possibly be so far away from an ion that it can be considered free. The situation is somewhat analogous to the case of electrons in a metal where the electrons are mobile yet trapped within the metal. Energy equivalent to the work function is needed to free such electrons.

However, the plasma electrons do not behave as electrons in a metal because of the random locations of the ions. The high mobility of electrons in a metal depends upon the regular array of ions in the crystal lattice. As the metal temperature is raised the lattice structure is perturbed and the mobility is decreased. The plasma might be considered as a metal at such extremes of temperature that the lattice structure is completely destroyed. Thus, the electron mobility would be low compared with the mobility of electrons in metal.

The electrons are considered to exist in quantum states which are established by small clusters of ions. An electron in such a state is then localized to the region of that cluster. As Harris has suggested, the electron is not a free particle and does not contribute to external pressure through translational degrees of freedom. (31, p. 430)

The electron quantum states change rapidly with time because the high velocities and high densities of the ions produce a very high collision rate among the ions. (3, p. 261) The time that an electron can be identified with any particular quantum state is probably less than 10^{-10} sec because of the rate at which the ion configurations change.

Calculation of Energies a and b

The equation of state of the plasma is obtained by calculating a and b as functions of temperature and density. To perform the calculations several simplifying assumptions are made. The gross aspects of the plasma behavior then become apparent.

The first assumption is that the kinetic energy of the ions is 3/2 nkT. The temperature is sufficiently high that the ion gas can be treated classically with each degree of freedom contributing 1/2 kT of energy.

The total kinetic energy per pair of particles is $3/2\ kT$ plus the kinetic energy of the electron in its quantum state which is given by b'. Thus b is given by

$$b = b' + \frac{3}{2} kT \tag{7.17}$$

The assumption is made that the potential energy is given completely in terms of the potential energy of the electrons in the field of the ions. That is, the quantity a is the average potential energy of the electrons in the quantum states. The electron-electron and ion-ion interactions are neglected as being small compared with the electron-ion interactions. The neglect of like particle interactions is suggested by the Wigner-Seitz calculation of the cohesive energy of sodium in which the contribution was minor. (34)

The average kinetic and potential energies of the electrons are related by some factor, g, which is defined by

$$b' = - g\, a \tag{7.18}$$

For a collection of isolated hydrogen atoms, g must be $1/2$ because of the results of the virial theorem for a single atom. Yet, in general, g will be different from $1/2$ because the quantum states of the electrons will be determined by potentials other than isolated coulomb potentials. If the quantities a and b' are replaced with g and with $c = a+b'$, which is the average total energy of the electron, then the virial equation and the energy equation become

$$\frac{P}{n} = kT + c\,\frac{1-2g}{3(1-g)} \tag{7.19}$$

$$\frac{u}{n} = \frac{3}{2} kT + f + c \tag{7.20}$$

The significance of g becomes apparent from these equations. For g of $1/2$, the equations reduce to the neutral ideal gas equations. However, when g is different from $1/2$, a correction term is introduced into the pressure equation. Thus, a relation has been established between the distortion of the electron quantum states in terms of g and the pressure correction in the equation of state.

Whether the correction to the pressure equation is positive or negative depends upon whether g is greater or less than $1/2$. (The quantity c which is the bound state energy is less than zero.) The physical interpretation of g depends upon the amount of confinement of the electron. For the case of

interest here, the electron is not as tightly confined as for an isolated atom because it has quantum states defined over a cluster of ions. In such a case b' is less than -1/2 a. However, for the hydrogen atom in a rigid spherical container the volume available to the electron is restricted and the kinetic energy of the electron is larger than -1/2 a. The application of the model of the restricted atom to a study of the compression of solids is discussed in the literature. (32, pp. 264-271)

To evaluate c and g, a series of quantum states for the electrons must be defined in such a way that average values of a and b' can be computed over the series. The series is very complex because of the variety of ion configurations which give rise to the quantum states; the accuracy of the results depends upon how well the states can be represented. A simple model is used here to obtain some equations which show orders of magnitude for P and u.

The average total energy c is evaluated by assuming the available states to be the first two energy levels of the unperturbed hydrogen atom. The first two levels are chosen because the Bohr radius of the second state is less than the radius of a sphere with a volume equal to the volume per atom, while the Bohr radius of the third state greatly exceeds the sphere radius. A more rigorous analysis would account for perturbations of the energy levels which would produce a spectrum of energies over the range limited approximately by the two states which were chosen.

The energy levels of the states are -13.55 ev and -3.4 ev while the degeneracies are 2 and 8. The Fermi distribution function determines the distribution of electrons in the states. In terms of Fermi energy E_f and the state energies of E_0 and E_1, and the ratio of numbers of electrons in the two types of states is

$$\frac{n_1}{n_0} = \frac{g_1}{g_0} \frac{e^{\frac{E_0-E_F}{kT}} + 1}{e^{\frac{E_1-E_F}{kT}} + 1} \qquad (7.21)$$

The Fermi energy is determined by the condition that

$$\frac{n_0}{n} = \frac{g_0}{e^{\frac{E_0-E_F}{kT}} + 1} \qquad (7.22)$$

where n is the sum of the numbers of electrons in the two states.

The energy c is determined from the ratio of the particle densities by finding the fraction of the total number of electrons in each state and summing over the energies of each state to obtain

$$c = \frac{n_1}{n} E_1 + \frac{n_o}{n} E_o \tag{7.23}$$

Results are given in Table 9 for various temperatures.

TABLE 9

AVERAGE ELECTRON ENERGY c

Temperature, °K	E_f, volts	n_1/n_o	n_o/n	c, joules
3.0×10^4	-14.23	0.137	0.880	-19.7×10^{-19}
3.2	-14.41	0.170	0.855	-19.4
3.8	-15.07	0.283	0.780	-18.1
4.0	-15.30	0.328	0.753	-17.7

The equation of state is much more sensitive to the value of g than it is to the value of c, which was just calculated. Even though perturbations were neglected in the computation of c, they must be considered in the calculation of g. In general, g can be found by evaluating b' and a with an average over the Fermi distribution of electrons in the various perturbed quantum states.

The calculation of g can be simplified if the perturbed states are defined in terms of a distorted coulomb potential which is given by

$$\varphi = K r^{n'} \tag{7.24}$$

where n' is different from -1. By the virial theorem, the kinetic energy of an electron in such a state is given by

$$b' = \frac{1}{2} \int \psi^* \left(r \frac{\partial \varphi}{\partial r} \right) \psi \, dr = \frac{1}{2} n' \int \psi^* \varphi \, \psi \, dr \tag{7.25}$$

where n' is the degree of homogeneity of the potential function. When n' is equal to -1, the result is that $b' = -1/2\, a$, but, in general, b' and g are given by

$$b' = \frac{1}{2} n' a , \quad g = -\frac{1}{2} n' \tag{7.26}$$

where a is given by

$$a = \int \psi^* \varphi \psi \, dr \tag{7.27}$$

The basis for a computation of n' is illustrated in Fig. 25. Two ions are located a distance of $2r_o$ from each other where

$$\frac{4\pi}{3} r_o^3 = \frac{1}{n} \tag{7.28}$$

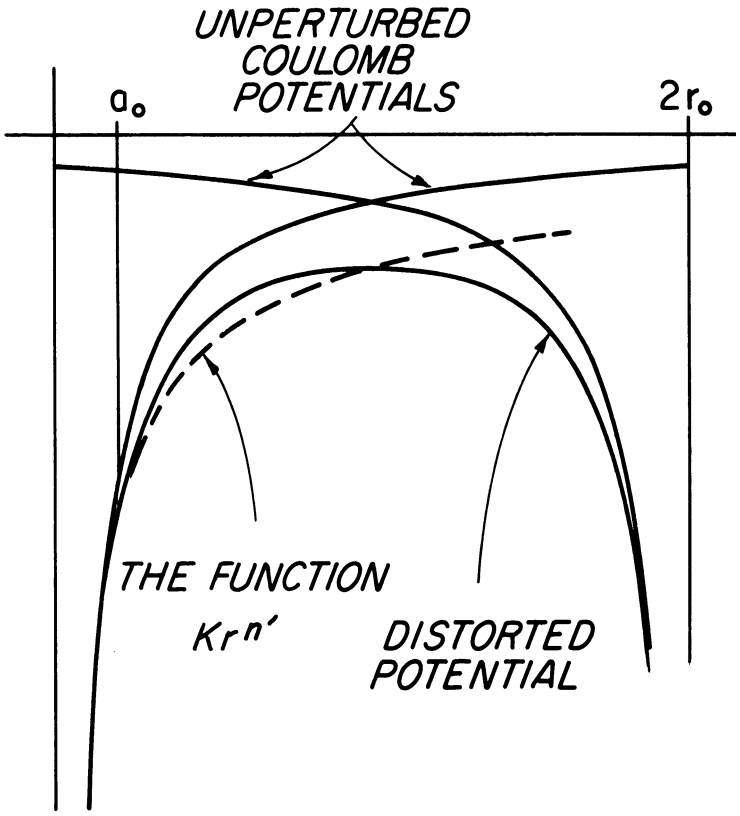

Fig. 25. Determination of the function $K r^{n'}$.

The potential along a line joining the ions is evaluated by summing the potentials of each ion. The combined potential is approximated by $K r^{n'}$, the constants of which are evaluated by setting the function equal to the distorted potential function for r equal a_o and for r equal r_o. The two conditions determine K and n'. Thus, the exponent n' is determined as a function of the ion density n. Results are shown in Table 10.

TABLE 10

THE DISTORTION PARAMETER g

n, m^{-3}	r_o, Å	n'	g
1×10^{27}	6.20	-0.737	0.369
3	4.28	-0.699	0.350
7	3.24	-0.664	0.332
10	2.88	-0.647	0.324
20	2.28	-0.612	0.306
30	1.99	-0.583	0.292

Comparison of Theories and Data

With c and g known as functions of T and n, the virial equation and the energy equation can be solved for P and u in terms of T and n. Results are shown graphically in Fig. 26. Also the magnitude of the correction term in the pressure equation is compared with kT in Table 11.

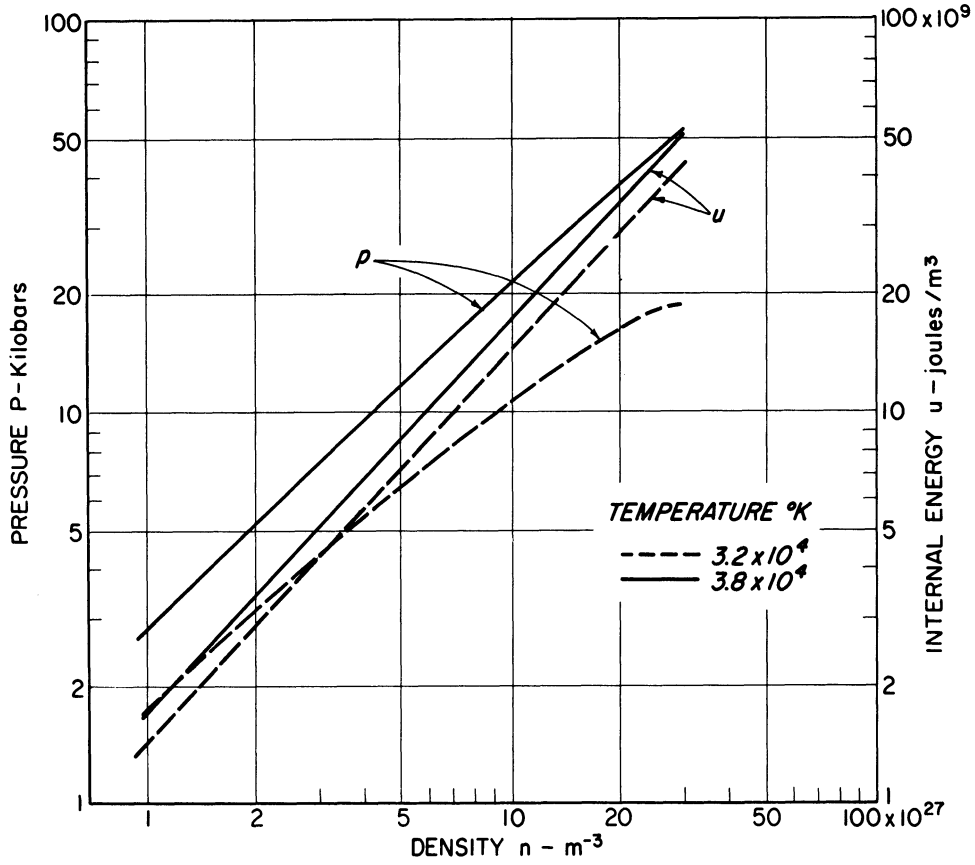

Fig. 26. Pressure and internal energy as predicted by the virial theorem.

TABLE 11

PRESSURE EQUATION CORRECTION TERM

(in joules)

Density n, m^{-3}	Temperature	
	32 000°K	38 000°K
	$kT = 4.42 \times 10^{-19}$	$kT = 5.24 \times 10^{-19}$
1×10^{27}	-2.70×10^{-19}	-2.52×10^{-19}
3	-2.99	-2.79
7	-3.26	-3.04
10	-3.38	-3.15
20	-3.61	-3.37
30	-3.79	-3.53

The principal difference between the results of the virial theorem and the results of the Debye-Hückel theory are readily seen. Although internal energy per particle is nearly the same in the two cases, the virial theorem predicts a strong condensation so that a much greater density of particles is obtained at a given pressure than for the Debye-Hückel theory. Because of the higher particle density, a higher internal energy per unit volume is obtained.

The strong condensation which has been observed is supported by an experiment done by Cook and McEwan. (35) The retention of size and shape of a plasma, consisting of a detonating explosive material, implied that strong cohesive forces existed in the plasma.

Measured data and the results of each theory are compared in Table 12. Although there is not close agreement between the results of the application of the virial theorem and the data, the virial theorem is a significant improvement over the Debye-Hückel theory. With a more detailed analysis, the method based upon the virial theorem might produce quantatively accurate results. However, such an analysis is not attempted in the present work.

The parameter g can be evaluated from experimental data instead of being calculated theoretically if the energy c is known. When c is known, the density n is determined from the measurement of u. Then the only unknown in the equation for P is the parameter g. The values of c from Table 9 were used to determine g for the measured data. Results are shown in Table 13. Because the values of g are substantially different from $1/2$, the perturbations of the electron wave functions are large and theoretical computations of the perturbed levels would be difficult.

TABLE 12

COMPARISON OF DATA WITH PREDICTIONS
OF THE VIRIAL THEOREM AND THE DEBYE-HÜCKEL THEORY

State	Measured internal energy, J/m^3	Virial theorem		Debye-Hückel theory	
		Internal energy, J/m^3	Density, $atom/m^3$	Internal energy, J/m^3	Density, $atom/m^3$
4 kilobars 38 000°K	8.4×10^9	2.6×10^9	1.5×10^{27}	1.4×10^9	0.55×10^{27}
7.7 kilobars 32 000°K	16	9	6.4	2.7	1.4

TABLE 13

PARAMETER g AND DENSITY n
DETERMINED FROM DATA WITH VALUES OF c TAKEN FROM TABLE 9

State	n, $atom/m^3$	g
4 kilobars 38 000°K	5.03×10^{27}	0.207
7.7 kilobars 32 000°K	11.3	0.297

VIII. THE PLASMA AT 115 KILOBARS

Because the plasma at 115 kilobars is much cooler than the plasmas at lower pressures, it has entirely different properties. At the temperature of 10 000°K the fraction of particles which are ionized is approximately 10^{-4} according to Saha's equation and many of the atoms are bound in molecular form. The plasma is therefore treated as a neutral gas which is in an equilibrium state of partial molecular dissociation. Because of the high densities, a correction of the van der Waals form expressed as $P(1-b)$ is included in the equation of state.

The irregular formations of plasma to be discussed in Section IX suggest the possibility of a highly conductive state at even lower temperatures of 6000 to 7000°K. The electrons are apparently mobile because of the high density even at the low temperature. The possibility of such a state is supported by the calculations of Harris. (33, p. 1836) However, for the plasma temperature of 10 000°K, the discussion is limited to the conventional model of thermal dissociation and ionization.

Equations for Analysis

As in the Debye-Hückel theory for the plasma at lower pressure, a pressure equation and an internal energy equation are required. A Saha equation for ionization is not needed because the fraction of ionization is too low to effect either u or P. However, dissociation equations are required in place of Saha equations.

The pressure equation is

$$P(1-b) = \left(\sum_i n_i\right)kT \tag{8.1}$$

where the sum includes the densities of each of the molecular species which exist. The correction b is the van der Waals covolume normalized per unit volume of plasma rather than per mole. In general, b cannot be equated to handbook values of covolume which apply near the critical points of gases.

Internal energy is given by

$$u = \frac{1}{2}kT\sum_i (f_i n_i) + tn_n - \sum_i n_i D_i \tag{8.2}$$

The number of degrees of freedom of a molecule of type i is given by f_i which includes the contributions of rotation and vibration as well as translation. The temperature is sufficiently high so that all types of molecular

motion are classical. Thus, for an atom, $f_i = 3$, and for a diatomic molecule, $f_i = 7$. The expression tn_n represents the energy required to convert water from its normal state to a collection of neutral atoms at zero temperature. The number of atoms is n_n and the energy per atom is $t = 5.21 \times 10^{-19}$J which consists mainly of dissociation energy. The expression for internal energy is then reduced by the sum of dissociation energies D_i of molecules in nondissociated states.

For a molecular equilibrium reaction given by

$$a + b \rightleftarrows ab \tag{8.3}$$

where a and b are atoms, the dissociation equation is (36, p. 320)

$$\frac{n_a n_b}{n_{ab}} = \frac{g_a g_b}{g_{ab}} \frac{(2\pi MkT)^{3/2}}{8\pi^2 IhkT} (1-e^{-s}) e^{-D/kT} \tag{8.4}$$

The constants are given by

g = statistical weight of the atom or molecule
M = reduced mass—$M_a M_b/(M_a+M_b)$
I = moment of inertia of molecule
h = Planck's constant
s = $h\nu/kT$
ν = fundamental frequency of vibration of the molecule
D = dissociation energy

Three types of reaction are considered in this calculation. They are the three types of two-particle interaction given by

$$\begin{aligned} H + H &\rightleftarrows H_2 \\ O + O &\rightleftarrows O_2 \\ O + H &\rightleftarrows OH \end{aligned} \tag{8.5}$$

Reactions involving three atoms are neglected as being of secondary importance. The inclusion of such reactions would complicate the system of equations considerably. Also the dissociation equation is intended only for two atom reactions. P and u would each be less for a given density if three atom interactions were considered.

Molecular parameters were obtained from Russell and from a tabulation of molecular properties in Leighton. (36, p. 322; 37) Table 14 shows the numerical values needed for the calculations.

TABLE 14

NUMERICAL CONSTANTS FOR USE IN THE DISSOCIATION EQUATIONS

	$\frac{g_a g_b}{g_{ab}}$	M, amu	I	$h\nu/k$	D
H_2	4	0.504	0.459×10^{-47}	6620	7.15×10^{-19}
O_2	27	8.00	19.33	2270	8.13
OH	3	0.948	1.482	5370	6.97

The constant ratio of hydrogen atoms to oxygen atoms imposes the condition that

$$n_H + 2n_{H_2} + n_{OH} = 2(n_O + 2n_{O_2} + n_{OH}) \tag{8.6}$$

Calculations

The equations are solved at 10 000°K for different particle densities. The procedure is to assume a value for n_H, the density of uncombined hydrogen atoms, and to compute the other densities from the dissociation equations. Then u and P(1-b) can be determined from the densities.

The three dissociation equations can be evaluated at 10 000°K by using the molecular parameters with the results as follows:

$$\frac{n_H^2}{n_{H_2}} = a_H = 6.52 \times 10^{27}$$

$$\frac{n_O^2}{n_{O_2}} = a_O = 13.6 \times 10^{27} \tag{8.7}$$

$$\frac{n_O n_H}{n_{OH}} = a_{OH} = 3.76 \times 10^{27}$$

These results can be combined with the equation which fixes the ratio of hydrogen to oxygen to obtain an expression for n_O in terms of n_H which is

$$n_0^2 \frac{4}{a_0} + n_0\left(2 + \frac{n_H}{a_{OH}}\right) - \left(n_H + \frac{2n_H^2}{a_H}\right) = 0 \qquad (8.8)$$

A plot of results as a function of n_n, the total number of atoms whether or not in molecular association is shown in Fig. 27.

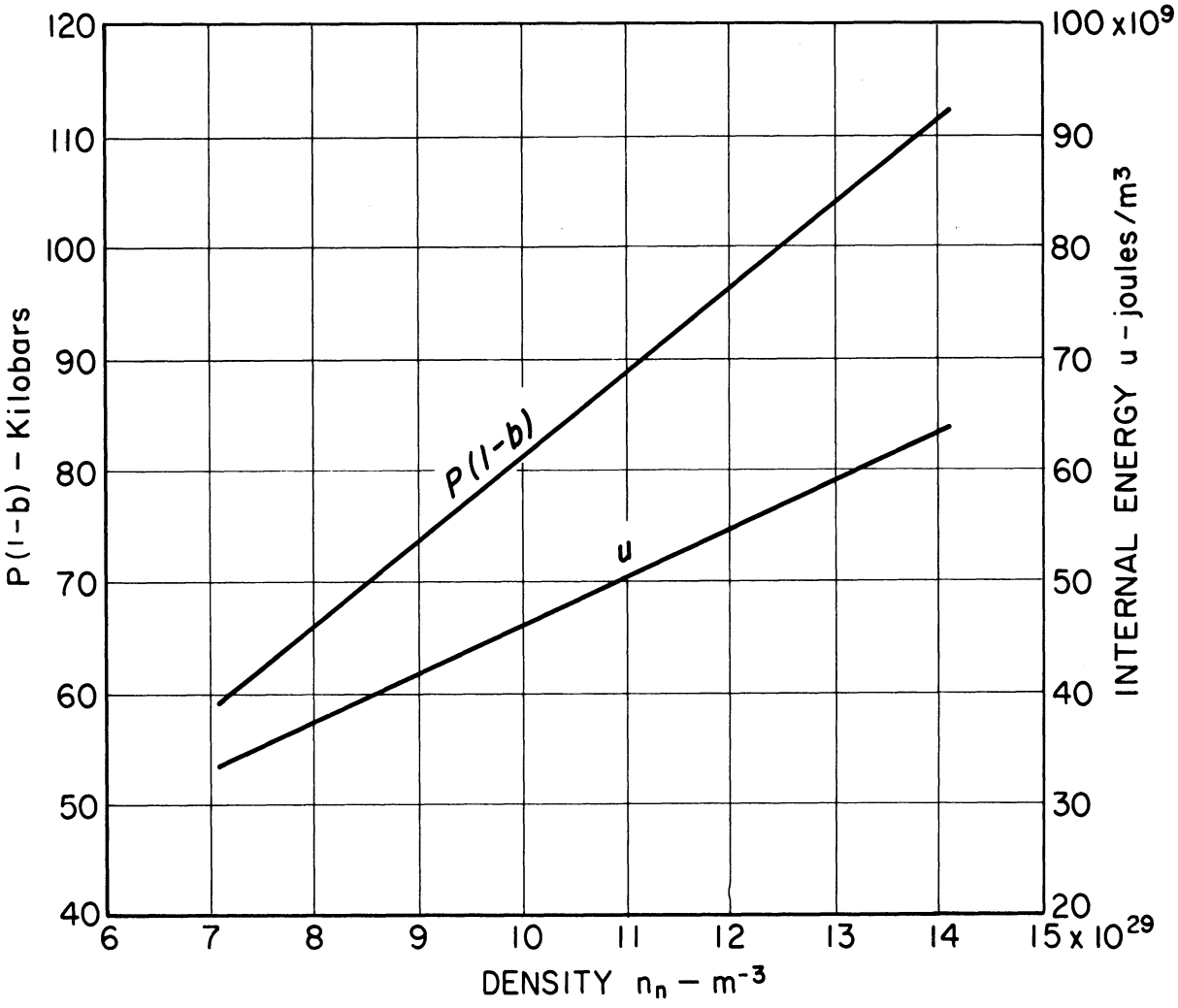

Fig. 27. Calculations of P(1-b) and u for plasma at 10 000°K.

Interpretation of Calculations

The experimentally measured value for u of 50 x 10^9 joules per cubic meter at 115 kilobars corresponds to a value for P(1-b) of 88 kilobars according to the results of the calculations. Thus, b has a value of 0.307. This value of b will be shown to be a reasonable expectation of the plasma model.

In the van der Waals equation which is normally applicable near the critical point, the constant b' (per mole) is one third of the critical volume. The constant has been tabulated for many different gases. However, b' cannot be a true constant because otherwise pressure would become infinite as volume per mole approached b'. In general, b' is a decreasing function of both density and temperature.

For the plasma at 115 kilobars, b can be shown to be less than the handbook value which, for water, is 0.0305 liter per mole. With 3 atoms per molecule of water, b' becomes 1.66×10^{-29} cubic meters per atom. In terms of n_n, the number of atoms per cubic meter, the handbook value for b' in dimensionless form is

$$b' = \frac{n_n}{6.02 \times 10^{28}} \tag{8.9}$$

However, from the calculations, n_n equals 1.09×10^{29} and b equals 0.307. Thus, b must be given by

$$b = \frac{n_n}{35.5 \times 10^{28}} \tag{8.10}$$

and the effective value of b is found to be approximately one fifth of the handbook value.

The value for b can be checked in terms of the density of water which has been compressed by the explosive shock wave with no electrical discharge. When the shock front passes through water, the atomic density, n_n, becomes 1.6×10^{29} and the temperature becomes nearly 1000°K at 115 kilobars. (13) If the kinetic contribution to pressure is assumed to be $n_n kT/3$ where the number of molecules is 1/3 the number of atoms, then the pressure equation is

$$P\left(1 - \frac{n_n}{K'}\right) = \frac{n_n kT}{3} \tag{8.11}$$

If numerical values are substituted, the denominator of b, designated as K', becomes 17.1×10^{28} and b becomes

$$b = \frac{n_n}{17.1 \times 10^{28}} \tag{8.12}$$

This value of b is somewhat larger than the value from the plasma measurements which is reasonable because of the lower temperature. However, it is

smaller than the handbook value which certainly does not apply in this case.

Therefore, the value for b, which was determined from the measurements, lies in a region which is acceptable. Certainly b should be less than the handbook value and not greatly different from the value obtained with an analysis of the explosively compressed water.

IX. ADDITIONAL OBSERVATIONS AND INTERPRETATIONS

The first attempts to confine plasma with pressure from an explosive charge produced some unexpected plasma growth characteristics. The electrical discharge was timed to begin after the shock wave from the explosive had swept over the discharge electrodes and surrounded them with a region of water at high pressure. The plasma then grew in an irregular pattern which was formed from two types of conducting media at significantly different temperatures.

To avoid the irregular growth, a uniform plasma column was formed before the shock wave reached the electrodes. Then the shock front passed through the plasma and compressed it to a uniform column at high pressure. The plasma column and the water around it had different shock propagation characteristics so that reflected shock waves were generated wherever the front passed through an interface. Thus, the plasma column was not as uniform as it might have been if the first attempt to produce a uniform plasma had been successful. Furthermore, with the latter method, the plasma column split into two parallel columns of plasma after about 1.0 μsec of uniform growth.

Irregular Plasma Growth

When the high pressure from the explosive charge was established about the tungsten initiating wire before the discharge began, the plasma formation was very irregular. Several tests were performed at different rates of current rise and at different pressures with the pressure depending upon the distance of the plasma from the explosive charge. The irregular growth occurred in all cases.

A delay of a few tenths of a microsecond often occurred after the discharge was triggered before appreciable current began to flow. Light-emitting plasma was formed at the time that the current flow was established. Thus, the tungsten wire was not as effective in initiating the plasma formation as it was in the case without the high pressure about the wire.

The type of formation which occurred is illustrated in Fig. 28. Current flows horizontally in the photograph. The plasma consisted of several globular regions of hot plasma which were separated from each other by regions of cool plasma. Apparently, there was no continuous column of hot plasma which connected the electrodes and which might have been the principal path of current flow. Because of the lack of a continuous hot column, the cool regions as well as the hot regions had to carry discharge current.

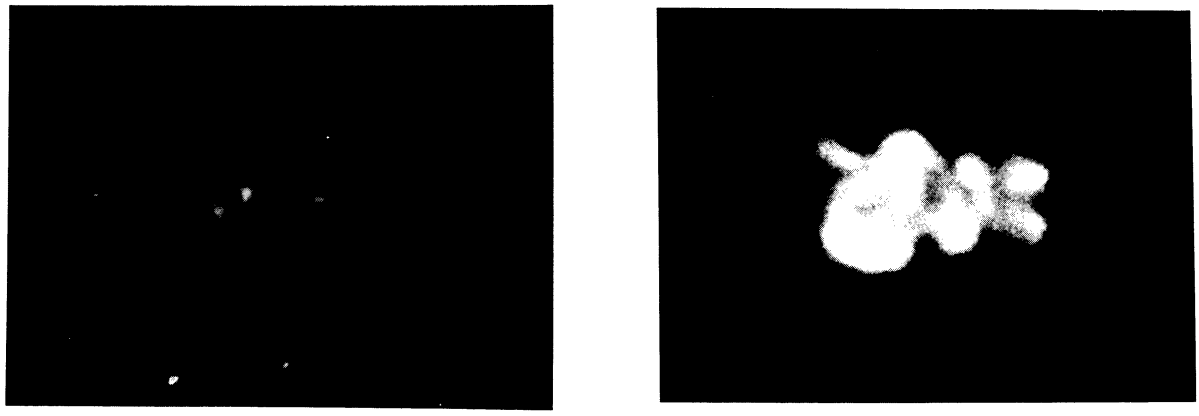

Fig. 28. Two photographs showing the irregular growth of a plasma column formed in explosively compressed water.

The irregularities in the 100 kilobar plasmas do not fade out with time but they actually become more pronounced. The various regions also maintain their identity over a period of time. Two photographs of the same test show how small irregularities which exist early in the plasma lifetime grow to become more prominent. The two photographs of Fig. 28 illustrate the growth pattern for that particular experiment. Figure 29 shows two photographs which also illustrate the growth of the irregular formations. In particular, the large ball of plasma, which has grown in a central location between the electrodes, is split by a wedge of cool plasma which is not obscured or consumed by the growing ball of hot plasma.

Fig. 29. Two photographs showing the irregular growth for another experiment.

Two photographs which were taken for two different tests about 0.1 μsec after the beginning of current flow are shown in Fig. 30. These photographs, supposedly taken for identical conditions, illustrate two different modes of plasma behavior during the early stages of plasma formation.

The various observations suggest the existence of two types of plasma which have greatly different properties. In a well developed discharge,

Fig. 30. Two photographs from different experiments showing alternate modes of plasma development.

regions of hot and cool plasmas exist. Also, the formation of the discharge path may occur in different ways, one being the development of a small and relatively hot plasma column and the other being the development of a rather diffuse and cool conducting region.

The two types of plasma might be distinguished by their conductivity mechanisms. The hotter plasma might be considered as a dense gas which contains a low fraction of ionized particles migrating under the influence of an electric field. However, the cooler and consequently more dense plasma might be considered as a type of lattice where all valence electrons contribute to conduction as in a metal. Neither type of plasma can be understood in terms of gaseous or metallic conduction as they are described by present theories, yet the need for some distinction of this type is apparent if an explanation is to be found for the plasma formations which have been observed.

The conductivity of the plasma might be represented as a function of plasma density for constant pressure. As temperature drops below 10 000°K and density increases, the number of free charge carriers and the conductivity drop. However, at higher densities corresponding to temperatures of about 6000°K, the overlap of electron wave functions gives rise to a different mode of conductivity which is an increasing function of density.

Reflected Shock Waves

When the shock front from the explosive passes through a plasma column which has already been formed, reflected shock waves are produced at the interface between the plasma and the water. One such wave is reflected back into the water when the shock front passes from water into the plasma. Another is reflected back into the plasma when the shock front passes from the plasma into the water on the other side of the plasma column.

A photograph of the reflected shock front in the plasma is shown in Fig. 31. The photograph was taken about 0.1 μsec after the principal shock front had traversed the plasma column. The view was normal to the direction of shock propagation and through a hole in the side of the brass extension. The reflected shock front is moving downward in the photograph.

Fig. 31. Reflected shock front in a plasma column which has been compressed with an explosive shock wave.

Development of the Plasma After Shock Wave Compression

In the case where an existing plasma column was compressed, the explosive shock front first arrived at the plasma column after the column had been growing for 0.3 μsec. Over the interval from 0.3 to 0.5 μsec, the plasma was being traversed by the principal shock wave and reflected waves. Then a period of about 0.4 μsec occurred during which the column of plasma had a fairly uniform temperature of about 10 000°K. The quantitative measurements were made then. Finally, at about 1.0 μsec, another change occurred in the plasma column as it split into two parallel columns during an interval of 0.2 to 0.3 μsec.

The process of splitting is illustrated in the sequence of photographs shown in Fig. 32. The three photographs were taken from more than one test to show the entire change which occurred. The first shows the plasma in its uniform state before the splitting begins. The second shows the plasma in an intermediate state where, except for a small region in the center, the plasma temperature has fallen to the lower range near 6000°K. The third figure shows the plasma after the split is complete with the hot center region having disappeared completely. The new columns have temperatures approximately the same as the plasma temperature before the change began. The variations of temperature are suggestive that the process of splitting may be related to existence of the two types of plasma which were discussed earlier.

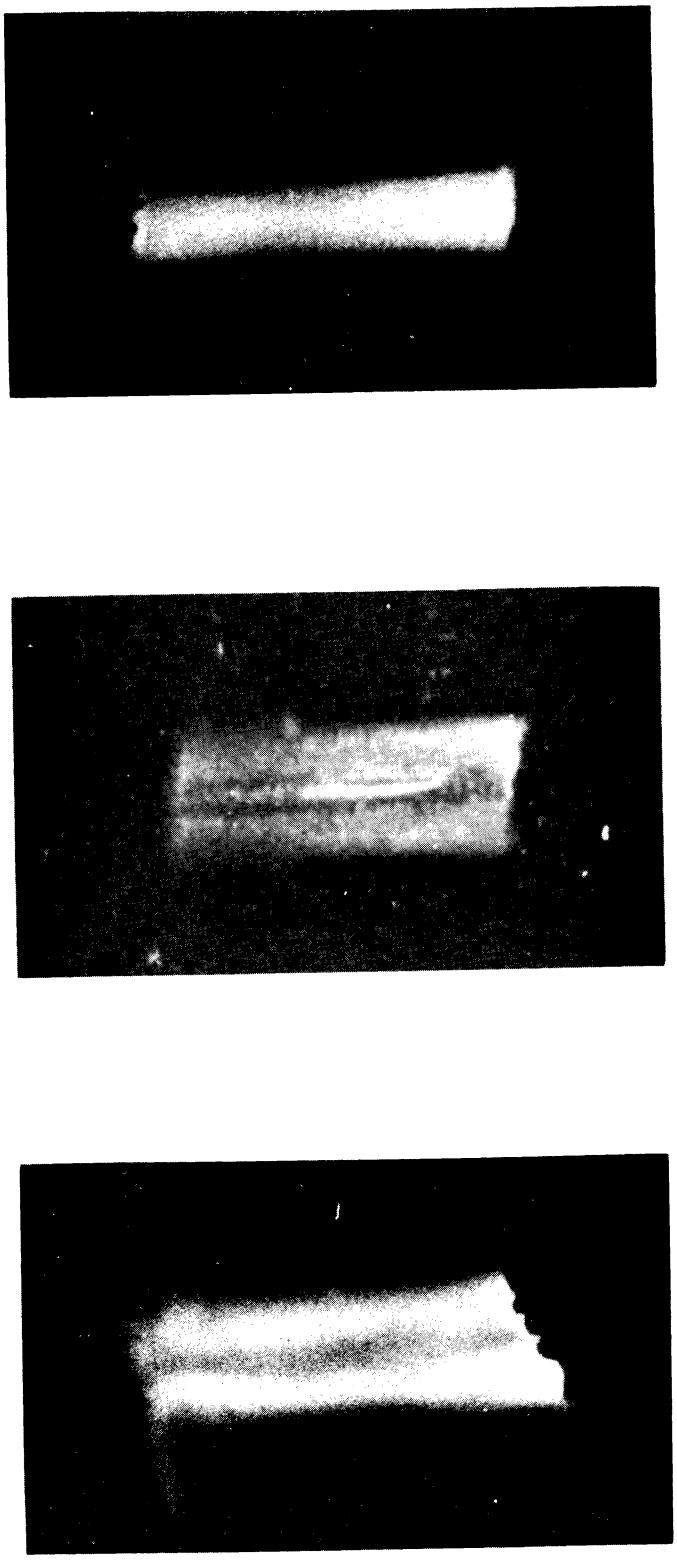

Fig. 32. Three photographs showing the splitting of a plasma column after approximately 1/2 μsec of confinement at 115 kilobars.

CONCLUSION

For the various experimental conditions which were investigated, numerical values were obtained for temperature, pressure, and internal energy. These data provided criteria for the applicability of theoretical equations which were used in calculating the thermodynamic properties of the plasmas. The two regions of pressure which were studied required different theoretical models for their descriptions.

For pressures from 4 to 8 kilobars, the plasma temperature was in the range from 30 000 to 40 000°K. The Debye-Hückel shielding theory was used to calculate values of internal energy from pressure and temperature data, and the calculated values were found to be smaller than the measured values by a factor of five.

Strong cohesive forces existed because of the interactions of the closely-spaced particles. Because of the cohesive forces, the density was several times greater than the Debye-Hückel theory predicted, and the internal energy per unit volume also was greater. However, the energy per atom was slightly lower. A more realistic theoretical prediction was based upon the virial theorem which was applied to highly distorted electron quantum states. The cohesion was related to the distortion which occurred because of the high density.

At a pressure of 115 kilobars, the plasma at 10 000°K was treated as a partially dissociated gas of water molecules with a very low fraction of ionization. The concept of covolume was introduced to complete the interpretation of the experimental data. The computed covolume was a small fraction of the covolume for water at the critical point. This result is expected at pressures much higher than the critical pressure.

Irregular plasma growth patterns at the higher pressure under certain conditions indicated that ionization was occurring because of the high density. However, the term ionization cannot be interpreted in the usual manner. A large number of electrons were mobile at temperatures in the range from 6000 to 7000°K, even though Saha's equation predicted a very low level of ionization. The close proximity of particles produced a type of lattice conduction through the overlap of wavefunctions.

REFERENCES

1. Feynman, R. P.; Metropolis, N.; and Teller, E.: Equations of State of Elements Based on the Generalized Fermi-Thomas Theory. Phys. Rev., Vol. 75, 1949, p. 1561.

2. Suits, C. G.: Measurements of Some Arc Characteristics at 1000 Atmospheres Pressure. J. Appl. Phys., Vol. 10, 1939, p. 203-206.

3. Martin, E. A.: Experimental Investigation of a High-Energy Density, High-Pressure Arc Plasma. J. Appl. Phys., Vol 31, 1960, p. 255-267.

4. Sherk, P. M.: Temperatures of Plasmas Produced by Exploding Wires Under Water. Phys. Fluids, Vol. 7, 1964, p. 913-915.

5. Komelkov, V. S.; Skvortsov, Yu X.; Kuznetsov, N. M.: Broadening of the Spark Channel in Liquids. Soviet Phys.—Tech. Phys., Vol. 5, 1961, p. 1100-1112.

6. Roi, N. A.; and Frolov, D. P.: On the Electroacoustical Efficiency of a Spark Discharge in Water. Soviet Phys.—Doklady, Vol. 3, 1958, p. 118-121.

7. Zingerman, A. S.: The Dependence of the Pressure at the Front of a Shock Wave Upon the Steepness of the Energy - Pulse Front When an Electrical Discharge Takes Place in a Liquid. Soviet Phys.—Tech. Phys. Vol. 1, 1956, p. 2454-2455.

8. Seay, G. E.; Seely Jr., L. B.; Fowler, R. G.: Production of High Ion Densities in Helium by Means of High Explosives. J. Appl. Phys., Vol. 32, 1961, pp. 2439-2447.

9. Courant, R.; Friedrichs, K. O.: Supersonic Flow and Shock Waves. Interscience, New York, 1948.

10. Cook, J. A.: The Science of High Explosives. Reinhold, New York, 1958, Chapter 12.

11. Cole, R. H.: Underwater Explosions. Princeton University Press, 1948.

12. David, H. G.; Hamann, S. D.: The Chemical Effects of Pressure: Part 5—The Electrical Conductivity of Water at High Shock Pressures. Trans. Faraday Soc., Vol. 55, 1959, pp. 72-78.

13. Walsh, J. M.; Rice, M. H.: Equation of State of Water to 250 Kilobars. J. Chem. Phys., Vol. 26, 1957, pp. 824-830.

14. Harris, A. J.: The Decay of Plane, Cylindrical and Spherical Shock Waves. Vol. 1 of Underwater Explosion Research. Office of Naval Research, Department of the Navy, 1950, pp. 1053-1056.

15. Walsh, J. M.; Rice, M. H.: Dynamic Compression of Liquids from Measurements on Strong Shock Waves. J. Chem. Phys. Vol. 26, 1957, pp. 815-823.

16. Cullington, E. H.; Chace, W. G.; Morgan, R. L.: Lovotron—A Low Voltage Triggered Gap Switch. (AFCRC-TR-55-227), Air Force Cambridge Research Center, 1955.

17. Zarem, A. M.; Marshall, F. R.; and Hanser, S. M.: Millimicrosecond Kerr Cell Camera Shutter. Rev. Sci. Instr. Vol. 29, 1958, p. 1043.

18. Attwood, S. S.: Electric and Magnetic Fields. Third Ed., Wiley, New York, 1949, p. 286.

19. Rouse, C. A.: Ionization—Equilibrium Equation of State: III. Results with Debye-Hückel Corrections and Planck's Partition Function. Astrophys. J. Vol., 136, 1962, pp. 636-634.

20. Rouse, C. A.: Ionization—Equilibrium Equation of State: IV. Dense Plasmas and Liquid Metals. Astrophys. J., Vol., 136, 1962, pp. 665-670.

21. Debye, P.; Hückel, E.: Zur Theorie der Elektrolyte. Physikalische Zeitschrift, Vol. 24, 1923, pp. 185-206.

22. Mayer, J. E.: The Theory of Ionic Solutions. J. Chem. Phys., Vol. 18, 1950, pp. 1426-1436.

23. Villars, D. S.: Equation of State of Gaseous Metallic Plasmas. Phys. Fluids, Vol. 6, 1963, pp. 745-748.

24. Tolman, R. C.: The Principles of Statistical Mechanics. Clarendon Press, Oxford, 1938, pp. 565-576.

25. Haar, D. ter.: Elements of Statistical Mechanics. Holt, Rinehart and Winston, New York, 1960, p. 82.

26. Landau, L. D.; Lifshitz, E. M.: Statistical Physics. Addison—Wesley, Reading, Massachusetts, 1958, p. 91.

27. Theimer, O.; and Gentry, R.: New Method for Determining the Thermodynamic Functions of Dense Gases and Plasmas. Ann. Phys. (N.Y.), Vol. 17, 1962, pp. 93-113.

28. Green, H. S.: Statistical Thermodynamics of Plasmas. Nuclear Fusion (International), Vol. 1, 1961, pp. 69-77.

29. Ecker, G.; Kroll, W.: Lowering of the Ionization Energy for a Plasma in Thermodynamic Equilibrium. Phys. Fluids, Vol. 6, 1963, pp. 62-69.

30. Moore, C. E.: Atomic Energy Levels. Circular No. 467, National Bureau of Standards, 1949, 1952, 1958.

31. Harris, G. M.: Equilibrium Properties and Equation of State of a Hydrogen Plasma. Phys. Rev., Vol. 133, 2A, 1964, pp. 427-437.

32. Hirschfelder, J. O.; Curtiss, C. F.: Molecular Theory of Gases and Liquids. Wiley, New York, 1954.

33. Harris, G. M.; Trulio, J. G.: Equilibrium Properties of a Partially Ionized Plasma. Phys. Rev., Vol. 119, 1960, pp. 1832-1841.

34. Wigner, E. P.; and Seitz, F.: Qualitative Analysis of the Cohesion in Metals. Vol. 1 of Solid State Physics, Frederick Seitz and David Turnbull, Eds., Academic Press, New York, 1955, pp. 97-99.

35. Cook, M. A.; McEwan, W. S.: Cohesion in Plasma. J. Appl. Phys., Vol. 29, 1958, pp. 1612-1613.

36. Russell, H. N.: Molecules in the Sun and Stars. Astrophys. J., Vol. 79, 1934, pp. 317-342.

37. Leighton, R. B.: Principles of Modern Physics. McGraw-Hill, New York, 1959, p. 731.